Link Quality in Wireless Sensor Networks

Ana Bildea

UNIVERSITÉ DE GRENOBLE

THÈSE

Pour obtenir le grade de

DOCTEUR DE L'UNIVERSITÉ DE GRENOBLE

Spécialité : **Informatique**

Arrêté ministérial : 7 août 2006

Présentée par

Ana BILDEA

Thèse dirigée par **Andrzej Duda**
et codirigée par **Olivier Alphand**

préparée au sein de **UMR 5217 - LIG - Laboratoire d'Informatique de Grenoble**
et de **École Doctorale Mathématiques, Sciences et Technologies de l'Information, Informatique (EDMSTII)**

Link Quality in Wireless Sensor Networks

Thèse soutenue publiquement le **19 Novembre 2013**,
devant le jury composé de :

M. Noel De Palma
Professeur, Université Joseph Fourier, Président
Mme. Isabelle Guérin-Lassous
Professeur, ENS de Lyon, Rapporteur
M. Stéphane Ubeda
Professeur, INSA de Lyon, Rapporteur
M. Pascal Berthou
Maître de Conférences, Université Paul Sabatier - Toulouse III, Examinateur
M. Andrzej Duda
Professeur, Grenoble INP – Ensimag, Directeur de thèse
M. Olivier Alphand
Maître de Conférences, Grenoble INP – Ensimag , Co-Directeur de thèse

Acknowledgements

I would like to express my deepest appreciation and my sincere gratitude to my thesis director, Prof. Andrzej Duda. Without his great guidance and persistent help I would have never completed this work. Thank you for mentoring me throughout the entire thesis venture, for engaging me in new ideas, and teaching me how to put complex ideas into simple terms.

I would like to thank my committee members, Prof. Isabelle Guérin-Lassous and Prof. Stéphane Ubeda for taking their time to judge my work. I am extremely grateful for your suggestions and helpful comments regarding my work.

I place on record, my sincere gratitude to my co-supervisor, Olivier Alphand for its supervision, support, suggestions, valuable comments that I benefit in the completion of this dissertation.

Also, I would like to address my deep gratitude to our team R&D ingineer, Etienne Double that provided me with technical answer each time I needed.

I will like to express my sincere thanks to Prof. Bernard Tourancheau, Associate Prof. Franck Rousseau, and Prof. Martin Heusse, for advising and providing me with answers in delicate research matters I had to tackle along my thesis.

In addition, a thank you to Pascal Poulet and Ghislaine Gaillard for easing the bureaucratic road in achieving the working rights in France.

I would like to acknowledge my colleagues and in the same time friends from Drakkar team. A special thank you for Isabel, Carina, Maru, Maciej, Nazim, Bogdan, Michal, as well as for friends from other teams, especially Sofia, Azzeddine, Reinaldo.

I am thankful to my friends outside the laboratory, especially to AlinaR, Cristina, Ioana, and Elena, Francois, Paul, Adi, Diana, Laurentiu, Bruno, Francesco F., Ting Ting, Andy, Tony, Teo, Geta, Rossy, Max, Anca, Radu, Sorin, Hannan, Andrei. Moreover, I convey a thank you to Paolo for continually encouraging in achieving my goal.

I am also thankful to all that I forgot and who, directly or indirectly, provided me with help in this challenging experience.

A very special thank goes to Genereso for supporting and understanding me on the last part of my venture.

Finally, my greatest appreciation goes to my family for your unceasing love and support throughout my entire life, for believing in me, and encouraging me in all my struggles and frustrations.

Contents

List of Figures

List of Tables

Notation

ACK	Acknowledgment
BER	Bit Error Rate
CSMA/CA	Carrier Sense Multiple Access/Collision Avoidance
CSMA	Carrier Sense Multiple Access
DAO	Destination Advertisement Object
DIO	DODAG Information Object
DIS	DODAG Information Solicitation
DODAG	Destination Oriented Directed Acyclic Graph
DSSS	Direct-Sequence Spread Spectrum
DUCHY	Double Cost Field Hybrid Link
ED	Energy Detection
ETX	Expected Transmission Time
F-LQE	A Fuzzy Link Quality
GFSK	Gaussian Frequency-Shift Keying
ICMP	Internet Control Message Protocol
IEEE	Institute of Electrical & Electronics Engineers
IETF	Internet Engineering Task Force
IP	Internet Protocol
ISO	International Standard Organization
IPT	Inter Packet Time Interval
KLE	Kalman filter-based Link quality Estimator
HoPS	Holistic Packet Statistics
LETX	LQI-based ETX
LEEP	Link Estimation Exchange Protocol
LQI	Link Quality Indication
LQIBM	The Link Quality Indication Based on Metric
LQE	Link Quality Estimator
LQR	Link Quality Ranking
LLN	Low power and Lossy Network
LNA	Low Noise Amplifier
LOS	Line of Sight
MAC	Medium Access Control
MP2P	Multi Point to Point
O-QPSK	Offset QPSK
OS	Operating System
PDF	Probability Density Function
PDU	Protocol Data Unit
PDR	Packet Delivery Ratio
P2P	Point to Point
P2MP	Point to Multi Point

PHY	Physical Layer
PRR	Packet Reception Ratio
QPSK	Quadrature Phase Shift-Keying
RA	Router Advertisement
RF	Radio Frequency
RFID	Radio Frequency Identification
RNP	Required Number of Packet Retransmissions
RPL	Routing Protocol for Low power and Lossy Networks
RSSI	Received Signal Strength Indication
SFD	Synchronization Frame Delimiter
SFD	Start-of-Frame Delimiter
SHR	Synchronization Header
SNR	Signal to Noise Ratio
SN	Sequence Number
TCP/IP	Transport Control Protocol/Internet Protocol
UDP	User Datagram Protocol
UI	User-Interface
WLAN	Wireless LAN
WMEWMA	Window Mean with Exponential Weighted Moving Average
WRA	Weighted Regression Algorithm
WRE	Weighted Regression Estimator
WSN	Wireless Sensor Network

Abstract

The goal of the thesis is to investigate the issues related to the temporal link quality variation in large scale WSN environments, to design energy efficient link quality estimators able to distinguish among links with different quality on a short and a long term.

First, we investigate the characteristics of two physical layer metrics: RSSI (Received Signal Strength Indication) and LQI (Link Quality Indication) on SensLAB [75], an indoor large scale wireless sensor network testbed. We observe that RSSI and LQI have distinct values that can discriminate the quality of links.

Second, to obtain an estimator of PRR, we have fitted a Fermi-Dirac function to the scatter diagram of the average and standard variation of LQI and RSSI. The function enables us to find PRR for a given level of LQI. We evaluate the estimator by computing PRR over a varying size window of transmissions and comparing with the estimator.

Furthermore, we show using the Gilbert-Elliot two-state Markov model that the correlation of packet losses and successful receptions depend on the link category. The model allows to accurately distinguish among strongly varying intermediate links based on transition probabilities derived from the average and the standard variation of LQI.

Finally, we propose a link quality routing model driven from the F-D fitting functions and the Markov model able to discriminate accurately link categories as well as high variable links.

Keywords Received Signal Strength indicator (RSSI), Link quality indicator (LQI), Link quality, Indoor Senslab-testbed, RPL, uIPv6, Duty Cycle Medium Access Control (MAC), Wireless sensor networks (WSN).

Résumé

Résumé L'objectif de la thèse est d'étudier la variation temporelle de la qualité des liens dans les réseaux de capteurs sans fil à grande échelle, de concevoir des estimateurs permettant la différenciation, à court terme et long terme, entre liens de qualité hétérogène.

Tout d'abord, nous étudions les caractéristiques de deux paramètres de la couche physique: RSSI (l'indicateur de puissance du signal reçu) et LQI (l'indicateur de la qualité de liaison) sur SensLab, une plateforme expérimentale de réseaux de capteurs à grande échelle situés à l'intérieur de bâtiments. Nous observons que le RSSI et le LQI permettent de discriminer des liens de différentes qualités.

Ensuite, pour obtenir un estimateur de PRR (Taux de Réception des Paquests), nous avons approximé le diagramme de dispersion de la moyenne et de l'écart-type du LQI et du RSSI par une fonction Fermi-Dirac. La fonction nous permet de trouver le PRR à partir d'un niveau donné de LQI. Nous avons évalué l'estimateur en calculant le PRR sur des fenêtres de tailles variables et en le comparant aux valeurs obtenues avec l'estimateur.

Par ailleurs, nous montrons en utilisant le modèle de Gilbert-Elliot (chaîne de Markov à deux états) que la corrélation des pertes de paquets dépend de la catégorie de liens. Le modèle permet de distinguer avec précision les différentes qualités des liens, en se basant sur les probabilités de transition dérivées de la moyenne et de l'écart-type du LQI.

Enfin, nous proposons un modèle de routage basé sur la qualité de lien déduite de la fonction de Fermi-Dirac approximant le PRR et du modèle Markov Gilbert-Elliot à deux états. Notre modèle est capable de distinguer avec précision les différentes catégories de liens ainsi que les liens fortement variables.

Mots-clés Indicateur de Puissance du Signal Reçu (RSSI), Indicateur de Qualité de Liaison (LQI), Plateforme de test (Senslab), RPL, uIPv6, Méthodes Duty Cycle d'accès au Médium (MAC), Réseaux de Capteurs (WSN).

Chapter 1

Introduction

Contents

1.1 IP for Wireless sensor networks (WSN)

WSN started over a decade ago to become popular mainly due to a wide range of scenarios in which they can be used. More specifically, the idea of embedding in the same device a communication module with sensing and processing capabilities contributed to the increased interest in the WSN.

The current progress of WSN is due to: hardware solutions such as Micro Electro-Mechanical Systems (MEMS), low-power communication hardware, low-power micro-controllers, as well as advanced software optimizations (lightweight communication protocols, real time systems).

A WSN is a set of objects deployed indoor or outdoor aiming at a common goal. The objects contain tiny autonomous sensors that allow monitoring large regions for short or long periods of time. Each sensor node has a limited memory, so it needs to report periodically collected data to a base station. Communication happens over a radio device having a range from several meters up to about 100m. Furthermore, data is usually communicated at a low bit rate of 250 kbps or even lower (60kbps). The main power supply of a sensor node is a AAA battery with a lifetime that can reach at maximum about 5-10 years for low traffic scenarios. In terms of cost, we have sensors with prices down to few $s that render deployments low-cost.

Each deployment targets a long lifetime. Basically, the lifetime is a vital factor for WSN, as sensor nodes dispose of non-renewable energy resources that make them dependent on energy consumption. Among the energy consumption sources we mention transmissions, sensing, signal and data processing, the phases during which the CPU continues to consume energy.

WSN networks need to meet other requirements: they need to be *reactive*, to act as quickly as possible aiming to respect the imposed deadlines, they need to be *robust* to adapt to the topology, density, and environmental changes, and moreover, the *connectivity* with the sink should be guaranteed.

The applications of WSNs spread across multiple domains such as home automation, industrial manufacturing, environmental monitoring, military, habitat or natural

phenomena surveillance etc. Each particular application may rely on a small or large scale. However, a large scale raises new challenges as the environmental conditions may change unexpectedly.

The research community has already carried out several large scale experiments, for instance, performed in the forests, where sensors monitor the habitat or open fields to track wild animals.

Generally, applications can be classified according to different targets: improve productivity, enhance security, support health care, ensure the maintenance, save energy in smart grids, render buildings intelligent. Another way to classify applications is by the deployment size, cost, topology, or mobility of nodes. Data they generally gather is mostly humidity, temperature, pressure, or lightning.

Table 1.1 presents a brief classification of existent applications. One predominant application is *home automation*. As it monitors and controls the living conditions, nodes have to be integrated into buildings.

One of the first applications of this type dates from 2002. It was initiated by Intel Research Laboratory from Berkeley University. The experiment consisted of a collection of more than 1 million of data readings from 32 nodes deployed along the Great Duck Island [61]. The reached lifetime of a sensor node was about 9 months.

Another pioneer application on WSN was the Zebranet project [61] headed at Mpala Research Center, Kenya. It consisted of tracking zebras using mobile sensors equipped with GPS technology. In medicine, E-health brings new perspectives through distance monitoring. Regarding natural phenomena, an example application was deployed around the Tungurahua volcano in Equator, where infrasonic signals during eruptions were monitored.

Today applications focus more on offering services, for instance, the Smart PARKing (SPARK) System [78] monitors and delivers information concerning available parking places. BorderSense, a patrol border service [86] is another common surveillance service. Multimedia sensors can detect intruders while mobile nodes are in charge of tracking the intruders.

The mentioned applications helped to better understand the issues that may arise in real deployments. For instance, it is important that communication protocols are designed and tunned fully considering the application scenario requirements, e.g. traffic pattern [65].

WSNs have recently evolved into the concept of the *Internet of Things (IoT)*. It aims at interconnecting sensor nodes with the Internet. The communication in IoT relies on unique addresses for each "object". The IoT tends to make use of the existing technologies and infrastructure of the Internet. More specifically, we can define the IoT as a merge between three following visions.

The first one concerns simple objects such as RFID (the pioneers of the IoT) and sensor nodes. Both, RFIDs and sensor nodes, are simple to use allowing to track objects, to read their status, to identify, to monitor.

In the second vision, the IP for Smart Objects (IPSO) Alliance boosts the Internet Protocol (IP) as a key for a worldwide spread of smart objects. They promote the IP protocol stack as a lightweight protocol working on the tiny and constrained devices.

Home automation	To improve comfort and safety, light monitoring, heating control, remote device control.
Industrial	Manufacturing automation, process control.
Environmental	Monitoring soil, water and air, agriculture.
Traffic	Highway, bridge monitoring.
Biology	Patient monitoring, body sensors, e-health.
Services	Electricity, water, gas sensors to storage the usage statistics, e-money, e-learning, commercial.
Phenomena	Volcano monitoring, habitat sensing and monitoring, natural disastrous detection.
Entertainment	Improving TV, smart phones experience.
Military	Border patrol sensors, battlefield management, area discovery, surveillance, defense.

Table 1.1: WSN applications.

IPSO advises as a solution for IoT connectivity an adaptation of the IP protocol on top of the IEEE 802.15.4 standardization.

The last aspect concerns the "semantic vision", in which sensors are queried to get relevant data, organize them, and reason upon.

In this struggle to find feasible solutions, it is important to mention the major constraints that slow down the IoT progress: energy, limited resources, highly unstable radio links, dense topologies in terms of the number of nodes etc.

However, an optimistic view of IoT foresees that in 10 years from now, the real world will join the digital one. Such a widespread adaptation of the IoT raises challenges: how to store all data, how to search for the needed information, how to guarantee privacy. Hence, once the IoT will satisfy all the requirements including (privacy, reliability, scalability), a widespread presence of smart objects will be predictable.

1.2 Motivation and Contributions

To benefit from all the potential of WSN, robust and reliable communication should be achieved on low-power, low-cost, tiny, autonomous, secure devices. Therefore, to achieve inter-connected constrained devices, the Internet Engineering Task Force (IETF)[37] created working groups that explore different directions: routing (Low Power and Lossy Networks(ROLL)[39]), IPv6 over Low power WPAN (6LoWPAN) [77], or the application layer CoRE [38]. Researchers address the challenges of interconnecting constrained devices to the Internet in two ways. The first one relies on designing protocols with low energy consumption. The second one consists of designing appropriate hardware systems.

In this thesis, we analyze a large scale WSN testbed to identify the factors that impact signal propagation, the relation and the pattern deviation of the hardware metrics that result in energy waste when communication protocols are used.

We propose a link classification for lossy environments. Based on this classification,

we propose two mathematical models (a fit function and a Markov model) able to predict the packet reception rate.

Furthermore, we propose a link quality estimator that takes as input hardware and software factors and combine them to reduce the overhead and the collisions introduced by retransmission while gaining in energy and packet delivery ratio. Finally, we conclude our work with future perspectives and needed further studies.

The thesis is organized into six chapters as follows:

Chapter 2 gives an overview of existing studies on the main factors that influence link quality. Furthermore, we discuss the main characteristics of the hardware metrics (RSSI/LQI/SNR). We present the main link characteristic studies as well as the existing link quality estimators based on simple or composed hardware metric combinations. We emphasize the existing efforts that use Markov chain model to achieve link assessment

Last, an overview of routing in IPv6-based 6LoWPAN networks is offered. We point out the main aspects of the metrics used by the most popular distance-vector based routing protocols (RPL, LOAD, CTP).

Chapter 3 presents an empirical study of the link quality factors based on the large scale testbed. The aim is to capture temporal fluctuations as well as link asymmetry in a given indoor environment. Furthermore, the investigation allows us to distinguish links based on their channel dynamics, and classify links using CC1101 and CC2420 radio chips based on hardware metrics such as the link quality indicator (LQI) and the received signal strength indicator (RSSI). We report on a study of good link proportion, environmental factors impacting signal propagation, and the bi-directionality of links varying the output power, the inter-packet time interval, and the length of the packet.

Chapter 4 statistically analysis the link quality. To obtain an estimator of the packet reception ratio (PRR), we have fitted a Fermi-Dirac function to the scatter diagram of the average and standard variation of LQI. The function enables us to find PRR for a given level of LQI. The estimator leads to better neighborhood management and routing metrics in wireless sensor networks.

Chapter 5 presents a study of the Gilbert two state model to catch the temporal evolution of each link category. To discriminate high variable links, we have found that the GE stationary probabilities derived from avg and std LQI can decide well the lowest variable links. Considering that the neighborhood relies only on high intermediate links, the good stationary probability of the avg LQI is able to distinguish the best one.

At the end of the Chapter, we discuss in details our routing metrics proposal. More specifically, we propose to use our fit function (LQI average and LQI deviation) and the stationary probabilities given by the Markov model to choose among links with high link variation. The idea is to put together the fit functions over average and standard deviation LQI to predict PRR and further use the stationary probabilities computed by the Markov model to discriminate more accurately the high variable intermediate links.

Chapter 6 We conclude the work by summarizing the main contributions. We also address the issues that continue to challenge the community. Moreover, we end up with the perspectives for the future work.

Chapter 2

State of the art

Contents

We will mainly concentrate on the link quality estimation approaches regarding the Media Access Control(MAC) and routing protocols (RPL/LOAD). The principal goal is to design a link quality estimator able to construct stable topologies and reduce energy consumption.

First, we present existing empirical studies performed on various radio chips (CC1100/CC1101/TR1000/CC2420) with respect to several metrics, such as received signal strength (RSSI), link quality indicator (LQI), and packet reception ratio (PRR). Environmental factors that prone to radio signal propagation distortion are discussed.

Second, we briefly overview the existing link assessment mechanisms that make use of RSSI, LQI, PRR, or Markov chain model.

Finally, we point out the main aspects of several distance-vector based routing protocols (RPL, LOAD, CTP).

2.1 Introduction

Wireless sensor networks rely on low complexity circuits and very low power radio hardware that enable battery supply nodes to last at most 10-15 years depending on their duty cycle. Therefore, to achieve such a long lifetime any energy waste should be avoided.

Low power links are sensitive to the environment and interferences. In this context, robust MAC protocols and stable routing protocols are difficult to design since the next hop choice may depend on an unreliable link quality estimator.

So, as long as the link quality estimation remains an open issue, much work considered the problem of characterizing wireless link quality [96, 106, 101, 6, 16, 80, 55, 95]. Moreover, in the link characterization process, the fluctuation of link quality rises continuous challenges due to the great impact on MAC and network layers. Figure 2.1 illustrates the link quality estimation process.

The quality of a link may vary as a function of time or distance. In particular, the temporal fluctuation of the link quality was reported by several studies on various

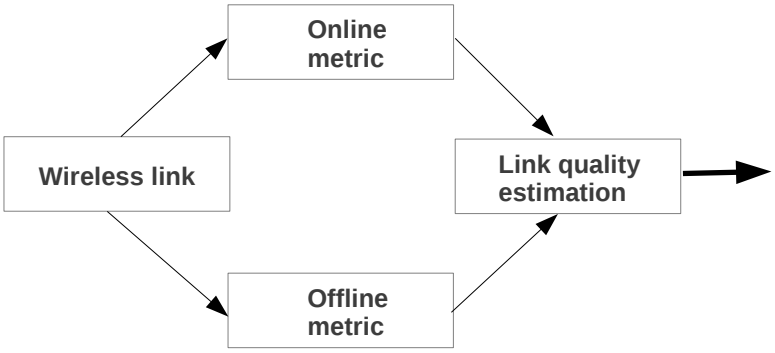

Figure 2.1: The link quality estimation process.

environments such as urban, habitat, university outdoor, offices [16, 83, 101, 80]. Likewise, the spatial variation of the link quality has been shown [103, 15, 105]. A common observation is that the link quality changes depending on the RSSI zone (connected, transitional, disconnected) the link is part of [101, 6, 28, 103, 97]. Generally, links in the connected zone are stable, contrary to the transitional and disconnected zones.

Furthermore, most of the studies used various platforms. We can cite platforms such as Mica 1, Mica 2 [23], Moteiv Tmote Sky [54], TelosB [60] equipped with CC1100/CC1101 [76], TR1000 [52], or CC2420 [22] low-power RF transceivers, among which the CC2420 radio is the most widespread.

Thus, the goal of this chapter is to overview the efforts done in characterizing lossy wireless links as well as on routing protocols (RPL, CTP, LOAD).

The chapter is organized as follows: first, we address the link characterization stressing out the impact of the physical layer on the link behavior. Second, we discuss the metrics that rely on online and offline link assessment mechanisms. The metrics are aiming to achieve energy consumption by estimating the stability of the links referring short and long term fluctuation of link quality. Likewise, we emphasize the advantages and the drawbacks of both mechanisms.

Finally, we overview the main features of the RPL, LOAD and CTP routing protocols followed by a brief discussion on their used routing metrics.

2.2 Link characterization

2.2.1 WSN context

Communication in WSN relies on low-power and cheap radio chips such as (TR1000/ CC1100/CC1001/CC2420) that present irregular radio patterns and a limited transmission range.

Nevertheless, due to the low power constraints and the fact that they need to act near the noise level while they are equipped with very simple radio circuits, the communication depends on the environment, frequency, the specific modulation scheme, or antenna patterns. As a result, the RF signals in indoor and outdoor environments may be highly variable and prone to bit errors. Still, they have to offer good packet delivery

ratio in multi hop scenarios for upper layers (MAC/Routing) whereas targeting few retransmissions and energy high efficiency.

The IEEE 802.15.4 standardization [85] targets low-cost, low-power devices low-data rates. It achieves three targets: low-power, low-data rate, and low-cost for the wireless personal area (WPAN) networks. The standardization was approved back in 2003, but due to the interest it attracted along years various variants of the standardization were proposed.

We bring up below the hardware and the environmental factors that influence IEEE 802.15.4-Compliant (CC2420) and IEEE 802.15.4-non-compliant (CC1101) radio links.

2.2.2 IEEE 802.15.4 standard and devices

We present in this section the most common aspects of the physical characterization of IEEE 802.15.4-compliant radios such as bit stream (CC1101) and packet oriented (CC2420) radios.

2.2.2.1 IEEE 802.15.4 PHY

The IEEE 802.15.4 PHY layer defines a total of 27 channels among which 16 non-overlapping channels. Before the transmission starts, every 4-bit symbol is transformed into a 32-chip sequence. At the reception, to decode the chip-sequence, the symbol that gives the higher chip correlation is chosen Figure 2.2.

Figure 2.2: The IEEE 802.15.4 PHY transmission process.

Each transmission or reception happens on a chosen channel that employs a specific modulation and encoding technique Table 2.1. Lower frequencies have a lower receiver sensitivity that gives a larger transmission range. Moreover, the range depends on the transmission power and the receiver sensitivity.

The IEEE 802.15.4 PHY is responsible of :

- *Turning on/off the radio transceiver* as required by the MAC layer.
- *Energy detection (ED) within the current channel.* This measure helps to detect the state of the channel busy/occupied. In 802.15.4, the ED takes 128μs and serves for the Clear Channel Assessment (CCA) or the channel selection.
- *Link Quality Indication (LQI).* The LQI indicates the quality of the received signal computed either using the ED, the signal to noise ratio, or both. This measure is important at the network layer as the routing metric can benefit from this measure.
- *Received Signal Strength (RSSI).* RSSI gives the strength of the received signal. It is measured over the first 8 symbols following the start delimiter of a frame.

- *Clear Channel Assessment (CCA).* The purpose of CCA is to inspect the medium state if it is busy or idle. A CCA may be performed in three modes. Mode 1 depends on an Energy Detection Threshold whereas mode 2 and 3 are depending on carrier sensing. CCA Mode 1 senses the channel as busy if the detected power in the channel exceeds the chosen threshold (generally -77dBm). CCA Mode 2 is based on carrier sense that considers a channel busy only if a signal with an IEEE 802.15.4 modulation and spreading technique is detected. Then, CCA Mode 3 is a combination of the mode 1 and 2. More specifically, a channel is detected as busy if it detects a IEEE 802.15.4 signal and the energy in the channel overcomes the chosen threshold.

- *Channel Frequency Selection* The transceiver can send data over one of the 27 channels available in 802.15.4. Thus, the physical layer is in charge of choosing the channel over which the transceiver sends packets.

Band[Hz]	Number of channels	Bit rate [kbps]	Modulation	Sensitivity [dBm]
868M	1	20	BPSK	-92
915M	10	40	BPSK	-92
2.4G	16	250	O-QPSK	-85

Table 2.1: IEEE 802.15.4 channel characteristics.

More specifically, physical layer provides instant information (RSSI/LQI) right after it decodes a packet. Therefore, the information may be employed as a link quality indicator. However, due to the short-term link variation, it is hard to predict the link quality just on a single packet [83].

2.2.2.2 RF features

The literature reports on several hardware factors that impact the link quality [15, 63, 92], such as: frequency, modulation, antenna (gain, orientation), output power, receiver sensitivity, internal noise, and hardware mis-calibrated. Table 2.2 presents the parameters of the most popular transceivers already mention: CC1101 and CC2420.

Frequency: The impact of the *oscillation rate of radio waves* has been proven on bit stream (CC1101) or packet oriented (CC2420) radio technologies. The bit stream technology relies on older radio transceivers such as the CC1101 that operate on the 868MHz frequency, whereas packet oriented ones refers to newer radios such as CC2420 (IEEE802.15.4 compliant) that operate on 2.4GHz frequency.

In particular, the platforms operating in the 868MHz ISM band are less exposed to external interferences, whereas the ones operating on 2.4GHz are likely exposed to external interferences from WiFi, Bluetooth, or microwaves. The 868MHz frequency has been used in various deployments [16, 15, 103, 67, 13]. The reason is its larger range as the attenuation of a signal is proportional to the used frequency. *Modulation*: Moreover, a drawback of the older radios 868MHz-based is related to a less robust modulation. In particular, older radio chips (CC1101/TR1000) use a simpler modulation such as

Frequency Shift Key (FSK), Gaussian Shaped Frequency Shift Keying (GFSK), On/Off Key (OOK), Minimum-shift Keying (MSK), Amplitude Shift Keying (ASK) with low bandwidth requirements. Nevertheless, the most popular radio transceiver (CC2420) is a IEEE 802.15.4 compliant. It uses Direct Sequence Spread Spectrum (DSSS) and Offset Quadrature Phase-shift Keying (O-QPSK) modulation scheme.

Radio	**CC1100**	**CC2420**
Data rate(max)	500 kbps	250 kbps
Frequencies	315/433/915 MHz	2.4 GHz
Rx Current	14 mA	17.4 mA
Tx Current	15 mA	19.7 mA
Output Power	+10dBm:-30dBm	0dBm:-25dBm
Receiver Sensitivity	-88 dBm	-95 dBm
Modulation	2-FSK/GFSK/MSK/OOK/ASK	O-QPSK/DSSS

Table 2.2: Radio parameters of CC1101 [76] and CC2420 [22].

Antenna: Zhou et al. [104] identified the sources of radio irregularities as non-isotropic path-loss caused by multi-path effects and hardware calibration. Hardware calibration is explained as a manufacturing problem according to which antenna gain may not be the same for all directions.

Receiver Sensitivity: It refers to the minimum signal strength needed at the input of a receiver in order to guarantee the reception.

2.2.3 RF signal propagation

Signal propagation depends on the type of the environment: indoor (i.e. offices, home), outdoor (i.e. urban, habitat). Distortion of the RF signals is due to various environmental and hardware factors [63, 92]. For instance, environmental factors include path-loss, fading, and interference.

- Path-loss (signal attenuation with distance):
  - *Free space (no multi-path sources are present)* see Equation 2.2.
  - *Log-distance path loss model (includes multi-path sources)* see Equation 2.4.

- Fading
  - Multi-path (the radio signals propagate over multiple paths, therefore, receivers retrieve multiple copies of the a signal):
    - *scattering (the deviation of the signal from the straight line)* occurs when the signal mets objects (IT equipments, small pieces of furniture).
    - *reflection (the signal bounces off an object)* is present when the signal meets large objects or surfaces (wall, ceiling, metal, glass, pieces of furniture).

    - *refraction (bending of RF signal, one part is absorbed the other part is reflected)* from obstacles.
    - *diffraction (the signal is obstructed by sharp edges)* encountered due to obstacle presence.
  - Shadowing (large obstruction of the RF signal):
    - human presence, walls, doors.

- Interference:
  - Concurrent transmissions,
  - Presence of other transmitters in the same band: Wi-fi, Blue-tooth or Microwaves.

Path-loss models predict the average received strength of a signal at a certain distance from the transmitter. It depends on the distance (line of sight) between the sender and the receiver. In fact, most of the models are based on the Fries free space equation 2.1.

$$P_r(d) = P_t G_t G_r (\frac{\lambda}{4\pi d})^2, \tag{2.1}$$

where P_r denotes the available power at the input of the receiving antenna, P_t denotes the output power of the transmitting antenna, G_t and G_r are the antenna gains of the transmitter and receiver, d is the distance between transmitting and receiving antenna, and λ is the wavelength.

The equation is simple, it provides an estimation of the received signal strength when between the transmitting and receiving antenna is a clear line of sight.

$$P_r(d) = P_r(d_0)(\frac{d_0}{d})^2, \tag{2.2}$$

where $P_r(d_0)$ is the received power in Watts at distance d_0, and $d_0 < d$. Therefore, the received power at any distance is referred by Equation 2.2. Moreover, RF signal power deteriorates with the squared inverse distance.

Path loss of a channel is measured in dB and is the difference (attenuation of the RF signal) between the transmitted power and receiver power in dB (see Equation 2.3).

$$PL(dB) = -10log_{10}(\frac{\lambda^2}{(4\pi)^2 d^2}), \tag{2.3}$$

Once we include multipath sources and ground reflection the path loss equation becomes:

$$PL(dB) = 10nlog_{10}(\frac{d}{d_0}), \tag{2.4}$$

where n (common value ranges from 2 to 6) is the loss exponent that indicates that the rate of the loss increase with respect to the distance. The path loss exponent depends on the environment and takes lower values for indoor (2) and higher for outdoor (6) [63]. Ganesan et al. [28] reported that the path loss formula changes with hardware characteristics.

Fading is defined as the deviation of the attenuation of the signal. It depends on frequency, location, and time. It can result in multi-path (fast fading on the order of 10 to 100 ms) or shadowing (slow fading on the order of 1s to 5s).

Multipath fading is the most common factor that affects link fluctuation resulting in a large deviation from the path loss models [63]. Especially, multipath it is due to reflection, refraction, diffraction or scattering of RF signals. Indoor, multi-path depends on the placement of nodes and the spatial characterization of the environment (office, halls, home). In particular, reflection is one of the main factors of multi-path presence that may alter the link reliability trough huge drops of the packet reception ratio. It occurs due to the presence of good reflectors such as metal or glass, and leads not just to the multipath effect, but also to the noise increase and interference.

The second fading factor is *shadowing*, a large scale effect that steers to creation of shadow zones (deep fade) where no radio emission/reception is encountered. However, Watteyne et al. [92] claimed that the fading effects can be avoided by changing the node location or the carrier frequency. Pucinelli et al. [63] emphasized that fading has to be considered in the design of wireless channels.

Interference is another important factor harming signal propagation. As a result of interference presence, protocols may become unstable due to packet reception drops, retransmissions, and link instability. It occurs in the presence of concurrent transmissions (internal interface) or from external interfering technologies e.g. IEEE 802.11 (WLAN), 802.15.1 (Bluetooth), and 802.15.4 [80].

Furthermore, Polastre et al. [59] reported that the IEEE 802.11b interference may result in energy waste as it may wake-up the duty-cycle MAC protocols that use an energy detection threshold to enter in listen mode. For example, to overcome the false wake-ups, Srinivasan et al. [79] recommended the use of adaptation clear channel assessment mechanism that takes into account the eventual noise from 802.11 networks.

On the other hand, concurrent transmissions lead to constructive or destructive interference that distorts the signal reception by creation of deep fading zones [55]. A constructive interference within two waves is defined as a multiple of 2π phase difference, while a destructive interference designates an odd π phase difference.

In this section, we have highlighted that links are lossy due to environmental factors harming signal propagation (path-loss, fading, interferences). The main observations on link dynamics driven from existing empirical studies are presented below.

2.3 Link behavior through hardware metrics

Radio transceivers provide two hardware metrics able to estimate the strength (RSSI) and the quality (LQI) of the received packet. For instance, each received packet embeds both hardware metrics (RSSI and LQI). Numerous existing studies explored the temporal fluctuation of RSSI and LQI in order to predict temporal link behavior.

Generally, a stable link guarantees a successful packet reception whereas short signal drops results in unsuccessful reception.

2.3.1 RSSI/LQI Overview

Received Signal Strength Indicator (RSSI) is an estimation of the received signal power in the channel. The obsolete radios such as CC1000/CC1101 are not based on the IEEE 802.15.4 standard, still, they provide the RSSI hardware parameter [76]. As the CC1101 transceiver enters in the reception mode, the RSSI is read out in raw from the RSSI register. The reading stops when the sync word is detected. The readout value is converted from 2 complement (hexadecimal) to decimal (RSSI_dec), following by a subtraction of -78dBm (offset) for CC1100 and -74dBm for CC1101 at 868MHz and a data rate of 250kbps. Additionally, in case the decimal value is below 128 the value is scaled conform the Equation 2.5. Conversely, for a value above 128, the RSSI estimation becomes Eq. 2.6. The offset depends on the data rate and the used frequency.

$$RSSI\ [dBm] = (RSSI\_dec)/2 - RSSI\_offset \tag{2.5}$$

$$RSSI\ [dBm] = (RSSI\_dec - 256)/2 - RSSI\_offset \tag{2.6}$$

Figure 2.3 a) presents the CC1101 frame format. In the newer radios such as CC2420 [22], the RSSI is an 8-bit integer value. It is read from the RSSI register (in case of the signal absence, the value indicates the noise). RSSI for CC2420 radio chip is computed over the eight symbol period ($128\mu s$):

$$RSSI\ [dBm] = RSSI\_VAL + RSSI\_OFFSET \tag{2.7}$$

The RSSI_VAL is a 12 bit register and the RSSI_OFFSET is equal to -45dBm. RSSI ranges from -28dBm to -127dBm. Figure 2.3 b) presents the frame format for the CC2420 radio.

Another measure extensively used to quantify link behavior is SNR that denotes the strength of the signal. It is defined as the ratio of the received signal strength and the strength of the background noise. To estimate SNR, the receiver records at first the RSSI of the received packet, then it has to measure the background noise. RSSI of a signal is defined as:

$$RSSI\ [dBm] = 10log_{10}(Power\_received\_packet + Background\_noise), \tag{2.8}$$

RSSI of the ambient noise is estimated as $10log_{10}(Background\_noise)$:

$$SNR\ [dBm] = RSSI[dBm] - Backgroud\_noise\ [dBm] \tag{2.9}$$

The Link Quality Indicator (LQI) is a metric that estimates the current quality of the received information.

For CC1101, *LQI gives an estimate of how easily a received signal can be demodulated by accumulating the magnitude of the error between ideal constellations and the received signal over the 64 symbols immediately following the sync word [76]* (see Figure 2.3). It ranges between [0..127]. A low value indicates a good link quality. Thus, its values depend on the used modulation (2-FSK/GFSK/MSK/OOK/ASK).

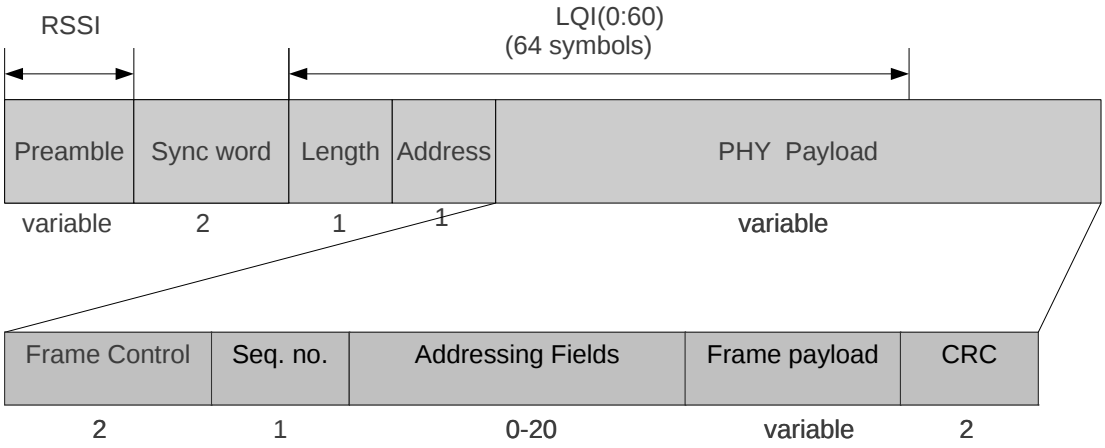

(a) RSSI/LQI metric for CC1101 radio.

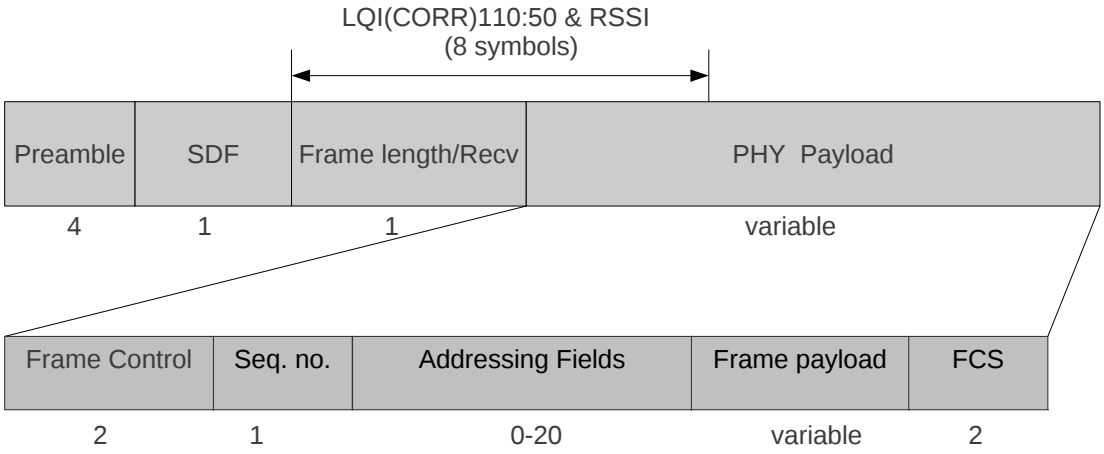

(b) Link quality indicator for CC2420 radio.

Figure 2.3: The frame format for CC1101 and CC2420 radio chips.

For CC2420 [22], *provides an average correlation value for each incoming packet, based on the 8 first symbols of the received PHY header (length field) and PHY Service Data Unit (PSDU).* The LQI software value is computed as in Eq. 2.10 and ranges from 0 to 255.

$$LQI = (CORR - a) * b \tag{2.10}$$

CORR represents the hardware correlation taking values between 50 and 110, a and b are constants whose values are specific to each hardware provider. For this reason, it remains unclear how LQI is computed. Specifically, a high correlation value of LQI gives better links. Figure 2.3 b) illustrates the RSSI and LQI computation for CC2420.

The strength of the signal (RSSI) and the link quality indicator (LQI) metrics are computed over each received packet. Since RSSI and LQI are correlated with the goodness of a signal, they may be used to predict link dynamics.

Generally, the quality of a link is estimated as a proportion of successfully received packets. Hence, the goodness of a link is linear to the proportion of received packets. Thus, a generic observation is that each link may belong to one of the following zones: high link quality, transitional ('gray zones') for intermediate link quality, and low link quality [28, 103, 97, 67, 101, 6]. Overall, previous efforts claimed that intermediate links are highly unstable.

In this context, we further present the work that was done to predict the link quality using hardware metrics. We mainly focus on several proposed link classifications according to PRR as well as on the temporal and spatial fluctuation of RSSI and LQI. Moreover, link asymmetry is discussed.

2.3.2 Link Classification based on PRR

Empirical studies carried out on various platforms resulted in a link classification based on the packet reception ratio (PRR). A PRR is defined as the ratio of the successful received packets to the total number of send packets. Generally, three classes of links are commonly mentioned such as good (high PRR), intermediate (intermediate PRR), and bad (low PRR): a common classification defines good links as the ones with a PRR above 90%, intermediate with PRR within 90% and 10%, and bad links for PRR below 10%. For example, Srinivassan et al. [79] claimed for the CC2420 transceiver that good links with $PRR > 85\%$ are above the receiver sensitivity threshold (-87dBm).

Table 2.3 summarizes the most common existing link quality classifications.

Considering the proportion of each link category on a large and small scale, it was reported a higher proportion of intermediate links on large scale platforms [28, 103]. Likewise, a study of the outdoor and indoor environments claimed a lower proportion of intermediate links in the outdoor with respect to indoor environments [67]. They conclude that the indoor environments are highly affected by multi-path effects.

Radio/Platform	**Good**	**Intermediate**	**Bad**	Reference
TR1001/ EYES	PRR$\geq$ 85%	$15\% < PRR < 85\%$	$15\% \geq PRR$	[67]
TR1000/Rene	PRR $\geq$ 65%	$15\% < PRR < 65\%$	$15\% \geq PRR$	[97]
TR1000&CC1100/Mica1&2	PRR$\geq$ 80%	$20\% < PRR < 80\%$	$20\% \geq PRR$	[15]
CC2420/Tmote Sky&JCreate	PRR$\geq$ 75%	$35\% < PRR < 75\%$	$35\% \geq PRR$	[13]
CC2420/TelosB,Micaz	$90 \geq PRR\%$	$10\% < PRR < 90\%$	$10\% \geq PRR$	[80, 92, 95]

Table 2.3: Link classification highlighted by various research efforts.

Moreover, we present below several findings on temporal fluctuation.

2.3.3 Temporal fluctuation

The literature investigated the RSSI/LQI temporal variation aiming to distinguish the fluctuation factors and patterns. Please note that the fluctuation term refers to RSSI

and LQI value changes over successive readings. Distinct factors such as environment, temperature, humidity, interference, were identified in Section 2.2.

2.3.3.1 RSSI fluctuation

First, the fluctuation of the RSSI indicator has been intensively analyzed in the literature [83, 63, 101, 66, 87].

Boano et al. [11] reports that RSSI is affected by the temperature change (day/night). The humidity seems to be another factor that generates RSSI variation [46]. External interference generates high fluctuation of RSSI [100]. They proposed an interference classifier that distinguishes between the potential interference sources (WLANs, Bluetooth, microwave ovens) that disturb the RSSI readings on the IEEE 802.15.4 channel. In addition, constructive and destructive interferences generated by the concurrent transmissions or environment factors result in high fluctuation of the RSSI [55]. Moreover, RSSI may encounter variance due to the antenna alignment (with the following degrees 0, 90, 180, and 270) [104]. It proposes a non-circular radio irregularity model (RIM) based on registered degree of the RSSI variation.

Tang et al. [87] concluded that RSSI fluctuation is due to hardware configuration, in particular, the transmitter and the receiver variability may vary for each radio chip. In addition, the antenna orientation is another important factor due to its non uniform radiation pattern and its magnetic pole position [92].

However, the conclusions of the studies are contradictory as they claim a small variation of the RSSI when above the radio sensitivity -87dBm for CC2420 chip [83], a large variation [101, 66] or even RSSI does not fluctuate in time [63]. The large temporal variation of the RSSI can reach 11dBm with a time-scale variation about 0s-20s or few hours [66]. However, RSSI is unreliable if the channel is in contention between several interfering motes.

Furthermore, considering SNR, Srinivasan et al. [81] claimed that its variation is correlated with the fluctuation of RSSI as the noise is quite stable.

2.3.3.2 LQI fluctuation

In terms of LQI, low variation was claimed for packets coming from nodes placed in zones with good radio connectivity. On the other hand, the variation of LQI becomes large for lower radio connectivity. Therefore, several studies demonstrated that LQI may vary drastically if the node is in the transitional or the disconnected zone [55, 50, 12]. However, for the link in the connected zone, the LQI is highly stable [83], which may be a good indicator for link quality.

A generic observation is that LQI variation can determine if a link is very good or extremely bad. However, it is not a good predictor for the transitional links, which are highly unpredictable. For instance, Srinivassan et al. [79] claimed that LQI varies in a wider range compared to RSSI.

A wide conclusion is that RSSI/LQI/SNR metrics are individually inadequate to evaluate correctly the link quality as they are based only on a single received packet.

Hence, an exponential average with a sliding window over historical data is widely recommended to properly estimate the link quality [80, 99].

2.3.4 Spatial fluctuation

It was shown in several research efforts a distance dependence of the RSSI and LQI. For instance, RSSI values decrease due to the path loss while LQI shown a distance correlation for the connected (high RSSI) and disconnected (low RSSI) zone [101, 79, 70]. Hence, they argued no correlation of LQI with distance for the transitional (intermediate RSSI) zone affected by anisotropic radio pattern, multipath effect, reflection, and external interference.

On the other hand, Woo et al. [97] claimed that the temporal variability of packet reception ratio is correlated with the distance. The study proposed a link estimation model, where the quality of a link is associated with a certain distance it is situated. Still, due to various environmental factors and the radio pattern it is hard to predict properly the distance.

2.3.5 Link asymmetry

Another issue of wireless links, is the link asymmetry. The most common factors that lead to link asymmetry are argued to be the hardware or the environmental factors [103, 97, 4, 15, 101, 80, 95].

The asymmetry of a link can be defined as an absolute difference $|PRR_{sender_x->receiver_y} - PRR_{receiver_y->sender_x}|$, where x, y are the ids of the nodes whereas the arrow points at the receiver. A link is called asymmetric if the absolute difference is bigger than 1% [95].

On the contrary, Srinivasan et al. [80] calls a link asymmetric if the absolute difference is above 40%. They claimed the good links (PRR>90%) are likely symmetric over time independently of the output power. The observation was also confirmed by Mottola et al. [55].

It was shown that intermediate links present high asymmetry due to multi-path effects and hardware mis-calibration where as bad links are less asymmetric [103, 97, 4, 15, 101, 80, 95]. Thus, Srinivasan et al. [80] shown a non-persist temporal asymmetry for unstable links mainly presented in the transitional zone.

To sum up, RSSI varies much less that LQI for intermediate and bad links. Conversely, LQI seems to be stable for good links whereas, for intermediate and bad links is highly unstable. Thus, the high variation is an interesting approach that have been extensively studied. For instance, numerous authors have combined RSSI, LQI and PRR in their link estimation schemes to discriminate lossy and asymmetric links from the good ones.

2.4 Packet loss modeling

First efforts on capturing loss burstiness through the well-known 2-state Gilbert-Elliot model was applied to IP voice flows traces [41, 73] and to packet tains in computer network traffic [40].

A pioneer study that models packet losses of wireless links was elaborated by Syed et al. [43]. They proposed the Markov-based stochastic chains that model the 802.11b links behavior of bit errors and packet losses. To show that higher order Markov chains (i.e. Markov chains of order 9) model more accurately the channel behavior, a comparison for full-state, hidden, and hierarchic Markov chains was performed. However, they claimed that such high order models are far too complex to be integrated into real-time systems.

Sanneck et al. [73] claimed that to accurately model packet losses, more complex models are required. They have proven this affirmation through a comparison between a two-state and k^{th} order Gilbert model. Moreover, they concluded that the order of the Gilbert model should be chosen conform with the application requirements.

Kamthe et al. [42] proposed a multilevel approach to model short and long term link behavior, it uses Hidden Markov Models (HMMs) and Mixtures of Multivariate Bernoullis (MMBs). To build the multi-state model training vectors were used. The model has several limitations: having only one transition will lead to a lack of data, a slow dynamics of PRR makes the M&M model to converge to the value of PRR. Moreover, the model is inaccurate when a link encounters too long chains of consecutive successes or losses as data traces are divided into training vectors of predefined size. On the other hand, such M&M model is recommended for long time scale testbeds because the training process requires about 12 hours. Therefore, as link behavior changes with time a M&M model may not be properly trained.

To measure the burstiness of a link, Srinivasan et al. [81] introduced the β factor. It assesses if packet losses are independent or equally distributed. To do so, the estimator uses the conditional probability delivery function (CPDF). A CPDF function determines the probability that a packet will be successfully received according to previous failures or successes. They found that packet losses are correlated, so that they claimed that second layer has to delay the acknowledgements sending with 500ms, to avoid the short term spans of the links.

Alizai et al. [2] proposed a short term link estimator (STLE) to detect the short term reliable links. STLE sets a threshold of 3 to identify the intermediate links. The threshold choice relies on the hypothesis that any link becomes unreliable after three consecutive packet receptions over the link. Sending data packets at an inter-packet time interval of 250ms, they argued that intermediate links present short term stability over periods above 750ms. Aguayo et al. [1] claimed a short term correlation period above 1s for 802.11b mesh networks. However, in our study, we observed that packet losses correlation differs with the link category.

Heinzer et al. [34] came up with a link estimator that predicts the packet reception from the relationship between chip (coded bits of information on direct sequence spread spectrum) errors in symbols (4 bits–32 chips) at IEEE 802.15.4 physical layer. The

approach is interesting as it aims to estimate PRR over a single packet from the number of consecutive erroneous chips detected in the payload. Moreover, using β factor over chips, they did not attain any relevant estimation of the link quality, instead a geometric linear model performed well. However, by our knowledge, we suspect that a bit rate of 10kbps is not standard compliant, therefore, the estimator requires further investigation at a bit rate of 250kbps. Thus, we consider that one packet is insufficient for an accurate PRR estimation, because good links may miss a single packet at a certain instant of time, which leads to underestimation of the link quality.

2.5 Link assessment in WSN

Link assessment is required for a better comprehension of the environments we cope with. More specifically, a good perception on the link behavior helps to design robust link quality estimators (LQEs). In fact, a good LQE for routing has to guarantee low energy consumption, stable topology, a high throughput, a low end-to-end delay, reliable paths when retransmissions are present, and low churn (neighbor changes).

On the other hand, it should be reactive, able to predict short and long term link fluctuations, stable in time, to accurately discriminate link quality, should rely on simple computation (light memory footprint), or to have accurate predefined thresholds to discriminate unreliable neighbors (blacklist mechanism). Please note that a too low or a too high threshold for blacklisting mechanism may contribute to routing instabilities.

To overcome the energy waste, LQEs should properly foresee the quality of the link over few samples. Since a wrong decision leads to packet loss and neighbor changes, which are costly. More exactly, when routing relies on bad links, retransmissions at the MAC layer increase, which causes energy waste.

If the metric fails choosing an unreliable neighbor, interferences through concurrent transmissions are introduced. Interference that affects the quality of neighboring links.

Therefore, the main requirements related to the literature in designing a good link estimator are :

- *reliability* successful data delivery;
- *accuracy:* link quality should be properly predicted;
- *energy consumption*: low data overhead should be guaranteed;
- *reactivity*: the necessity to quickly adapt to network changes;
- *stability*: it has to avoid short term link fluctuations so that the routing does not have to reconsider alternative links, which is energy consuming;
- *little computation*
- *memory efficient* to required low memory.

In the light of fulfilling the main requirements of a good link quality estimator, much research have addressed numerous estimation techniques such as:

- average: Packet Reception Ratio (PRR), Required Number of Packets(RNP) [16], The Link Quality Indication Based on Metric (LQIBM) [102], Expected Transmission Time (ETX) [24],
- maximum: MAX-LQI [72],
- filter: Kalman filer algorithm (KLE) [74], Window Mean with Exponential Weighted Moving Average (WMEWMA) [97], LQI-based ETX (LETX) [72], 4Bit [27],
- standard deviation: σ_m metric [53],

- probability: β factor [81],
- weighted sum: Double Cost Field Hybrid Link (Duchy) [64], Holistic Packet Statistics (HoPS) [68],
- classification: Link Quality Ranking (LQR) [106],
- regression: Weighted Regression Algorithm (WRA) [98]
- fuzzy logic : A Fuzzy Link Quality (F-LQE) [5].

Basically, independently of the used technique, each quality link estimator relies on few stages such as: *monitoring* the link over a temporal window, *recording* the needed data, *analyzing* the data.

Active monitoring is based on broadcasts sent periodically over short periods to estimate the link quality [16]. Hence, the reception of packets is not confirmed by layer 2 acknowledgements, neither retransmissions are required. A primary concern is the trade-off between the periodicity of data probes. A too low rate will affect energy consumption as an important overhead will be introduced, and in dense networks it will lead to high congestion. On the other hand, a too large periodicity window renders impossible detection of links with short-term fluctuations.

Passive monitoring is the most common monitoring scheme [97, 72, 53, 81]. It estimates the quality of links based on received information. It is energy efficient as no additional overhead is introduced. Still, for low traffic communication, the link estimation may be inaccurate due to the lack of information.

Hybrid monitoring includes a broadcast phase for active monitoring followed by a passive phase in which it considers the information from received packets such as layer two acknowledgements. In fact, using passive monitoring and a constrained active monitoring that employs only data traffic yielded a much better link quality estimation in terms of energy consumption [64, 27]. Once the monitoring mechanism is chosen, the node records the hardware parameters and the statistics about the send/receive data and acknowledgements.

Afterwards, a defined technique such as average, filter, standard deviation, classification, regression are applied to estimate the link quality. An open question 'How many readings are needed for a good link quality estimator?', remains unanswered. However, various studies claimed to attain a reliable estimation over large historical data above 50 packets [66, 83, 97].

Overall, LQEs evaluate the quality of links based on hardware metrics (RSSI, LQI, SNR) or software metrics evaluated on the basis of routing information (i.e. PRR, RNP). Hardware metrics are easy to monitor (no computation is required), even so they are highly hardware and environment dependent. Conversely, software metrics count, average, or approximate packet receptions/retransmissions, which increases the overhead.

The majority of LQEs uses an exponential moving average to smooth readings and reduce the link quality metric to a single value. Thus, a bad choice of parameter setting

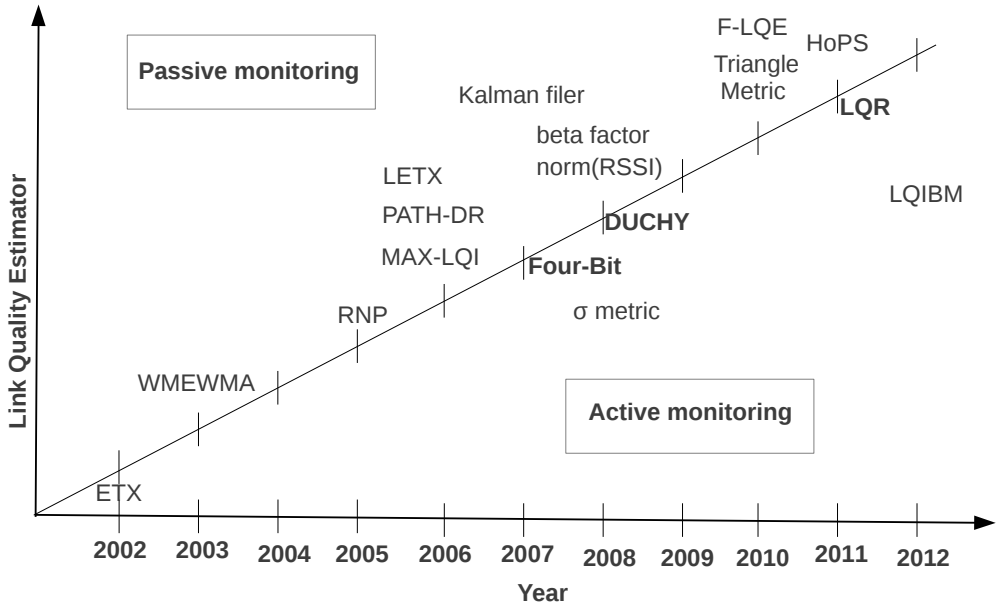

Figure 2.4: Temporal evolution of the main link estimators that use active, passive, or hybrid monitoring.

for the moving average algorithm may lead to bad decisions. Moreover, both hardware-based and software-based LQEs offer a partial link estimation, because they assess a single link propriety.

Several LQEs that employ statistical methods as regression or classification [81, 106] were proposed. Fuzzy logic opened a new perspective in combining different link proprieties in designing better estimators [5]. For instance, it outperformed PRR, WMEWMA, ETX, RNP, and Four-bit, but still, a drawback arose in terms of computation complexity, memory footprint [5]. Again, there is no LQE that offers a holistic link quality characterization.

Figure 2.4 illustrates the temporal evolution of the main link quality estimators.

Next, we proceed to offer a short overview into the main LQEs approaches. We classify the existent link quality metrics as link quality metrics (computed over link) and link quality routing metrics (computed over path).

2.5.1 Link quality metrics

Much research has considered the problem of characterizing the quality wireless links to derive metrics for finding the best routes in wireless sensor networks. Several empirical studies provided a better understanding of the complex behavior of low-power links. The transmission quality in terms of the PRR depends on the received signal strength, the level of interference, and the ability of the receiver to correctly decode transmitted information.

2.5.1.1 RSSI/LQI/PRR

Many studies revealed the importance of RSSI in the evaluation of link quality and analyzed the relation between RSSI and PRR.

One of the recent studies of Srinivasan et al. [83] showed that RSSI of CC2420 is a promising indicator when its value is above the sensitivity threshold. In particular, it allows to detect a threshold above which links present good PRR. Below the threshold, the PRR values largely vary and one RSSI value may correspond to several values of the PRR. Nevertheless, RSSI has a low variance compared to LQI, indicating that an RSSI value for one packet is a good estimator of an average RSSI value for consecutive packets. The authors also observed that LQI (Link Quality Indicator) presents a better correlation with PRR than RSSI, however, it needs to be averaged over many packets (about 120). Rondinone et al. analyzed the link quality in sensor networks and proposed to use as a link quality indicator the product of the PRR and the normalized average RSSI [71].

Similar analysis by Rondinone et al. led to the conclusion that neither RSSI nor LQI do not sufficiently discriminate the level of PRR for a successful link quality indicator [71]. They proposed to use as a link quality indicator the product of the PRR and the normalized average RSSI, which presents the advantage of distinguishing links with the same PRR, but with a different average RSSI. The drawback of this approach is that it requires the knowledge of PRR that we actually want to estimate in this thesis based on the RSSI and LQI indicators.

PRR accounts for the ratio between total send packet and the successfully received packets. It is not hardware dependent as RSSI and LQI. Cerpa et al. 2005 [16] claimed that PRR overestimates the link quality of intermediate links due to the distribution of losses. Its instability was also shown by Baccour et al. [6]. However, its granularity depends on the number of packets received over a temporal window.

In another paper, the authors modeled packet loss with a binomial distribution and concluded that good links are symmetric [97]. Meier et al. 2008 [53] analyzed measurements of an indoor sensor network with CC2420 exhibiting high link quality variability and considered metrics derived from modeling the loss process as a Bernoulli process, (i.e. ETX that depends on PRR, wide used by RPL [88] and LOAD uses the number of weak links in a path as a metric [19]).

2.5.1.2 Window Mean with EWMA (WMEWMA)-2003

Window Mean with EWMA (WMEWMA) estimator [97] is a simple and memory efficient estimator widely used in WSN. It uses an exponential weighted moving average (EWMA) filter to estimate the link quality based on the current recorded PRR and the historical PRR.

WMEWMA is responsible to filter the transient fluctuation of the PRR. It is computed at the receiver side through passive monitoring, so that additional overhead is not introduced. The algorithm calculates the average of the data reception rate following:

$$WMEWMA(\alpha, w) = \alpha * WMEWMA + (1 - \alpha) * PRR \tag{2.11}$$

where α [0..1] decides on the historical data importance, w defines the time window. The current PRR is more important than the historical PRR when $\alpha < 0.5$.

In a comparison study, WMEWMA outperformed the Time Weighted Moving Average (TWMA) , Moving Average, EWMA, Flip-Flop Packet Loss, and Success Interval with EWMA filters, being more reactive and more stable [96].

2.5.1.3 Required number of packets retransmissions (RNP)-2005

RNP [16] estimates short-time link fluctuation using passive monitoring. More specifically, it periodically broadcasts control packets for a short time, then it averages the number of sent packets (transmitted/re-transmitted) before a successful reception as follows:

$$RNP(w) = \frac{Total\ transmitted/re-transmitted\ packets}{Total\ acknowledged\ packets} - 1 \tag{2.12}$$

In the context of neighbors with the same packet reception rates, RNP favors links with less retransmissions which offers an advantage over PRR metric. As drawbacks we can mention instability and the energy waste due to additional messaging overhead. Moreover, Baccur et al. reported RNP as unreliable for link estimation because of the asymmetry presence [3].

2.5.1.4 Kalman filter (KLE)-2007

Kalman filter [74] estimates the link quality using passive monitoring. It predicts PRR using the signal-to-noise ratio (SNR) of the link and a pre-calibrated SNR-PSR curve. The SNR curve is decided offline by plotting the collected average SNR against PRR. Each receiver has to record the SNR using the Kalman Filter algorithm in order to minimize the error estimation. It claimed a fastest adaptation to the channel changes compared to RNP, PRR, or ETX.

2.5.1.5 The norm(RSSI)-2008

A normalized LQE metric is proposed by combining PRR and RSSI [71]. The metric is defined as follows:

$$LQIndicator = PRR * norm(meanRSSI) \tag{2.13}$$

$$norm(meanRSSI) = \frac{meanRSSI}{60} + \frac{100}{60} \tag{2.14}$$

They reported that the metric provides stable and accurate links estimation on the Moteiv's TelosB nodes equipped with the CC2420 radio transceiver. They concluded that sliding windows of 10 packets are appropriate to estimate the link quality. Moreover, PRR and RSSI are logged in neighbor discovery phase.

2.5.1.6 The beta factor-2008

β factor [81] measures the link burstiness using conditional probability delivery functions (CPDFs). CPDF was derived from packet delivery traces and determines the probability that a packet will be received after certain consecutive successes or failures. Therefore, a CPDF will call a link ideal bursty if it has a strong packet successes or failures correlation. This means that an ideal bursty link has long bursts of consecutive failures or successes. On the other hand, it calls a link independent, when no correlation of packet successes or failures was detected.

Yet, a β factor close to zero denotes a low correlation of packet successes or failures. It is computed as follows:

$$\beta = \frac{KW(I) - KW(E)}{KW(I)} \tag{2.15}$$

where KW() is the Kantorovich-Wasserstein distance (i.e. the KW distance between two vectors denotes the absolute difference of their corresponding elements), KW(E) represents the CPDF of the empirical data recorded over a link, whereas KW(I) is the CPDF of the ideal bursty link. In other words, KW will indicate how close the CPDF of an empirical is from the CPDF of the ideal bursty link.

β metric was tested on the Mirage testbed and it is integrated in the CTP routing protocol for which it improves its efficiency up to 15% when it copes with bursts [81].

2.5.1.7 (σ_m metric)-2008

σ_m metric [53] detects the degree of the link stability by comparing the standard deviation of the link with the deviation of a (stochastic) Bernoulli Process (σ_m^{rand}). It relies on active monitoring as nodes need to broadcast packets.

They claimed that good links have a reception sequence similar to a Bernoulli process. To prove their observation, they considered the sequence: 1 for a good packet reception and 0 for a lost packet. They found that a perfectly stable link is a Bernoulli process with independent random variables, where each has the probability P_r. Furthermore, to map the temporal PRR given an observation window of m packets to a stochastic Bernoulli process, they found a stochastic standard deviation:

$$\sigma_m^{rand}(P_r) = \sqrt{(\frac{1}{m}P_r(1 - P_r))} \tag{2.16}$$

where m is the number of aggregated packets (window size), and P_r the probability of each independent packet.

On the other hand, the standard deviation of the temporal PRR given an observation window of m packets (PRR_w) is:

$$\sigma_m^{PRR_w} = \sqrt{(std(PRR_w))}. \tag{2.17}$$

Last, a link stability factor γ_m gives the degree of link stability and is computed as follows:

$$\gamma_m = \frac{\sigma_m^{PRR_w}}{\sigma_m^{rand}(P_r)}. \tag{2.18}$$

They concluded that the estimator distinguishes among stable and unstable links whereas using limited resources.

2.5.1.8 F-LQE: A Fuzzy Link Quality-2010

F-LQE [5] considers four link properties such as packet delivery (PRR), stability of the link (SF), coefficient-of-variation over last 30 packets, asymmetry (ASL-PRR), absolute PRR difference within the uplink and the downlink link between two nodes, and the channel quality (SNR).

More specifically, F-LQE defines a good link as having good packet delivery ratio, low asymmetry, high stability, and high channel quality (high SNR). In addition, the EWMA filter is used to provide the smoothness of the F-LQE values:

$$F - LQE(\alpha, w) = \alpha * F\_LQE + (1 - \alpha) * LQ(w) \tag{2.19}$$

where, $\alpha = 0.9$, w-estimation window, $LQ(w) = 100 * \mu(i)$, $\mu(i)$ is defined as:

$$\mu(i) = \beta * min(PRR_{(i)}, ASL_{(i)}, SF_{(i)}, SNR_{(i)}) + (1-\beta) * mean(PRR_{(i)}, ASL_{(i)}, SF_{(i)}, SNR_{(i)}) \tag{2.20}$$

where $0 < \beta < 1$ gives the smoothness of the fuzzy value, $PRR_{(i)}$ is the average PRR of a link i, $ASL_{(i)}$ measures the asymmetry of link i, $SF_{(i)}$ is the deviation of PRR over last 30 packets for link i, $SNR_{(i)}$ is the average SNR of the link i.

$PRR_{(i)}$, $ASL_{(i)}$, $SF_{(i)}$, $SNR_{(i)}$ are normalized [0..1]. Hence, high values of $F-LQE$ denote good link quality.

F-LQE outperformed PRR, WMEWMA, ETX, RNP, and 4B regarding the stability, reliability, and asymmetry. However, F-LQE considers four link properties which lead to complex computation and large memory footprint. Additionally, an observation window of 30 may be too large because estimators should target estimation of link quality over few packets.

2.5.1.9 Triangle Metric-2010

The Triangle metric [13] combines PRR, LQI, and SNR to guarantee fast and reliable link quality estimation. It relies on active monitoring as each node broadcasts periodically 10 packets per second. It considers an observation window (w) of size m over which it counts the number of received packets, then, calculates mean LQI, and mean SNR:

$$\overline{LQI}_w = \frac{\sum_{k=1}^{n} lqi_i}{n} \tag{2.21}$$

$$\overline{SNR}_w = \frac{\sum_{k=1}^{n} snr_i}{n} \tag{2.22}$$

where n is the number of successfully received packets ($0<n \leq m$), lqi_i and snr_i denote the lqi and the snr of the received packet i.

Next, Triangle metric computes the distance between the node location characterized by a point($\overline{SNR}$, $\overline{LQI}$) and the origin (0,0).

$$distance = \sqrt{\overline{SNR}_w^2 + \overline{LQI}_w^2} \tag{2.23}$$

Hence, based on the computed distance, the link quality between sender and receiver is estimated. A large distance indicates a better link quality. However, an empirical threshold is used to discriminate between link categories. Thus, broadcasting 10 packets each second introduces overhead which enhance the energy depletion.

2.5.1.10 Holistic Packet Statistics (HoPS)-2011

HoPS [68] is measured at the receiver side and uses four link-quality descriptors (LQI, SNR, PRR, ETX), that are periodically updated. A first-order EWMA filter captures the short-term fluctuations of packet successful ratio (h_τ^{ST}). It aims to retrieve the deviation of PRR in the recent past:

$$h_\tau^{ST} = \alpha * h_{\tau-1}^{ST} + (1-\alpha) * q_\tau \tag{2.24}$$

where $0 < \alpha < 1$ gives the smoothness of the short term fluctuation, q_τ is a binary value that denotes whether an expected packet at time τ was received.

A second-order EWMA filter measures long-term fluctuations (h_τ^{LT}):

$$h_\tau^{LT} = \beta * h_{\tau-1}^{LT} + (1-\beta) * h_\tau^{ST} \tag{2.25}$$

where $0 < \beta < 1$ gives the smoothness of the long term fluctuation,

To track short and long term fluctuations, a third filter EWMA filter is applied:

$$\delta_\tau^+ = \gamma * \delta_{\tau-1}^+ + (1-\gamma) * \phi(h_\tau^{ST}, h_\tau^{LT}) \tag{2.26}$$

$$\delta_\tau^- = \gamma * \delta_{\tau-1}^+ + (1-\gamma) * \phi(h_\tau^{LT}, h_\tau^{ST}) \tag{2.27}$$

where τ is time, $0 < \gamma < 1$, h_τ^{ST} - short term fluctuation. h_τ^{LT} - long term fluctuation, and

$$\phi(x,y) = \begin{cases} x-y, & x > y \\ 0 \; else \end{cases}$$

Next, the absolute deviation estimation gives link stability as follows:

$$h_\tau^\sigma = \delta_\tau^+ + \delta_\tau^-. \tag{2.28}$$

An expected deviation estimation so called trend estimation is computed as follows:

$$h_\tau^\theta = \delta_\tau^+ - \delta_\tau^-. \tag{2.29}$$

Finally, HoPS is estimated due to the absolute and the expected deviation estimation:

$$HoPS_\tau = h_\tau^{LT} + \frac{|h_\tau^\theta|}{h_\tau^\sigma}(h_\tau^{ST} - h_\tau^{LT}). \tag{2.30}$$

HoPS argued to outperform RPN, F-LQE, LEEP, ALE in terms of stability and efficiency. Moreover, they claimed a lower memory footprint than F-LQE. Hops is an interesting approach as it uses three EWMA filters to track short and long temporal fluctuations. However, the complexity of computation and the need to store the output of three EWMA filters renders it heavy for usage.

2.5.1.11 Link Quality Ranking (LQR)-2011

LQR [106] metric is designed to identify best links when only unreliable links are present. It is a sender initiated metric: a sender periodically sends a predefined number of probes. Next, as soon as a receiver is reached by a probe, it triggers a timer and sends back to sender its physical metric indicators. Once a sender receives back the hardware information from its neighbors, it proceeds by selecting the best quality link to forward data.

The best link is chosen as a result of the comparison of the triplet (PRR, SNR, LQI) for each single link. For example, assuming that x_i, y_i, and z_i indicate the prr, snr, and lqi of link i, then, the comparison of these metrics for two independent links, i and j is given by as follows:

$$e =< sgn(x_i - x_j), sgn(y_i - y_j), sgn(z_i - z_j) > \tag{2.31}$$

where e represents the comparison of the PRR, SNR, LQI metrics for link i, and $sgn(x)$ is the sign function ($sgn(x) = \{1, 0, -1\}$ *depending if* $x = \{> 0, 0, < 0\}$).

LQR is meant for sparse deployments where data are required to be fast transfered to neighbors. Even if it argued to identify best available links, the application to multihop scenarios is limited by the large number of packets that have to be broadcast, i.e. 100.

2.5.2 Link quality routing metrics

2.5.2.1 ETX - Expected Transmission Count-2003

Expected Transmission Count (ETX) [24] is one of the well-known routing metrics used in WSN. ETX is due to find high throughput path on multihop networks. It offers an estimation of the link quality, channel noise, and asymmetry.

ETX is defined as the estimated average of the number of data and acknowledgements (ACK) frame transmissions necessary to successfully transmit a packet. ETX is an additive metric. The computation of ETX requires that nodes periodically broadcast small probes to compute forward (data frame (d_f)) and reverse (acknowledgement frame (d_r)) probability. Furthermore, ETX is computed as the product of data frame delivery probability and acknowledgement frame delivery probability:

$$ETX = \frac{1}{(d_f * d_r)}. \tag{2.32}$$

It assumes that the reception of data frames is same as the acknowledgement ones, independently on the packet size.

Equally important is the calculation of the path ETX as a sum of the ETX for each individual link of the path:

$$ETX(path) = \sum_{link \in path} ETX_{link} \tag{2.33}$$

To prove the performances of ETX, it was integrated to two routing schemes such as Destination-Sequenced Distance-Vector Routing (DSDV) and Dynamic Source Routing (DSR). The metric outperformed the hop count metric as it has knowledge about delivery ratio over the path and the total number of retransmissions.

Today, ETX metric filtered by WMEWMA is highly used in routing (i.e. CTP, RPL).

2.5.2.2 LQI-based ETX (LETX)-2006

LETX [72] metric is a LQI based metric, it relies on a PRR estimation based on LQI. LETX estimates the link cost as the overall transmission tries to achieve successful delivery during neighbor discovery:

$$LETX(link) = \frac{1}{\Phi(link)} \tag{2.34}$$

where $\Phi(link)$ is a function that estimates PRR from the LQI values of the link. The function is a polynomial order one function that estimates PRR from average LQI. Being the inverse of the estimated PRR, LETX aims same as ETX, a minimum number of retransmissions over a link. A path is the route along which packets travel from source to destination. The path cost is computed as the sum of the link costs of the path. Moreover, LETX is an additive metric that does not introduce overhead as it is computed online during the route discovery process.

2.5.2.3 PATH-DR-2006

PATH-DR [72] was designed to predict the link quality from the LQI value of a single packet reception. It relies on the neighbor discovery during which it reads the LQI values. The goal is to choose the path with the best packer delivery ratio (PDR):

$$p^* = arg\ max_{p \in P} \prod_{link \in L_p} ESTLDR(link) \tag{2.35}$$

where arg comes from the set of points the function attains the maximum value, ESTLDR(link) is the estimated hop by hop packet delivery ratio of the LQI values of the messages received during the discovery of neighboring motes. To estimate the PRR, they mapped the average LQI with a linear model.

2.5.2.4 MAX-LQI-2006

Each receiver selects the path with the highest minimum LQI value, to avoid weak links.

$$p^* = arg\ max\ min_{p \in P, link \in L_p} LQI(link) \tag{2.36}$$

where p is the path, P is the set of available paths, L_p is the set of path links. The MAX-LQI metric [72] is computed at the receiver side.

2.5.2.5 Four-Bit (4Bit)-2007

4Bit [27] metric aggregates the information provided by physical, link, and network layers. Is composed of four information bits. The first bit, so called 'white bit' denotes that the quality of the medium is high. The second bit (ack bit) is given by the link layer, and as soon a packet is acknowledged, the bit is set. The third bit (pin bit) is set by the network layer. If on, it designates that the link is part of the routing table entries. Last, the fourth bit (compared bit) tells if a link entry is better that the other one existing in the routing table.

Thus, it is initiated by the sender and makes use of the active and passive monitoring to compute the ETX needed to set the ack bit.

The ETX is computed after previously broadcast packets are sent for a short time, so that ETX from a receiver to sender:

$$ETX\_receiver\_sender(w, \alpha) = \frac{1}{WMEWMA(w, \alpha)} - 1 \tag{2.37}$$

where, $0 < \alpha < 1$, w is the observation window.

Furthermore, the sender estimates the ETX as following:

$$ETX\_sender\_receiver(w, \alpha) = \alpha * ETX\_sender\_receiver + (1 - \alpha) * RNP \tag{2.38}$$

Once the ETX is computed from receiver to sender and from sender to receiver, the four-fit expression becomes:

$$4B(w, \alpha) = \alpha * 4B + (1 - \alpha) * ETX\_sender\_receiver(ETX\_receiver\_sender) \tag{2.39}$$

4B provides a third layer neighbor's choice based on information coming from the first layer (LQI) and the second layer (ETX). Finally, it was concluded that 4B outperforms the LQI metric alone. Specifically, it obtained a better link delivery radio than ETX and RNP metrics.

2.5.2.6 DUCHY: Double Cost Field Hybrid Link-2008

The Duchy metric [64] is a routing metric that aims to choose shortest hops and good link quality. To do so, it uses RSSI information to discriminate good links, uses

LQI information to discriminate bad links, and a feedback scheme that relies on link-level ACKs. It embeds two estimators, one for channel instability (Channel State Information-CSI) and second for the path expected transmission count (ETX).

For instance, CSI relies on active monitoring thorough beacons. CSI considers both RSSI and LQI information measured from each received beacon, information that is normalized and then smoothed using a WMEWMA filter. The second used scheme is RNP that counts the number of layer-2 ACKs.

Duchy constructs an outer cost filed for depth control (RNP) and an inner field for parent selection (CSI). The two cost field information is embedded into each disseminated beacon. The outer field will keep track of the ETX cost, whereas the inner field contains the LQI and RSSI cost.

DUCHY was integrated with Arbutus routing protocol, and claimed to achieve shortest paths with good link qualities compared to the MultiHopLQI metric.

2.5.2.7 Link quality indication based on metric (LQIBM)-2012

LQIBM metric [102] combines mean and deviation LQI to accurately discriminate poor links.

Initially, probes have to be broadcast to estimate the mean and the variance coefficient of LQI. The metric tracks the mean and the deviation of LQI along the entire routing path as follows:

$$P = \alpha * P_{cm} - (1 - \alpha) * \frac{\sigma}{\mu} \tag{2.40}$$

where $0 < \alpha < 1$ gives the smoothness of the historical data, P denotes the selection probability of routing, μ indicates the mean LQI, σ indicates the standard deviation of LQI , and P_{cm} is a quantitative value that indicates the proximity degree of LQI mean with LQI maximum.

P_{cm} is given by:

$$P_{cm} = e^{-(\frac{100-\mu}{110-50})^2} \tag{2.41}$$

The metric is supposed to overcome the bottleneck links, congestion and retransmissions. Nevertheless, the LQI variance is unpredictable for intermediate links, so that it may occur that links with low mean LQI have low deviation, moreover, the asymmetry of links is not considered. Also, is not specified the type of the found fitting function or the observation window the mean and deviation LQI are computed.

2.5.3 Discussion

LQEs were designed as a result of extensive analyses carried on various platforms. Thus, the most common are Mirage [18] (Mica2 and Mica2Dot), MoteLab [93] (Mica2 or Telos), TWIST testbed [32, 106] (Tmote Sky), SCALE[15] (Mica 1&2). Except the existing testbeds, other studies were performed on local deployments such as offices, halls, buildings, parks. For example, the Berkeley mote platform was used to assess the

EWMA filter performance [97]. Recently, frameworks such as SWAT [82] or RadiaLE (TelosB motes) [6] were designed to ease the link estimator evaluation.

Empirical studies performed on the above platforms addressed mostly linear topologies [103, 67, 94] (868 MHz), grid [96] (868 MHz), [72] (2.4GHz), or random [79] (2.4GHz). In fact, empirical studies assessed the impact of link estimators by integrating routing protocols such as CTP [45, 103, 8, 27] for MultiHopLQI, 4Bit, β factor [81], DSDV and DSR for ETX [24], Not-so-Tiny Ad-hoc On-demand Distance Vector (NST-AODV) for LETX [72], AODV for LQIBM [102], Arbutus [62] for Duchy [64].

Moreover, ETX link estimator is one of the pioneer link estimators. Once it was proposed, it outperformed the classic hop count metric [24].

Each of the link assessment approaches we have discussed were confronted with existing approaches. We highlight the main observations of each performed comparison.

- RNP [96] gives a higher PRR as it keeps track of retransmissions [6] while PRR overestimates the link quality for intermediate links.
- LETX [72] outperformed hop count and PATH-DR in terms of packet delivery ratio.
- PATH-DR and MAX-LQI [72] outperformed hop count in robustness and overhead.
- F-LQE [5] metric is more stable compared with ETX, RNP, 4Bit, PRR. It as able to discriminate very good links ($PRR > 99\%$) and good links ($90 < PRR < 99\%$).
  - F-LQE considers three link proprieties such as PRR, stability (avoiding the short term fluctuation) and asymmetry.
  - ETX, RNP, 4B do not consider link stability property.
  - PRR and SPRR are less sensitive to short term fluctuation, therefore, both are more stable than RNP and 4B.
  - ETX is unstable for bad links, it tends to infinity whereas PRR reaches 0.
- Duchy [64] outperformed MultiHopLQI metric by achieving shortest paths with good links quality.
- HoPS [68] metric offered better stability and efficiency than RPN, F-LQE, LEEP, ALE metrics, because it considers short and long term fluctuations.
- 4Bit [27] attains better PRR than ETX, RNP, LQI metrics.

Several metrics were designed to achieve a specific target, for example $\beta factor$ (bursty traffic), LQR (choice of links among unreliable links at a certain instant). Table 2.4 presents the described LQEs.

Several studies use real testbeds to provide evaluation of the proposed link quality estimators in order to find out the best one. We present the conclusions of the most recent studies.

- WMEWMA outperforms filter-based LQEs [96] as it selects shortest paths, still, data collection is not reliable as retransmissions are omitted.

- Liu et al. 2009 [51] compared RNP, ETX, and 4Bit metrics in terms of path quality, delivery rate, cost per packet, routing overhead, and neighbor blacklisting (accurate predefined thresholds to discriminate unreliable neighbors). They concluded that RPN choses shorter paths compared with ETX and 4B and obtains a smaller overhead. Moreover, ETX outperforms RPN being more reactive when links encounter short-term drops. Besides, ETX introduces a high overhead compared to RNP and 4B. On the other hand, in dense networks, none of the three metrics guarantee a good path quality. Overall, ETX achieved the best delivery rate.

- Baccour et al. [3] claimed that ETX outperforms PRR, RNP, 4B, WMEWMA estimators with respect to energy efficiency, the number of retransmissions and the path length. They observed that estimators perform better when they consider the link layer retransmissions.

- Using the RadiaLE framework [6], the authors studied the performance of the following estimators: PRR, ETX, RNP, WMEWMA, and 4Bit. They found that four-bit and RNP underestimate the link quality whereas PRR, WMEWMA, and ETX overestimate the link quality [5]. The underestimation is due to the maximum number of retransmissions, for instance, RNP has to perform a maximum of 4 retransmissions before to drop a packet. A link is classified as bad link since the retransmission threshold of 4 is reached. For example, RadiaLE recorded that when RNP is used 90% of links performed packet transmissions after and average of 4 retransmissions. 4B underestimates less the link quality. Moreover, the underestimation is cause by the fact that the estimators do not know if the packet was transmitted or not after 4 retransmissions as layer 2 ACKs are not used. On the contrary, when retransmissions are avoided and decisions are taken from the successfully received packets, links may be overestimated since a received packet denotes a good link, even if the packet was received after numerous retransmissions. Furthermore, the authors claimed that WMEWMA and PRR are more stable than RNP and 4B, because of EWMA filter that soothes the short-term fluctuations.

We can see in Table 2.4 that among single and composite metrics, the composite metrics such as F-LQE, HoPs, LQIBM achieved a good reactivity, they are less sensitive to short term fluctuation of the links, considered the bi-directionality of links, and are reliable. However, HoPs remains the most interesting approach as it uses three EWMA filters to track short and long temporal fluctuations. Moreover, a drawback of HoPs is its heaviness for usage due to the complexity of the computation and the need to store the output of three EWMA filters.

LQE	Reactivity	Stability	Bi-directionality	Reliability	Fluctuation
PRR	yes	yes	no	no	short-term
WMEWMA	yes	yes	no	no	long-term or short-term
RPN	yes	no	yes	no	short-term
LETX	yes	no	yes	no	short-term
Path-DR	yes	no	no	no	short-term
MAX-LQI	yes	no	no	no	short-term
norm(RSSI)	yes	yes	no	no	short-term
β factor	yes	-	-	no	short-term
F-LQE	yes	*yes*	yes	yes	long-term
HoPS	yes	*yes*	yes	yes	long-term and short-term
ETX	yes	no	yes	yes	short-term
Triangle	yes	yes	no	no	short-term
LQIBM	yes	yes	yes	yes	short-term
Duchy	yes	no	no	yes	short-term
4B	yes	no	yes	yes	short-term
LQR	yes	no	no	yes	short-term

Table 2.4: Link quality estimators classification in terms of their attained reactivity (adapt to network changes) , stability (capacity to ignore small fluctuations of links), bi-directionality (asymmetry of links), reliability (successful data delivery).

2.6 Routing in IPv6-based 6LoWPANs

We focus our attention on the most common approach that enabled the Internet of Things. We highlight how to push IPv6 in sensor networks. We review on aspects of the distance-vector based routing protocols such as CTP, LOAD [19], and RPL [88].

2.6.1 Introduction

Ten years ago, putting a TCP/IP stack in a sensor was hardly possible. Nowadays, several operating systems including optimized IP stacks run on different resource and energy-constrained platforms already tested in real deployments. The standardization efforts are still on their way, but major problems were overcome progressively during the past decade.

Simultaneously, existing IP routing protocols raises several issues in the context of wireless multi-hop low power and lossy networks (LLN). Several routing protocols were proposed: CTP, LOAD, RPL.

Routing is an important feature of the WSN communication that presents various challenges with respect to other wireless networks like mobile ad hoc networks (MANET) or cellular networks. In this context, routing protocols have to ensure the next hop packet forward as well as the path calculation. Most of WSN application scenarios are multi-hop as WSN networks are deployed over large spaces and short radio range coverage. Packets should visit several intermediate nodes to reach a sink destination.

The destination plays the role of a collector that gathers data for further analysis

and evaluation. The collector may disseminate information back to nodes so, it also needs to communicate with rest of the nodes.

2.6.2 The Collection Tree Protocol (CTP)

Back in 2005, one of pioneering routing protocols for LLN was the Collection Tree Protocol (CTP) [69]. CTP is a hierarchical distance vector protocol based on multi-hop communication. It was designed to collect information from sensor nodes and delivered it to a central station (root). CTP constructs anycast route paths from each node to the collection point (root) defined in the network (cf. Figure 2.5).

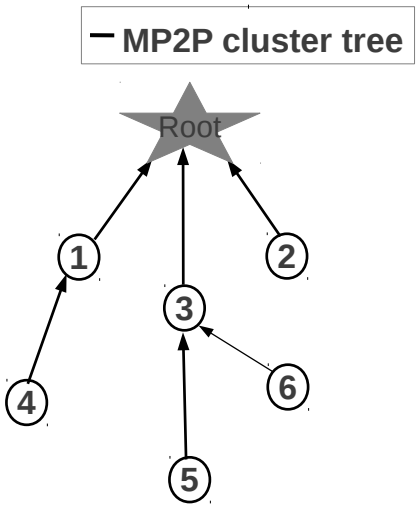

Figure 2.5: Cluster tree topology.

CTP aims at reactivity (quickly react to changes), efficiency (low energy consumption), and reliability (successful data delivery). It accounts for three mechanisms: link quality estimation, data-path validation, and adaptive beaconing. First, to cope with the lossy links while providing reactivity, it uses the 4Bit [27] link quality estimator (cf. Section 2.5.2.5).

Second, data path validation is meant to detect network inconsistencies such as short and long term link breaks, loops, leading to energy waste. Short data packets that embed link layer information (root distance) are generated (active monitoring). When a node needs to forward a packet coming from a lower or equal root distance, it may initiate a local repair by correcting the topology and then forward the packet.

The last mechanism, active beaconing relies on the trickle mechanism [47]. Routing control packets generation change dynamically from small time intervals around few milliseconds to large time intervals around dozen of minutes. A small interval gives better reactivity at the price of additional overhead and energy. On the other hand, a larger interval decreases energy waste and the overhead but may be slower to network changes.

CTP was used for clinical monitoring [17, 44], environmental monitoring (i.e. tropical forest), Greenorbs with more than 1000 motes [31], or protocol validation as β

factor [81]. Various implementations are available on nesC for TinyOS [49], Java for Sun SPOTs motes, C for ContikiOS [26], or C++ for Castilia simulator [56].

2.6.3 6LoWPAN Ad-Hoc On-demand Distance Vector (LOAD)

LOAD [19] protocol was proposed as an adaptation of AODV [57] to sensor networks. Its features are to establish and maintain multihop routing paths. It operates on top of the adaptation layer. LOAD uses several mechanisms: route discovery using broadcast, local structure maintenance (routing and route-request tables), local and global repair, and loop avoidance. It relies on point to point (P2P) traffic pattern.

LOAD routes are constructed on demand, so that when a packet has to be sent to a destination, the node checks for the destination in its routing table. In case the entry misses, it initiates route discovery by broadcasting a Route Request (RREQ) message. Each intermediate forwarder of the RREQ will add the originator address in the routing table. In this way, a reverse route from the destination to the source of the RREQ message is created. Once RREQ reaches the destination, to confirm the reception, a route-reply (RREP) message is sent to the originator using the reverse-route already created. Since the reverse route is installed, the bi-directional route is ready for use.

To keep track of connectivity, LOAD uses data link layer information. When a router detects a link breakdown, it may initiate a local repair (using route discovery mechanism in LOAD) by broadcasting a Route Request (RREQ). The bi-directional route is re-installed with the reception of the unicast reply-request (RREP), however, any packet reception for the destination the link is down, will be buffered for a further forward to the destination.

Whenever a node fails to repair a break link, it sends back to originator a unicast route-error (RERR) message that needs to drop buffered packets. Moreover, during local repair only the originator of a RRQE message is notified about the reachability of a destination, , whereas AODV will notify all the neighbors that have the respective destination as the next hop.

Unlike AODV, LOAD does not allow intermediate routers to reply to a route-request. Forbidding the intermediate nodes to respond respond with a RREP to a RREQ, LOAD assures loop freedom.

The route cost in LOAD is computed as the accumulated link cost and the hop count from the source to destination. To measure the link cost, it utilizes the Link Quality Indicator (LQI) hardware (cf. Section 2.5.1). LOAD will prefer in its routing decisions a route that contains a smaller number of weak links (links with LQI below a certain threshold value) and less hops from source to destination.

2.6.4 Routing in LLNs (RPL)

RPL [88] is a distance vector protocol for LLNs. It was designed by the Internet Engineering Task Force(IETF) working group, ROLL [88]. In March 2012, it became a standard (RFC 6550).

The principle of RPL relies on a Destination Oriented Directed Acyclic Graph (DODAG) generated based on few RPL signaling messages: DODAG Information Object (DIO), Destination Advertisement Object (DAO), and DODAG Information Solicitation (DIS).

Routing starts with the root (sink) that periodically generates DIO link-local multicast messages using the trickle algorithm [47].

The DODAG topology allows a node to have more than one parent at a time, Figure 2.6 shows the DODAG topology. Nodes in RPL can play the role of a edge router, router, or a leaf.

- An edge router (LBR) is in charge of the DODAG generation. It is a powered node with high storage capacity, able to store information from inside the DODAG. In addition, it ensures the communication with other DODAGs or the Internet.
- A router is responsible of forwarding messages to the next hop towards the destination and to disseminate DIO or DAO messages when needed.
- A leaf is an end-device that can only send data traffic.

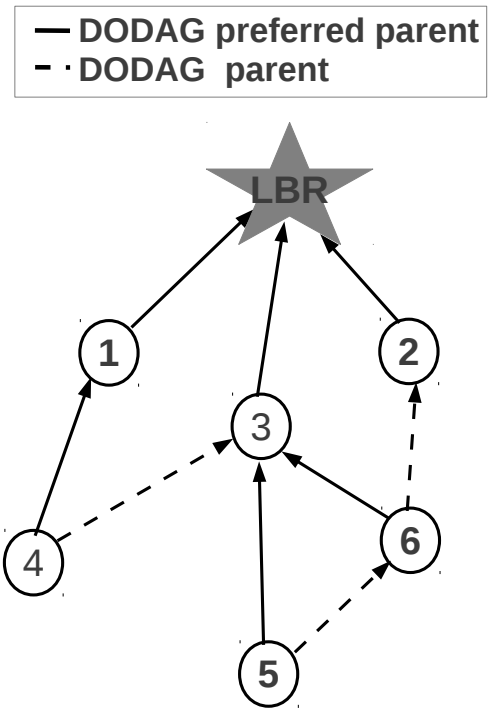

Figure 2.6: RPL DODAG.

Each DIO disseminates:

- *RPLInstanceID* gives the topology instance number associated with the current DODAG. Each RPL instance may hold several DODAGs initiated by different edge routers having identical objective function.

- *Rank*, is the node relative position with respect to the DODAG root. It increases monotonically following the requirements of the objective function (OF).
- *DODAGID* is the identifier of the DODAG, typically it is an IPv6 address given by the DODOAG root. Note that the root can initiate disjoint DODAGs with different objective functions.
- *DODAG VersionNumber* is a counter that gets incremented by the root each time the topology triggers changes. It is a way to track network updates.

The Objective Function plays different roles in RPL: estimates the rank value from a chosen routing metric (hop count, ETX, energy, etc.), decide optimal routing paths, and define constraints on path selection. Recently, two OFs were defined, hop count (OF0[91]) and ETX (OF1[30]). A node favors a path with a minimal number of hops towards the root (OF0), or a minimal ETX value (OF1). However, manifold metrics associate with nodes or links can be applied [91]. Node metrics may represent node characteristics such as:

- *Node state* indicating if the node can or not aggregate traffic flows.
- *Node energy* points out the available energy on the node. When the metric is used, a node should prefer the path (towards the root) that alleviates the energy cost.
- *Hop count* announces the number of visited nodes to reach the root.

On the other hand, link metrics represent the link quality towards neighbors. Each application scenario may require information such as:

- *Latency* – the time delay required for a specific data communication.
- *Throughput* – data rate per unit time may be used to discriminate nodes with low data rates.
- *Reliability* – reflects the link quality estimation. The proper algorithm for link estimation remains an open issue. Besides, we have discussed in Section 2.5.1 existing propositions. One link estimator is ETX (OF1), that estimates the number of retransmissions over a link (see Section 2.5.2.1).
- *Color* of the links denotes patterns of bit values predefined by the user. For example, encrypted links can be discriminated trough a flag value.

RPL supports three types of traffic patterns shown in Figure 2.7:

- Multi Point to Point (MP2P) or converge-cast for data collection: from nodes to LBR (upward routing).
- Point to Multi point (P2MP) for data dissemination: from LBR to a node or a group of nodes (downward routing). P2MP it is extensive use in building and industrial automation [88].

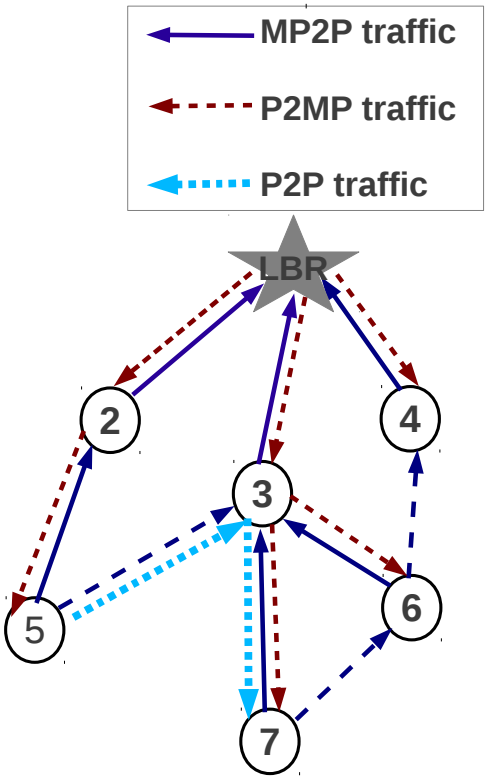

Figure 2.7: DODAG traffic patterns.

- Point to Point (P2P) for communication between any node inside the DODAG.

Topology generation process

Upward routes facilitate the MP2P communication. The root disseminates DIO messages on the link local multi-cast address to initiate the DODAG construction (upward routes). The LBR (sink) has the rank set to 1. At each received DIO, a node decides to join or not the DODAG topology according to the predefined Objective Function. Once it joins the DODAG, it creates an entry in the candidate neighbor list. Then, it computes its own rank as a sum between the rank in the DIO message and the link metric value (e.g. ETX [24]). A neighbor that proposes a lower rank towards the root is selected in the node's parent set as preferred parent. A default route is installed and inward traffic is forwarded to the preferred parent. The preferred parent should be updated whenever a lower rank is proposed or a new entry is recorded. Once a node has decided the upward default route, it should send DIO messages to announce its rank value. A node can ask for a DIO message through the generation of a DIS message.

To restrict extensive preferred parent changes due to instable links, low-pass filter, thresholds, or hysteresis algorithms are recommended.

To ensure upward routes maintenance, nodes periodically transmit DIOs at a frequency given by the trickle algorithm [47]. The mechanism is simple and is intended to detect network instabilities. Each node keeps track of a DIO transmission interval limited by a a minimum interval (I_{min} [ms]) and a maximum interval (I_{max} [minutes]).

The trickle algorithm sets the DIO interval to I_{min} when the network is unstable (lost of preferred parent, loops, updates), and it increases exponentially otherwise.

2.Downward routes installation enables the P2MP and the P2P communication. RPL may employ two types of operation modes to maintain downward routes. First, storing mode when each child has to send to the elected parent or to a multi-cast subgroup a DAO message to announce its prefix. The parent has to store each prefix received in DAO message, and further communicate the reachability to its own parent. An issue of this approach is the storing capacity of parents that have to hold all the routes to the leaves.

Second, in non-storing mode, once an intermediate parent receives an unicast DAO from its child, it cannot store the child prefix. Thus, it needs to forward the DAO packet to its legitimate parent after it appends its address to the DAO packet. Clausen et al. [21] reported that source-routes may result in fragmentation that may lead to packet losses as a packet is dropped if a single fragment is lost.

For downward routes, the periodicity of DAO emission remains open so that each implementation can decide when to send DAO messages, or successively send several DAO messages to ensure the reachability of the parent [20].

RPL properties

RPL provides mechanisms to avoid or detect loops, based on rank decision and path validation. Once a node losses all the parent set candidates, it may be tempted to attach to its own sub-DODAG in case it misses DIOs. To avoid this situations, RPL defines several rules: a node may not pick as parent the node having a higher rank than a maximal depth, a node may poison its sub-DODAG. A maximal depth is defined as a minimal accepted rank and a DAGMAXRankIncrease is specified by the user. The poison process assumes that a node out of the parent candidates table due to a lost connection or no more availability has to advertise an infinite rank to its children. Moreover, to prevent loops, nodes check that the forwarding direction is same as the traveling direction (upward/downward).

A lot of work concerns RPL, because of the interest it rises for large topologies such as building automation [25], home automation[14], and smart grids[58]. However, Levis et al. [48] due to detailed analysis of the existent routing protocol features concluded that none of them fulfill wholly the Low Power and Lossy Networks(LNN) requirements. Hence, efforts were directed to design a new protocol in charge to overcome the mentioned issues.

2.6.5 Conclusions

WSN protocols such as media access, routing, localization are highly depended on the efficiency and stability of LQEs. Therefore, much effort resulted in LQE proposals as a combination of hardware or software metrics. Hardware metrics (RSSI/LQI/SNR) are simple and easy to read from the radio device. For example, SNR and RSSI can differentiate between very good links that exhibit a PRR>99% and the other ones with a PRR below 99%. However, in the first section of this chapter, we have seen that they are highly dependent on the hardware and environmental factors. Hence, link

estimators only based on hardware metrics are not sufficient to discriminate the quality of links.

On the other hand, software link estimators may consider the number, the average, or approximate packet receptions/retransmissions using techniques such as filters, standard deviation, weighted sum, classification, regression, or fuzzy logic. Anyway, most of the estimators use the exponential moving average (EWMA) filter to smooth metrics.

Up to now, the most promising approaches are the composite metrics, because they aggregate several link properties e.g. 4Bit [27], F-LQE [5], Triangle [13], HoPS [68], LQR [106], LQIBM [102]. Clearly, composite metrics outperform simple metrics such as RSSI, LQI, SNR, PRR not able to track at once all proprieties of links (delivery, stability, asymmetry, reactivity).

LQIBM only models the LQI variance, which is highly unpredictable for intermediate links and does not catch the long term link behavior. HoPS outperforms F-LQE in terms of the memory footprint and short term link behavior. Thus, two main issues have been identified, one that a deeper temporal link behavior is needed to model mathematically the fluctuations of links, and therefore, avoid bad parent choices at the routing level, and second, the collected information (SNR, LQI, sequence number, ETX) are merged into one value, which may underestimate the link quality.

Nonetheless, the widest used metric in WSN is ETX, it presents few limitations, i.e. as it relies on counting packet retransmissions, it does not consider packet losses: considering that after 5 retransmissions, a packet has to be dropped, if a node records a dropped packet (5 retransmissions) and one successful transmission (1 retransmission), while the second node records, two successful transmissions (4 retransmissions), ETX will prefer the first node. Consequently, ETX is unstable and unreliable for dense networks where we may encounter high packet losses.

An ideal link estimator needs to: assure a good delivery rate, be accurate, be reactive (adapt to network changes), consider the link asymmetry, have low overhead, be reliable in dense and noisy networks, be stable (able to ignore small fluctuations of link quality).

An open issue remains the design of a link estimator able to consider all the above mentioned link proprieties and furthermore, to assure a holistic estimation. Moreover, estimators need to perform well in noisy and dense networks by avoiding unreliable links and choosing stable paths for multihop routing.

In this context, at first, we have observed that hardware metrics turn out to provide good information of the link characteristics (delivery, stability, asymmetry, reactivity). Second, composite metrics outperform single metrics. Even so, composite metrics need still further investigation in terms of the required computation time, complexity, memory footprint, behavior in noisy environments and dense networks. To reduce the memory footprint and complex computation of the existing composite metrics, we believe that link estimators should integrate mathematical models able to capture the dynamics of the hardware metrics (average RSSI, std RSSI, average LQI, deviation LQI).

In this thesis, we intend to find an approach able to predict the link behavior from hardware metrics that will require low computation and low memory storage.

Chapter 3

Link quality characterization in an indoor Wireless Sensor Network

Contents

We report in this chapter on the results of measurements on SensLAB [75], an indoor large scale wireless sensor network testbed equipped with CC1101/CC2420 radio chips. We have done extensive experiments on the SensLab platform and recorded two main hardware metrics: RSSI (Received Signal Strength Indicator) and LQI (Link Quality Indicator). LQI gives "an estimate of how easily a received signal can be demodulated by accumulating the magnitude of the error between ideal constellations and the received signal over the 64 symbols immediately following the sync word" *[89]. Further, we grouped the links function of their degree of fluctuation as good (*$80\% \leq PRR \leq 100\%$*), intermediate (*$20\% < PRR \leq 80\%$*), and bad (*$80\% < PRR < 20\%$*).*

We analyze RSSI and LQI behavior in what it concerns the correlation between link properties, temporal fluctuation and asymmetry aspect, to find the best way of detecting good *links in comparison to* weak *ones. To attain a deep understanding of*

link dynamics we are aware of the spatial displacement of nodes. Moreover, we present the main characteristics of links dynamics after previously we identify the external and internal factors that may contribute to signal distortion.

3.1 Introduction

In the literature, much research has explored the link quality on indoor and outdoor environments. In this chapter, we concentrate on an indoor environment. We focus on two hardware metrics such as RSSI and LQI. Their temporal fluctuation was reported to be the main issue of the link quality variation.

Referring to an indoor or an outdoor environment, signal distortion leads to decrease of RSSI, LQI increase for CC1101 with values between 0 (good)-110 (bad), and LQI decrease for CC2420 with values between 110 (good)-50 (bad). Generally, the distortion of the signal is due to the presence of various factors such as the presence of good reflectors (metal or glass) that lead to multi-path (reflections, fading, diffraction) effects, interference all named in Section 2.2.3. Hardware miss-calibration and antenna position are other two additional factors that may affect signal propagation [15, 63, 92].

A *link* by definition refers a two-way interconnecting system between two nodes in the purpose of transmitting or receiving data. Various studies classified links by their quality in three categories: bad links, intermediate, and good links. In particular, Table 2.3 presents an existing link classification. A good link improves the lifetime of a node thanks to the high packet delivery rate reducing energy consumption. On the contrary, intermediate links are highly variable which increase energy consumption.

In order to discriminate links by their quality, efforts analyzed the temporal deviation of RSSI and LQI hardware metrics. They concluded that either observed RSSI does not vary sufficiently, either LQI metric presents unpredictable variation. Therefore, remains a challenge the right methodology to estimate link quality, by merging LQI and RSSI behavior, or by other means.

Consequently, due to the temporal nature of signal propagation, existing studies showed through empirical studies the existence of three zones: good (high link quality), intermediate (intermediate link quality), and bad (bad link quality). Good zones or so known as connected are characterized by stable and mostly symmetric links. Thus, in intermediate or transitional (gray) zones link quality may vary drastically, and more, they are highly asymmetric. The bad or disconnected zones refer to very poor links that should be avoided [101, 6].

Back in 2003, Zhao et al. used a 60 node testbed to show a high variation in packet reception in intermediate zones [103]. Woo et al. observed that distance may discriminate signal zones. They claimed good connectivity of nodes up to 3m and a high variability between 3m and 12m [97].

In this chapter, at first, we aim to understand better the environmental factors that may affect the signal propagation in our large scale testbed (Senslab), equipped with two different radio chips (CC1101 and CC2420). Second, we want to stress out the main characteristics of CC1101, CC2420 links. Last, we provide observations on temporal

link behavior in terms of RSSI, LQI, PRR, and asymmetry. We have organized the chapter as follows:

Section 3.3 presents the experimental set up scenarios for CC1101 and CC2420 testbeds. Next, in Section 3.4, we provide a link classification based on the PRR (good, intermediate, bad). For each category, we report on how varying inter-packet time and output power affects the proportion of links.

Section 3.5 discusses the RSSI/LQI characteristics for good/intermediate/bad links. We consider individually each category to observe the main link property correlation, their temporal fluctuation, and their asymmetry.

Finally, we conclude this chapter by listing down the main characteristics of links that we further use for finding a link quality estimator able to accurately predict PRR.

3.2 Motivation

In this chapter, our main goal is to exploit the temporal deviation of the hardware metrics, namely, LQI and RSSI, in order to accurately distinguish the quality of links.

Initially, we conduct experiments to better understand the Senslab indoor environment. Once we identify the factors, we aim to elaborate a new approach to identify best the reliable links. Likewise, our findings may be used in the design of more accurate radio models in simulators. Finally, we elaborate recommendations on how a new testbed has to be properly deployed.

3.3 Experimental Set Up

We have run experiments on the Strasbourg platform of SensLAB [75] composed of 1024 nodes distributed across 4 sites (Grenoble, Strasbourg, Lille, Rennes). Each individual site comprises 256 WSN430 nodes. Designed to serve as testbed for the Internet of Things scenarios. Our study uses two sites, the SensLAB Strasbourg (CC1101) and SensLab Lille (CC2420).

We observe for CC1101 the quality of transmission of a node that broadcasts a total of 5000 packets of 110 bytes every 0.5s. There is no other ongoing transmission, so there is no interference nor contention between nodes. When one node broadcasts its packet, the other 79 nodes (Strasbourg) are active and ready to receive—they log the values of LQI and RSSI of the received packet. The values are recorded for the correctly received packets with good CRC and also for those with incorrect CRC. As there is one sender at a time, we are able to relate the sender and the receiver of a packet even if the receiver cannot decode a packet.

The receiver nodes do not acknowledge frames and the MAC layer does not retransmit frames in case of failed transmissions. After the experiment, we compute for each link:

- the average value of RSSI over all received packets,
- the average value of LQI,

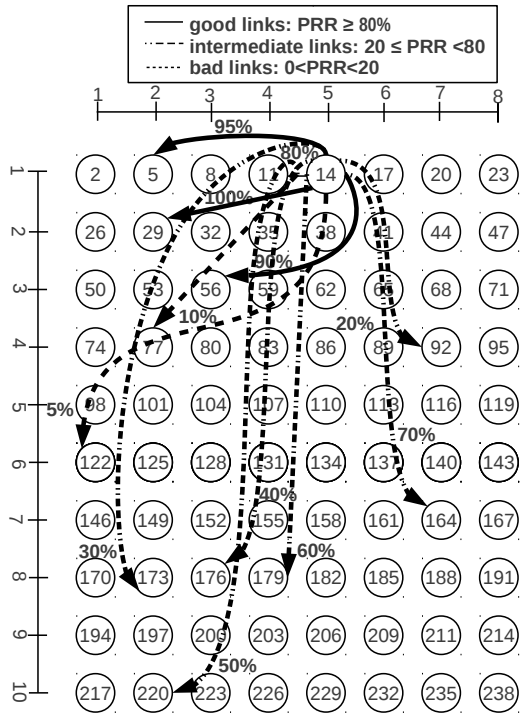

Figure 3.1: Topology of the second tray of SensLAB testbed in Strasbourg. An example of the measured PRR for Node 14 (transmission power: 0dBm): an arrow represents a link labeled with the measured PRR.

- the average value of the Packet Reception Ratio (PRR) of each link as the proportion between the number of correctly received packets (correct CRC) to the total number of sent packets.

We assume that all nodes can potentially communicate with each other. We further discuss separately the results obtained for CC1101 and CC2420.

3.3.1 Senslab-Strasbourg (CC1101)

SensLAB Strasbourg is composed of 240 WSN430 fixed nodes distributed across three trays at different heights. Each tray contains 80 nodes arranged in a regular grid (10x8) with a distance between each node of about 1m (cf. the topology of the second tray of the testbed in Fig. 3.1). A node is composed of a MSP430F1611 CPU (48KB ROM, 10KB RAM) and a CC1101 radio operating at 868MHz. Its transmission power ranges between -30dBm and 10dBm, and the reception sensitivity is set to -88dBm. In a single experiment, we use one tray at a time, i.e. 80 nodes. We run the experiments with two levels of the transmission power: 0dBm and -10dBm. The bit rate is 60kb/s and nodes use the Frequency Shift Keying (2-FSK) modulation and channel 30. Table 3.1 summarizes the parameters of the experiments.

We assume that all nodes can potentially communicate with each other, the total number of unidirectional links is 6320 (80 sender nodes times 79 receiver nodes).

Table 3.1: Experiment parameters

Experiment area	9m x 7m x 2m
Number of nodes	3 x 80
Traffic type, inter-packet interval	broadcast, 0.1s/0.2s/0.5s/1s/30s
Number of sent packets	5000
Packet size	110 & 6 bytes
Transmission power	10dbm, 5dbm, 0dBm, -10dBm, -30dBm
Topology	grid

3.3.2 Senslab-Lille (CC2420)

SensLAB Lille [75] composed of 256 WSN430 nodes scattered across two horizontal trays of different heights and one vertical tray. Each of the horizontal tray contains 100 nodes regulate in a grid of (20x5) with a distance of about 0.6m between nodes. A node is composed of a CC2420 radio operating at 2.4GHz. Table 2.2 presents its main parameters.

We use for our study one tray of 100 nodes.

Table 3.2 shows the parameters of the experiment. We run experiments with three levels of transmission power: 0dBm, -15dBm, and -25dBm. The bit rate is 250kb/s and nodes use the orthogonal quadrature phase shift keying (OQPSK) modulation. We concentrate on the 0dBm output power on our study.

Thus, either in the case of Lille-Strasbourg (CC2420) the receiver nodes do not acknowledge frames so that the MAC layer does not retransmit frames in case of failed transmissions.

Moreover, we assume same as in Strasbourg platform that all nodes can potentially communicate so that the number of unidirectional links is 9900 (100 sender nodes times 99 receiver nodes).

Experiment area	11.4m x 2.4m
Number of nodes	20 x 5
Environment: testbed	Senslab Lille
Traffic type, inter-packet interval	broadcast, 0.1s/0.2s/0.5s/1s
Number of sent packets	1000
Packet size	110 & 6 bytes
Transmission power	0dBm, -10dBm
Topology	grid

Table 3.2: Parameters of the WSN430, CC2420-based testbed.

3.4 Link categories

We consider three main categories of link quality: *good* links with a PRR above 80%, *intermediate* with PRR between 20% and 80%, and *bad* ones with PRR below 20% (such categories appear in previous studies Table 2.3 where the most common

threshold is 90%–10%). Please note that the decision of the three categories is due to the temporal deviation values of LQI. For example, a density distribution of the LQI deviation picks around the value of 1 for good links, 2.5 for intermediate links, and 5 for bad links.

We discuss the impact on link proportion for three cases. One when we decrease power down to -10dBm (CC1101) and to -25dBm (CC2420), and last, a short (6bytes) and long packet (110bytes) case.

3.4.1 Link proportion for CC1101

Table 3.3 gives the proportion of links in each category (over all 6320 unidirectional links). Figure 3.2 shows the portion of links in terms of PRR over the whole experiment. We encounter an important percentage of links with PRR>80% and PRR<20% links. $PRR = 0\%$ corresponds to the case in which a given node did not receive any packet.

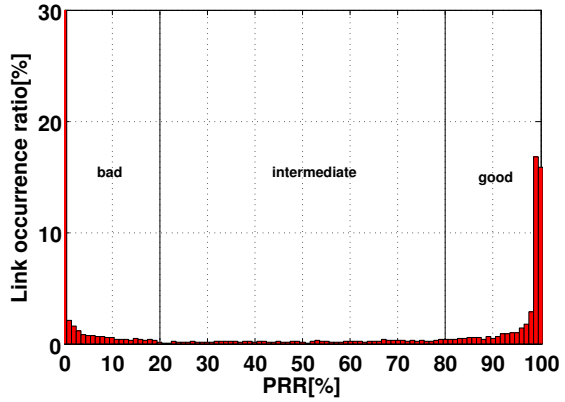

Figure 3.2: The link occurrence ratio for links with a given PRR at 0dBm output power on CC1101.

Parameters	$PRR \geq 80\%$			$20\% \leq PRR < 80\%$			$0 < PRR < 20\%$			$PRR = 0\%$		
Trays	t1	t2	t3	t1	t2	t3	t1	t2	t3	t1	t2	t3
110B, 0.5s, 0dBm	48%	49%	38%	9%	8%	10%	12%	10%	10%	31%	33%	42%

Table 3.3: Proportion of links in each category: good ($PRR \geq 80\%$), intermediate ($20\% \leq PRR < 80\%$), bad ($0 < PRR < 20\%$) for each of the three available trays (t1-tray1, t2-tray2, t3-tray3), with transmission power: 0dBm.

We can observe in Table 3.3 that at 0dBm output power and an inter-packet interval of 0.5s there is a large proportion of good links. Besides, the number of intermediate links is fairly low.

Table 3.4 shows that the decrease of the transmission power to -10dBm only slightly affects the proportion of good links for the first and second tray.

The third tray decreased significantly the number of good links at -10dBm, which shows that nodes are highly affected by multipath effect as third tray is close to metal fixed supports. We can say that the presence of reflectors at a low power affect more the proportion of good links.

Parameters	$PRR \geq 80\%$			$20\% \leq PRR < 80\%$			$0 < PRR < 20\%$			$PRR = 0\%$		
Trays	t1	t2	t3	t1	t2	t3	t1	t2	t3	t1	t2	t3
110B, 0.5s,-10dBm	46%	44%	13%	8%	6%	7%	6%	9%	15%	40%	41%	65%

Table 3.4: Proportion of links in each category: good ($PRR \geq 80\%$), intermediate ($20\% \leq PRR < 80\%$), bad ($0 < PRR < 20\%$) for each of the three available trays (t1-tray1, t2-tray2, t3-tray3), with transmission power:-10dBm.

We have also noticed that at an output power of 5dBm or 10dBm, the intermediate and bad links are in-existing, they are below 1%. We observe a proportion of good links of 65% for 5dBm and 83% for 10dbm.

Consequently, when we decrease the output power down to -30dBm, the majority of links are bad. Aside from the power decrease impact on the link proportion, we are interested in how interference and long or short packets impact link proportion.

In Table 3.5 we show the concurrent interference case. We set up node 86 as an interferer that concurrently transmits data packets of 110 bytes each 0.5s. The second tray presents at -10dBm a proportion of good links about 45% whereas in the presence of high interference, the proportion of good links decreases drastically and reached only 7%, a drop of 85% is observed. A similar observation was made by Mottola et al. [55]. They reported that concurrent transmissions substantial increase the interference resulting in important packet delivery drop.

Parameters	$PRR \geq 80\%$	$20\% \leq PRR < 80\%$	$0 < PRR < 20\%$	$PRR = 0\%$
110B,0.5s,-10dBm	44%	6	9%	40%
110B,0.5s,-10dBm,+int.	7%	5%	32%	56%

Table 3.5: Proportion of links for the second tray-Strasbourg with concurrent interference.

Table 3.6 presents that on CC1101 radio, good links increase from 65% at 100ms to 69% at 1s for packets of 110B, and from 87% at 100ms to 89% at 1s. Intermediate links also increase from 2% (100ms) to 5% (1s) for long packets and from 2% (100ms) to 4% (1s) for short packets.

To conclude the link proportion study for CC1101, we can observe that link proportion changes with power decrease as well as with interference presence.

Parameters	$PRR \geq 80\%$	$20\% \leq PRR < 80\%$	$0 < PRR < 20\%$	$PRR = 0\%$
110B, 0.1s, 0dBm	65%	2%	2%	31%
110B, 0.2s, 0dBm	66%	1%	3%	30%
110B, 0.5s, 0dBm	64%	2%	2%	32%
110B, 1s, 0dBm	69%	5%	2%	24%
6B, 0.1s, 0dBm	87%	2%	9%	2%
6B, 0.2s, 0dBm	86%	2%	8%	4%
6B, 0.5s, 0dBm	87%	1%	10%	2%
6B, 1s, 0dBm	89%	4%	6%	1%

Table 3.6: Proportion of links for short and long packets, grid of 80 nodes, Strasbourg-CC1101 at 0dBm output power.

Still, while varying the inter-packet interval for 100ms, 200ms, 500ms, 1s, to 30s we observe that it does not affect link proportion. On the other hand, at an inter-packet interval of 30s we encounter a small drop of about 6% of good links and an increase in intermediate links of only 3%. Therefore, we claim that for CC1101 the proportion of good links may be affected by the output power decrease and by large inter-packet intervals, no matter the packet size, long (100B) or short (6B).

3.4.2 Link proportion for CC2420

We consider the same three categories of link quality: *good*, *intermediate*, and *bad*. Table 3.7 gives the proportion of links in each category (over all 9900 unidirectional links).

A first observation is that CC2420 (2.4GHz) radio records a percentage of 20% of good links for long data packet (110B) scenarios, while for CC1101 (868MHz) we reached 46%. In terms of intermediate links, we record a proportion of about 70% for CC2420 radio and aprox. 10% for CC1101. These observations agree with previous studies that claimed about 35% to 50% for Mica 1 platform (CC1101) [103, 107] and 5% to 60% for TelosB (CC2420) [80].

A second observation regards the impact of intermediate link proportion with the decrease of the output power. Choosing a too low output power (-25dBm), the radio range diminishes considerably, so that we may not have enough radio range to reach neighbors, and run properly our experiments. For instance, the good links proportion goes below 1% at -25dBm output power.

Parameters	$PRR \geq 80\%$	$20\% \leq PRR < 80\%$	$0 < PRR < 20\%$	$PRR = 0\%$
110B, 0.5s, 0dBm	24%	71%	1%	4%
110B, 0.5s, -15dBm	4%	38%	7%	51%
110B, 0.5s, -25dBm	0.2%	13%	4%	%82.8

Table 3.7: Proportion of links for data packets of 110 bytes, grid of 100 nodes, Lille-CC2420 at 0dBm, -15dBm, and -25dBm output power.

Furthermore, we analyze the impact of the packet size on the proportion of the links. Table 3.8 illustrates that short packets (6 bytes) result in 80% of good links, because of a lower probability of a packet loss. Likewise, for CC1101 radio, the proportion of good links holds around 80%, see Table 3.6.

Moreover, Table 3.8 shows that good links proportion increases from 25% at 100ms to 27% at 1s for 110B packets, and from 81% at 100ms to 91% at 500ms for packets of 6B. The intermediate link proportion increases with 4% from 67% at 100ms to 73% for packets of 110B and with 6% from 4% at 100ms to 10% for 6B packets.

Parameters	$PRR \geq 80\%$	$20\% \leq PRR < 80\%$	$0 < PRR < 20\%$	$PRR = 0\%$
110B, 0.1s, 0dBm	25%	67%	1%	5%
110B, 0.2s, 0dBm	26%	59%	5%	11%
110B, 0.5s, 0dBm	24%	71%	1%	4%
110B, 1s, 0dBm	27%	73%	1%	1%
6B, 0.1s, 0dBm	81%	4%	1%	14%
6B, 0.2s, 0dBm	90%	5%	0.5%	4.5%
6B, 0.5s, 0dBm	87%	6%	1%	2%
6B, 1s, 0dBm	91%	7%	0.5%	1.5%

Table 3.8: Proportion of links for short/long packet, grid of 100 nodes, Lille-CC2420 at 0dBm output power.

Therefore increasing the inter-packet time result in increase of intermediate link proportion for long packets, observation made as well by Srinivasan et al. [81]. In following, we study the temporal fluctuation of RSSI and LQI.

3.4.3 Temporal fluctuation of link quality

We analyze the temporal deviation of LQI and RSSI. We have observed on CC1101 that RSSI varies between 0dBm-4dBm for good links and slightly increases for the intermediate and bad links, up to 10dBm.

On the other hand, for CC2420, RSSI has a larger variation (std. RSSI that takes values higher than 5) for intermediate and bad links, see Figure 3.9, which corresponds to the literature [101, 66].

In addition, we confirm the observation that intermediate links drop from high to low PRR over short time spans, similarly to Bas et al. [7] who claimed a RSSI variability of 5dBm-6dBm for CC2420.

We have looked at the temporal variation of the RSSI over 24 hours for two links, one with a PRR=100% and the second with a PRR=50%. Figure 3.3 shows that good links have a steady RSSI over the long term whereas for intermediate links, the RSSI variation is more important.

Furthermore, with respect to LQI, a generic observation is that LQI varies little over time for good links while a high variation occurs for intermediate and bad links.

In spite of a LQI variation of 1 encountered for a good link on CC1101 radio, CC2420 has a higher fluctuation about 5. Even though, to discriminate best the intermediate

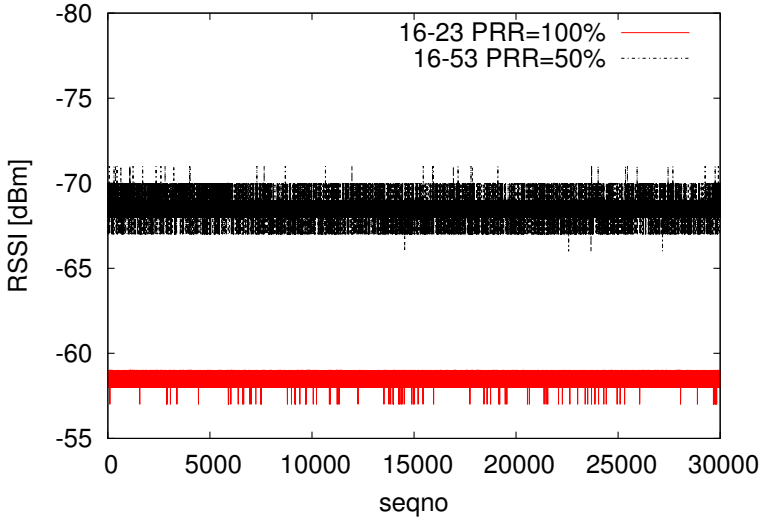

Figure 3.3: The RSSI evolution over 24h for 16 → 23 (PRR=100%) and 16 → 53 (PRR=50%) links for on the CC1101-testbed.

from good and bad links, the fluctuation of LQI may not be sufficient. For this reason, we elaborate a deeper analysis of the standard deviation and the average values of RSSI and LQI.

Referring to the short term link dynamics, a challenge remains of how large the observation should be, or how long the link drops last for individual link categories.

The research claimed an observation sliding window size of 10 [12] or within 40 and 120 [79]. However, the interval of 120 data packets to make decisions regarding the quality of links is too large for low rate traffic or dense networks.

Furthermore, the average model over historical data was claimed as a solution [80, 99]. In the last chapter we provide a deeper insight on the short term link drops correlation through a 2-state Markov model.

3.5 RSSI/LQI

In this section, we investigate the quality of a link in terms of RSSI and LQI. Moreover, we study the bi-directionality of links.

3.5.1 RSSI

At first, we consider the RSSI hardware metric at different output power by tracing the probability density function of the averaged and standard deviation of RSSI values corresponding to each link.

A) Probability density function of RSSI

Figure 3.4 shows the probability density function of the RSSI averaged and RSSI standard deviation for CC1101. Figure 3.4 a) shows that the probability density function

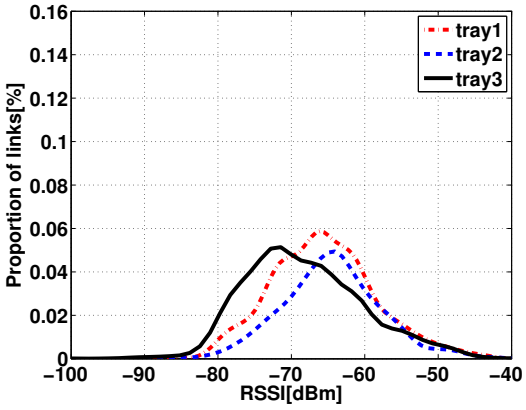

(a) PDF of avg. RSSI - Strasbourg trays: 1,2,3 at 0dBm.

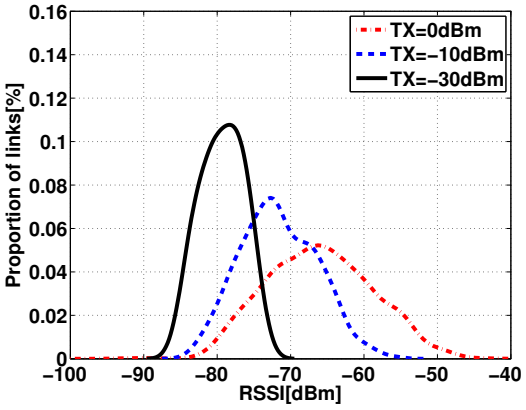

(b) PDF of avg. RSSI - Strasbourg tray 2 at 0dbm, -10dBm, -30dBm.

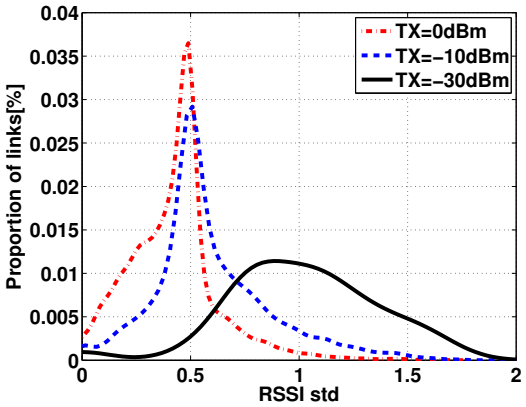

(c) PDF of std. RSSI - Strasbourg tray 2 at 0dbm, -10dBm, -30dBm.

Figure 3.4: The Probability Density Function (CC1101) of a) avg. RSSI for Strasbourg trays: 1,2,3 at 0dBm, b) avg. RSSI for Strasbourg tray 2 at 0dbm, -10dBm, -30dBm, c) std. RSSI for Strasbourg tray 2 at 0dbm, -10dBm, -30dBm.

for the third tray has a pick around -72dBm, while the first and the second tray have both a density pick around -66dBm. This is the effect of the multi-path presence on the third tray coming from fixed metal supports holding the RJ45V cables and the light lamps.

In Figure 3.4 b), we see a shift of 13dBm from -65dBm at 0dBm down to -78dBm at -30dBm. Interestingly, Figure 3.4 c) shows that decreasing the output power to -30dBm stirs the RSSI standard deviation from 0.5 to 1.

Figure 3.5 a) shows that at 0dBm output power the RSSI values for CC2420 con-

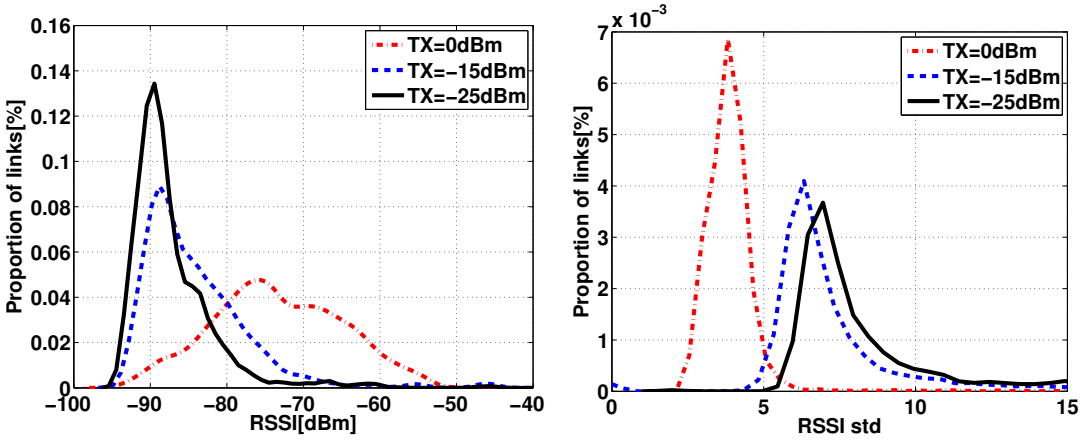

(a) PDF of avg. RSSI

(b) PDF of std. RSSI

Figure 3.5: The Probability Density Function for 100 nodes on Lille (CC2420) for a) avg. RSSI at 0dbm, -10dBm, -30dBm output power, b) std. RSSI at 0dbm, -10dBm, -30dBm output power.

centrate around -75dBm, unlike to CC1101 3.4 b) where values concentrate around -65dBm. This is due to the environment, more specifically, the Strasbourg testbed is less exposed to multipath effects and also the distance between nodes is 1m with respect to Lille testbed that has 0.6m.

We have come to the conclusion that neither packet size nor inter-packet interval do not impact the probability density function of the averaged RSSI. However, the probability density function of the standard deviation and average RSSI are affected by the output power decrease. For example, the standard deviation of RSSI picks around 0.9 at 0dBm, 0.5 at -10dBm and -30dBm.

B) Cumulative density function of RSSI

Figure 3.6 shows the RSSI readings for all received packets for the main subcategories of good links at 0dBm. More specifically, Figure 3.6 a) and b) shows that good links may be distinguished on CC1101 by a threshold of -65dBm, independently of the packet size 6 bytes (a) or 110 bytes (b).

Hence, we noticed that good links with a PRR above 99% have a RSSI above -65dBm. Additionally, we have observed that the threshold keeps around -65dBm either at -10dBm with or without concurrent transmissions.

We investigated the cumulative distribution function of average RSSI and deviation RSSI over the entire experiment for each sub-category of links at a step of 10%. First and foremost, we have observed that for CC1101, the average RSSI overlaps for subcategories with a PRR below 99%. Yet, links with PRR above 99% go over -63dBm.

Adversely, regarding std RSSI, the deviation is too little about 1, resulting in an overlap of CDF curves and therefore, may not be used to discriminate link categories.

At the same time for CC2420 (0dBm), Figure 3.6 c) (6 byte packet size) and 3.6 d) (110 byte packet size) show that a value -65dBm can discriminate up to 90% of the RSSI readings for links with PRR above 99%, and 70% for PRR [95%-99%). Figure 3.7 shows that the threshold value depends on the chosen output power for both radio chips CC1101 and CC2420.

On CC2420 radio, Figure 3.8 shows a -70dBm avg RSSI value that can distinguish links with PRR>95%, a proportion of $\sim$ 50% of links $80\% \leq PRR \leq 95\%$, and $\sim$ 20% of links $70\% \leq PRR \leq 80\%$. Contrary to CC1101, the CDF curves of avg RSSI for good and intermediate links do not overlap, therefore, avg RSSI may be used to distinguish good and intermediate links.

Figure 3.9 a) shows that a std RSSI of 4 can distinguish links with a PRR ($95\% \leq PRR \leq 100\%$). Moreover, Figure 3.9 b) shows that intermediate links ($20\% \leq PRR \leq 80\%$) have a std RSSI within 4 and 10 while links with low PRR ($PRR \leq 20\%$)) the std RSSI is significantly higher (above 10). Please note that the mentioned std RSSI values of 4 and 10 are observed on the CDF curves. We mainly want to point out that the std RSSI can discriminate link categories.

We observe that avg RSSI and std RSSI can well discriminate links with a high reception ratio (PRR>95%) for CC1101, though for CC2420, they can discriminate all link categories.

More specifically, on CC2420, good links may be discriminated by an avg RSSI higher than -75dBm and a std RSSI below 4; intermediate links have a avg RSSI generally between -75dBm and -90dBm at 0dBm output power, and a std RSSI between 4 and 10; bad links overlap intermediate avg RSSI whereas, the std RSSI higher than 10 distinguishes bad links.

To conclude this subsection, we point out, at first, that the probability density function of the averaged RSSI is not affected neither by packet size nor by the inter-packet interval. Second, we observe that links having a PPR above 99% (CC1101) can be discriminated easily with a value of -65dBm, and -75dBm for CC2420 radio.

Third, we point out that the avg RSSI and the std RSSI can discriminate on CC1101 only links with reception ratio (PRR>99%). Moreover, for CC2420, std RSSI and avg RSSI can discriminate better links with a reception ratio below 99%.

Likewise RSSI, we investigate below the features of the LQI measured on our testbed.

3.5.2 LQI

We want to find the correlation between LQI and PRR. We record for each link 5000 (CC1101) / 1000 (CC2420) readings during each experiment. We group links into sub-categories, and we consider the average and standard deviation LQI to understand better the link behavior and further benefit of observations to improve routing performances.

To have a deeper insight on the std LQI, we investigate the level of std LQI (CC1101/CC2420) for each sub-group of links at a step of 10. LQI values for good

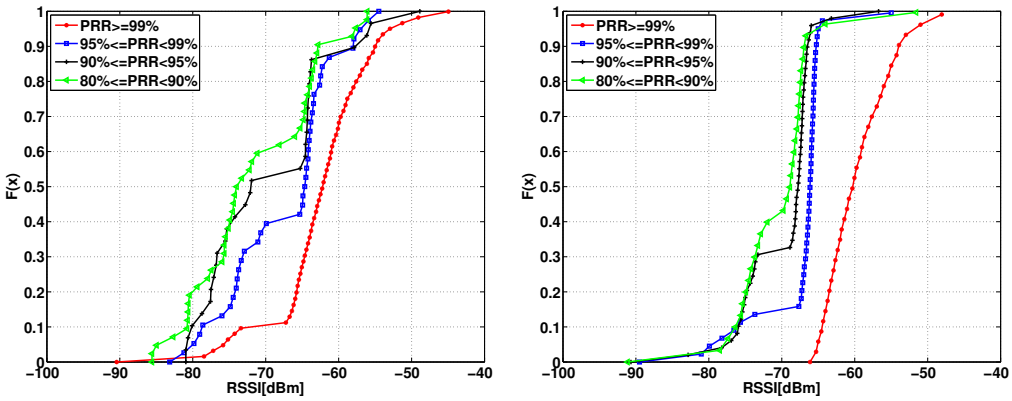

(a) 6 byte packets, CC1101.

(b) 110 byte packets, CC1101.

(c) 6 byte packets, CC2420.

(d) 110 byte packets, CC2420.

Figure 3.6: The cumulative distribution function for good links (PRR>80%) as a function of RSSI at an transmission power set to 0dBm for a) 6 byte packets, CC1101, c) 110 byte packets, CC1101 c) 6 byte packets, CC2420, d) 110 byte packets, CC2420

links are close to 0 for CC1101 radio, whereas for CC2420 the values are close to 110.

Figure 3.10 a) shows that avg LQI keeps below 1.5 for good links. Figure 3.10 b) shows that links with a PRR within 40% and 80% reaches an avg LQI of 4. Figure 3.10 c) presents that for bad links with PRR below 10% the avg LQI goes to much higher values. Also, it reveals that average LQI is enough to discriminate links with a $PRR \geq 99$ which are stable, observation confirmed by literature [83, 50, 12]. Bad links with $PRR \leq 10$ may be also easily discriminated only with the average LQI.

Observing std LQI, Figure 3.11 illustrates that a threshold of 1.5 for std LQI is able to identify links 90%<=PRR<=100% Figure 3.11 a). Figure 3.11 b) shows that raising

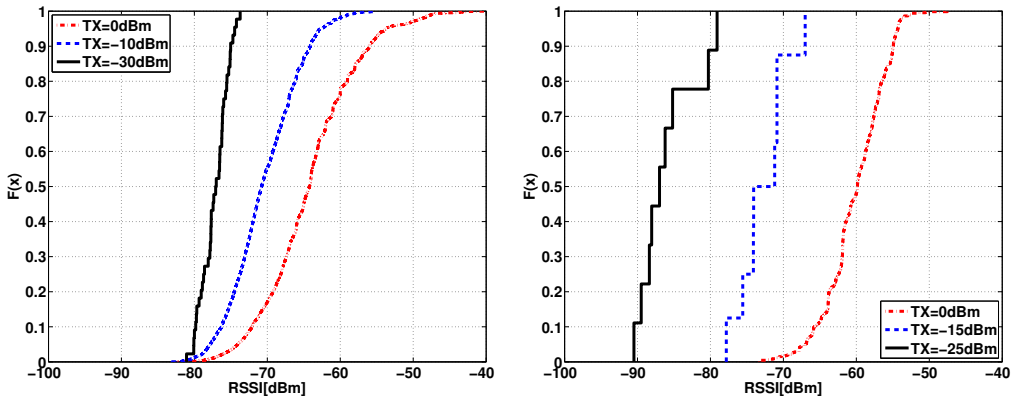

(a) 110 byte packets, CC1101.

(b) 110 byte packets, CC2420.

Figure 3.7: The cumulative distribution function of RSSI for links with $PRR \geq 99\%$ for various output power: a) CC1101: 0dBm, -10dm and -30dBm; b) CC2420: 0dBm, -15dBm and -25dBm.

the threshold from 1.5 to 3, can distinguish almost all links from 90% to 40% of PRR along with 60% of links with a PRR from 40% to 20%. In particular, Figure 3.11 c) presents a high std LQI, typically, more than 4, for links with less that 20% of PRR.

Figure 3.12 a) shows for CC2420 that avg LQI is around 105 for links with PRR above 80; avg LQI decreases for intermediate links down to 70, see Figure 3.12 b), whereas for bad links, it continues to decrease to 50, see Figure 3.12 c). The decrease of avg LQI with the link quality shows that LQI can be a good indicator for the quality of links.

On the other hand, Figure 3.13 illustrates that std LQI overlaps for good and intermediate links , showing a range within 5 and 10. However, std LQI helps to discriminate bad links that exceed a deviation of 10.

As we can see, avg LQI helps to discriminate good links, their value is less than 1.5 for CC1101 and between 104-107 for CC2420. Thus, std LQI remains below 2 for CC1101 and is between 5 and 10 for CC2420. Therefore, to discriminate good links of CC2420 radio, we need to combine avg LQI and std LQI.

Then, intermediate and bad links may be discriminated using avg LQI and std LQI for both CC1101 and CC2420 radios.

To conclude, we can draw a first conclusion that, avg LQI and std LQI for good links vary little. On the other hand, intermediate (20%<=PRR<80%) and bad links (PRR less than 20%) have high average LQI and deviation LQI. Therefore, we can use avg LQI and std LQI to discriminate link categories.

It may occur that bad links exhibit low std LQI because of a sequence of bad packet receptions (high number of errors). In this case, avg LQI is important as it will denote a high LQI (CC1101), or low LQI (CC2420).

Second, we believe that avg LQI coupled with std LQI will give a more accurate

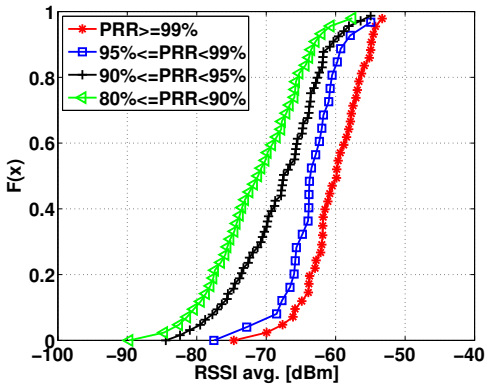

(a) avg RSSI for links (80%<=PRR<=100%).

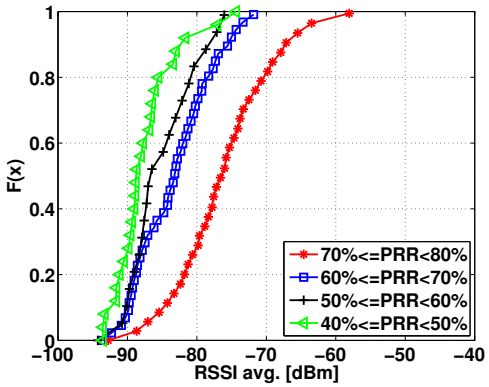

(b) avg RSSI for links (40%<=PRR<80%).

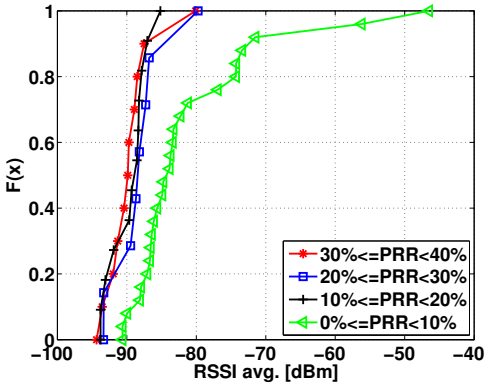

(c) avg RSSI for links (0%<PRR<40%).

Figure 3.8: The cumulative distribution function of avg RSSI for sub-groups of links spaced at a step of 10: a) 80%<=PRR<=100%, b) 40%<=PRR<80%, c) 0%<PRR<40% at an output power of 0dBm, CC2420.

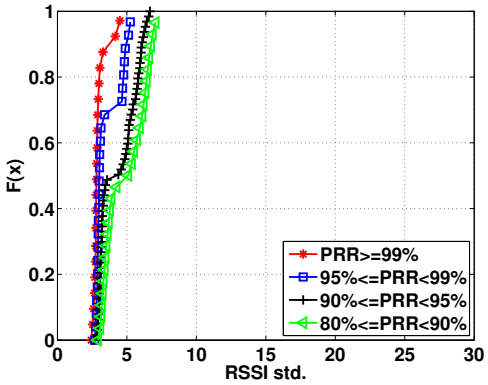

(a) std RSSI for links (80%<=PRR<=100%).

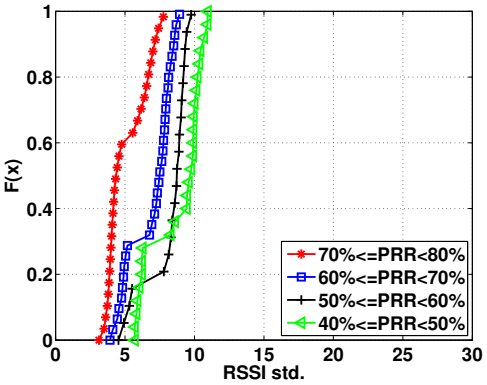

(b) std RSSI for links (40%<=PRR<80%).

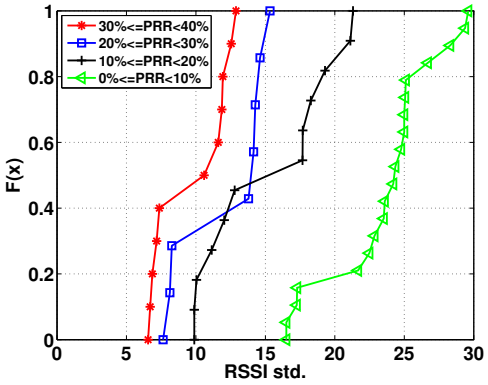

(c) std RSSI for links (0%<PRR<40%).

Figure 3.9: The cumulative distribution function of std RSSI for sub-groups of links spaced at a step of 10: a) 80%<=PRR<=100%, b) 40%<=PRR<80%, c) 0%<PRR<40% at a transmission power set to 0dBm on CC2420.

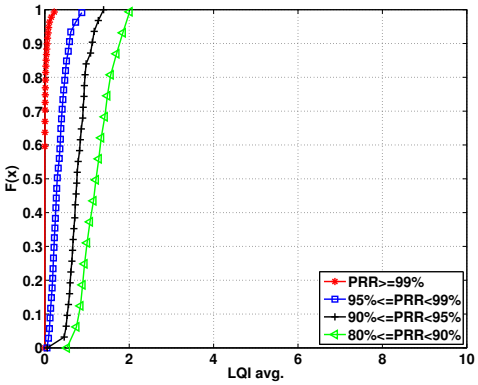

(a) avg LQI for links (80%<=PRR<=100%).

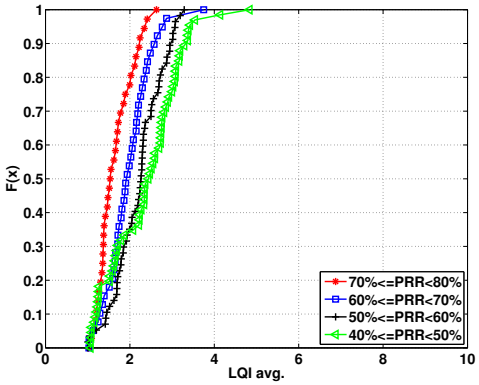

(b) avg LQI for links (40%<=PRR<80%).

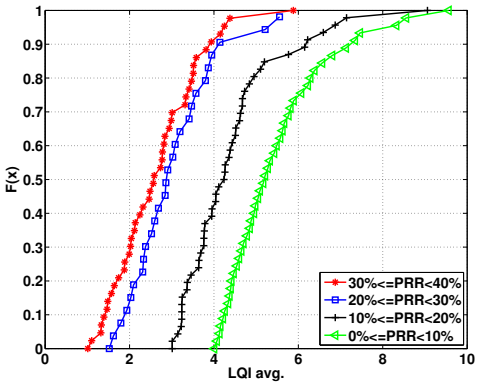

(c) avg LQI for links (0%<PRR<40%).

Figure 3.10: The cumulative distribution function of avg LQI for sub-groups of links spaced at a step of 10: a) 80%<=PRR<=100%, b) 40%<=PRR<80%, c) 0%<PRR<40% at a transmission power set to 0dBm on CC1101.

estimation, avoiding bad discrimination of links with close qualities.

In the next chapter, we show how together LQI and RSSI can accurately discriminate links on long and short term.

3.6 Link Asymmetry

Another issue of wireless links is link asymmetry as it may dissolve the assumptions adapted in routing protocols. The reasons may be: receiver sensitivity, hardware miscalibration, radiation patterns (multi-path effects), integrated antenna in the printed circuit board, and low-noise amplifier (LNA) [35].

We compute the asymmetry of a link as the absolute difference $|PRR_{x->y} - PRR_{y->x}|$,

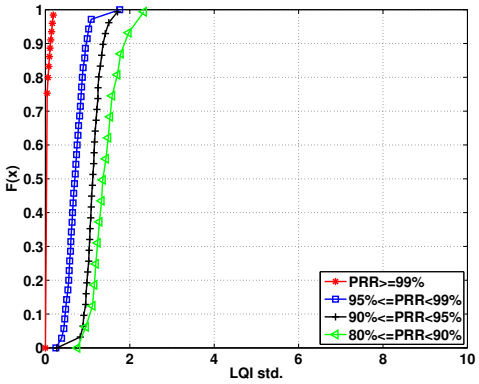

(a) std LQI for links (80%<=PRR<=100%).

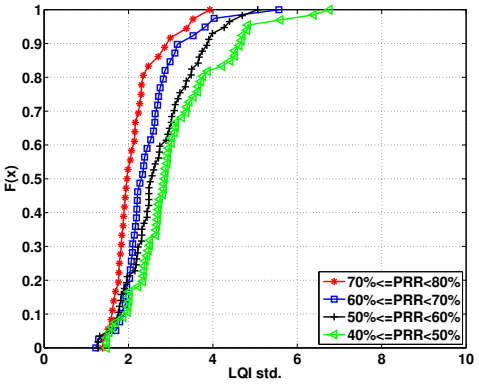

(b) std LQI for links (40%<=PRR<80%).

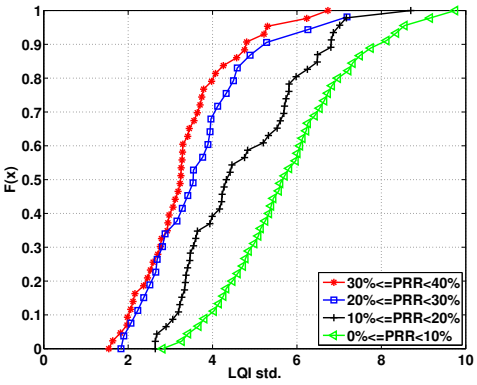

(c) std LQI for links (0%<PRR<40%).

Figure 3.11: The cumulative distribution function of std LQI for sub-groups of links spaced at a step of 10: a) 80%<=PRR<=100%, b) 40%<=PRR<80%, c) 0%<PRR<40% at a transmission power set to 0dBm on CC1101.

where x, y denote the nodes and the arrow points to the receiver node.

Hence, we consider that a link presents asymmetry if the absolute difference is higher than 1%, and at least one packet was exchanged. Moreover, in our study we call an asymmetry as: *stable* if the absolute difference is less than 20%, *average* for an absolute difference between 20% and 80%, and *strong* if the absolute difference is above 80%. Also, we use the term of bi-directional link, for a link that has an absolute difference less than 1 within uplink and downlink. We call unidirectional link, a link that received data packets on the forward and do not record any successful packet reception on the backward link, or reverse.

Figure 3.14 shows that RSSI is symmetric (CC1101) for long (110bytes) and short (6bytes) packets. Instead, when we decrease the output power to -10dBm, and -30dBm, the number of unidirectional links increases. For instance, we see in Figure 3.14 c) that

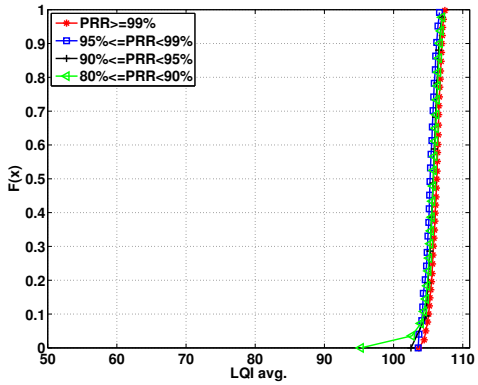

(a) avg LQI for links (80%<=PRR<=100%).

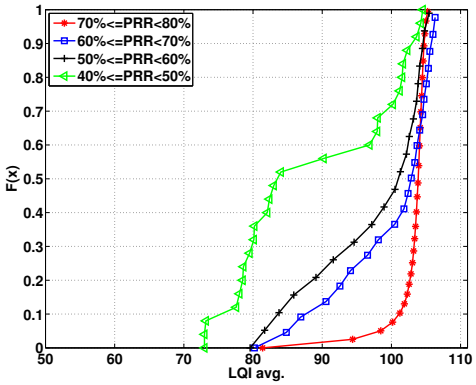

(b) avg LQI for links (40%<=PRR<80%).

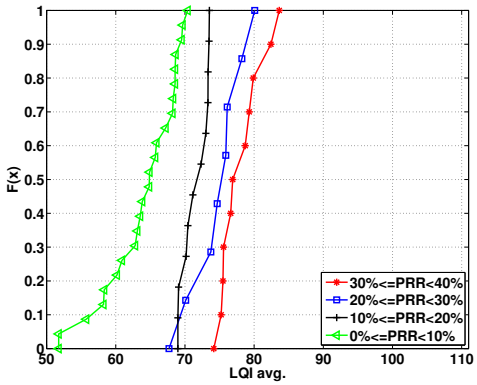

(c) avg LQI for links (0%<PRR<40%).

Figure 3.12: The cumulative distribution function of avg LQI for sub-groups of links spaced at a step of 10: a) 80%<=PRR<=100%, b) 40%<=PRR<80%, c) 0%<PRR<40% at a transmission power set to 0dBm on CC2420.

at -10dBm we have numerous links at -100dBm, which represents the noise, meaning that these links are unidirectional, and that are part of the group with strong asymmetry. We observed that once we decrease the output power, the unidirectional links multiply.

For CC2420 radio, Figure 3.15 shows that the symmetry of RSSI is not affected by the packet size. Once we decrease the output power to -15dBm, or -25dBm we lose on RSSI symmetry, see Figure 3.15 c).

Figure 3.16 illustrates that links with a 100% of reception ratio are symmetric in proportion of 97%. We notice also that the size of packets affects with only $\sim 2\%$ the proportion of links that are asymmetric. Thus, short packets recorded only 1% of the total links as asymmetric, while for long packets we record 3%. However, decreasing the output power to -10dBm results in an increase of asymmetric links from 3% to 5%.

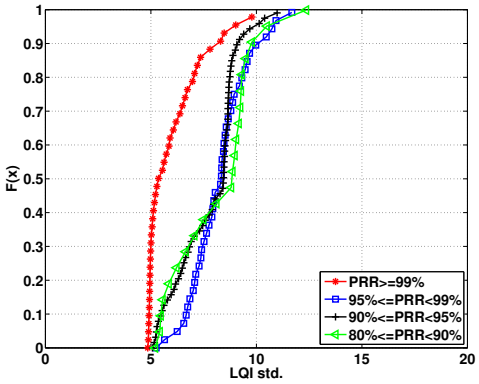

(a) std LQI for links (80%<=PRR<=100%).

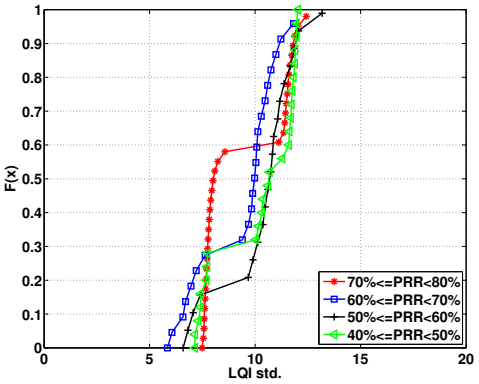

(b) std LQI for links (40%<=PRR<80%).

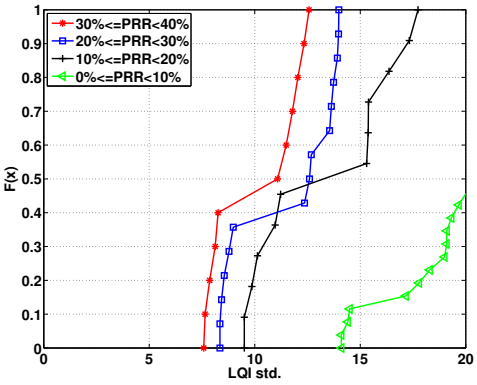

(c) std LQI for links (0%<PRR<40%).

Figure 3.13: The cumulative distribution function of std LQI for sub-groups of links spaced at a step of 10: a) 80%<=PRR<=100%, b) 40%<=PRR<80%, c) 0%<PRR<40% at a transmission power set to 0dBm on CC2420.

Moreover, links with PRR ($80\% \leq PRR < 100\%$) have a stable asymmetry of maximum 20%, while the intermediate links have an average asymmetry from 20% to 80%. Also, the packet size or the power decrease do not affect the symmetry of good and intermediate links.

Still, we observed that at 0dBm 40% of bad links have strong asymmetry, whereas at -10dbm the percentage of bad links with strong asymmetry is 90%.

On the other hand, for CC2420 radio, Figure 3.17 shows that increasing the packet size from 6 bytes to 110 bytes leads to a lost of 5% of perfect symmetric links (same PRR in both directions), along with a asymmetry increase for intermediate and bad links. Again, similarly to CC1101, reducing the output power to -15dBm leads to a slightly asymmetry increase for intermediate and bad links, while the perfect symmetric links are completely lost.

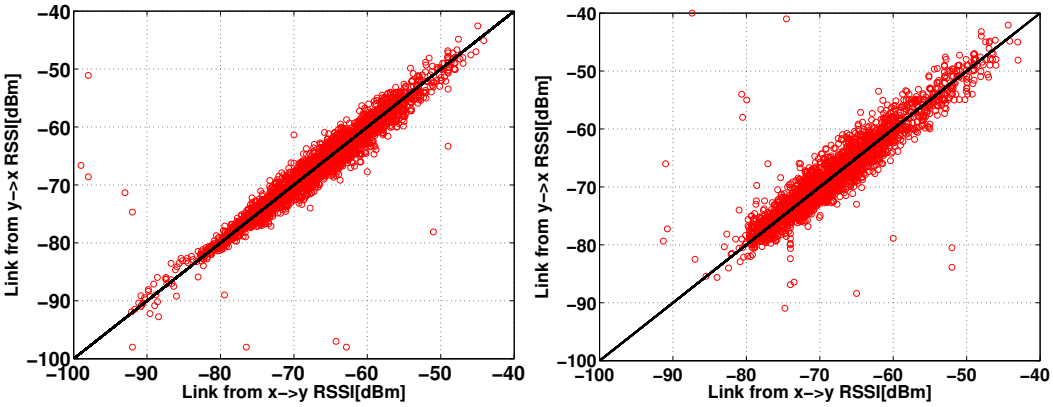

(a) 6 byte packets size at 0dBm.

(b) 110 byte packets size at 0dBm.

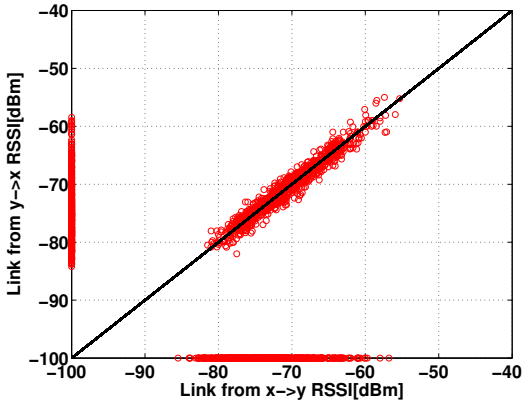

(c) 110 byte packets size at -10dBm.

Figure 3.14: RSSI of bidirectional links ($x \rightarrow y$ and $y \rightarrow x$) for CC1101: a) 6 bytes, output power of 0dBm, b) 110 bytes, output power of 0dBm, c) 110 bytes, output power of -10dBm.

Figure 3.18 and 3.19 highlight that unidirectional links exist mostly in zones with low RSSI. Also, bi-directional links are not influenced by packet size, whereas the unidirectional links widen the RSSI range once the packet size increases. However, the RSSI range of unidirectional links narrows with the decrease of power for both radio chips CC1101 and CC2420.

Table 3.9 presents the symmetry degree for CC1101 and CC2420 radio chips at different emission power: 0dBm, -10dB, -15dBm and different packet size, 6 bytes, 110 bytes, respectively.

To sum up, as we can see in Table 3.9 that links with PRR=100% are slightly influenced by the packet size. On the contrary, when we decrease the power to -10dBm we observe that we record with 20% links with A=0%. Even so the good links maintain

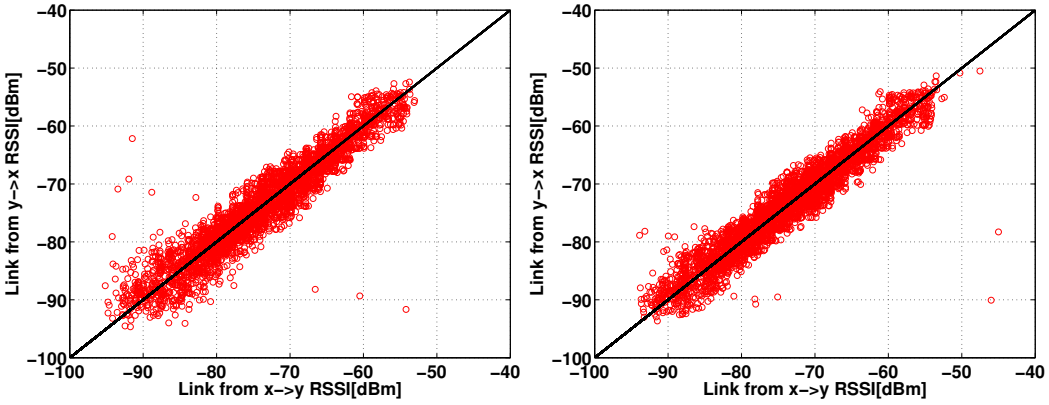

(a) 6 byte packets size at 0dBm.

(b) 110 byte packets size at 0dBm.

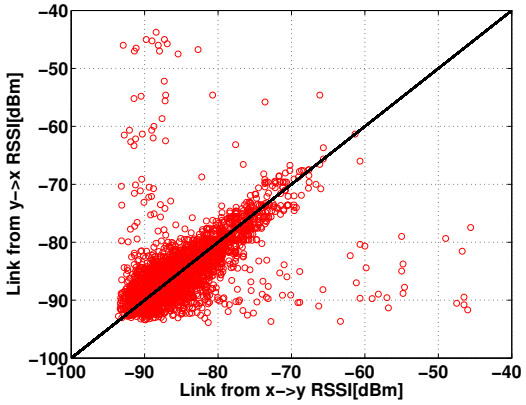

(c) 110 byte packets size at -15dBm.

Figure 3.15: RSSI of bidirectional links ($x \rightarrow y$ and $y \rightarrow x$) for CC2420: a) 6 bytes, output power of 0dBm, b) 110 bytes, output power of 0dBm, c) 110 bytes, output power of -15dBm.

Parameters	$PRR \geq 80\%$				$20\% \leq PRR < 80\%$				$0 < PRR < 20\%$			
Asymmetry	A=0%	0%<A<=20%	20%<A<=80%	A>80%	A=0%	0%<A<=20%	20%<A<=80%	A>80%	A=0%	0%<A<=20%	20%<A<=80%	A>80%
CC1101,0dBm,6B	72	18	0	0	0	20	80	0	0	18	32	50
CC1101,0dBm,110B	79	21	0	0	0	20	80	0	3	47	30	20
CC1101,-10dBm,110B	90	10	0	0	0	10	90	0	2	5	4	89
CC2420,0dBm,6B	23	77	0	0	0	87	13	0	15	27	56	2
CC2420,0dBm,110B	50	50	0	0	10	86	4	0	10	40	43	3
CC2420,-15dBm,110B	15	85	0	0	14	71	15	0	5	45	50	0

Table 3.9: Link asymmetry (A[%]:absolute difference) for each category: good ($PRR \geq 80\%$), intermediate ($20\% \leq PRR < 80\%$), bad ($0 < PRR < 20\%$) for CC1101 and CC2420 with a packet size of 6 bytes and 110 bytes at various transmission power: 0dBm, -10dB, -15dBm.

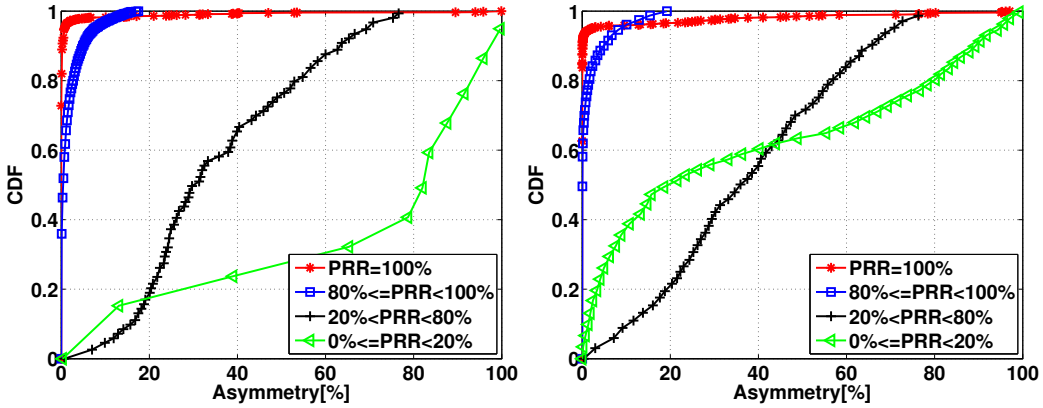

(a) 6 byte packets size at 0dBm.

(b) 110 byte packets size at 0dBm.

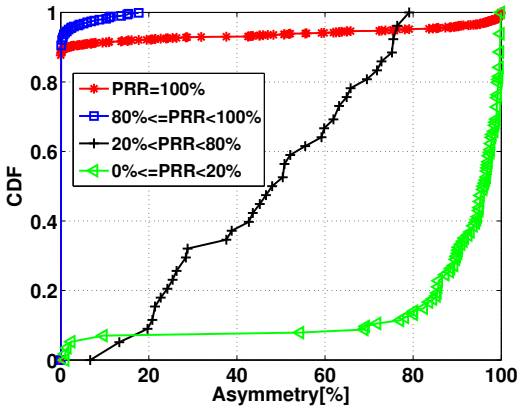

(c) 110 byte packets size at -10dBm.

Figure 3.16: The RSSI symmetry for perfect ($PRR = 100\%$), good ($80\% \leq PRR \leq 99\%$), intermediate ($20\% \leq PRR < 80\%$), bad ($0 < PRR < 20\%$) links for CC1101: a) 6 bytes, output power of 0dBm, b) 110 bytes, output power of 0dBm, c) 110 bytes, output power of -10dBm.

an asymmetry below 20% for CC1101 and CC2420.

Moreover, for CC1101, intermediate links ($20\% \leq PRR < 80\%$), are not influenced by the packet size neither. We record a majority of links with average asymmetry for CC1101 and a majority of link with stable asymmetry for CC2420. of 20%<asymmetry<=80% for CC1101 and a majority of 0%<=asymmetry<=20% for CC2420. Overall, decaying the output power results in a decline of the number of strong asymmetric links. Thus, most percentage of bad links have a strong asymmetry for CC1101 and an average asymmetry for CC2420.

Lastly, for CC1101 and CC2420, the power decay leads to an enhance the number of links with average and strong asymmetry while reduces the percentage of links with

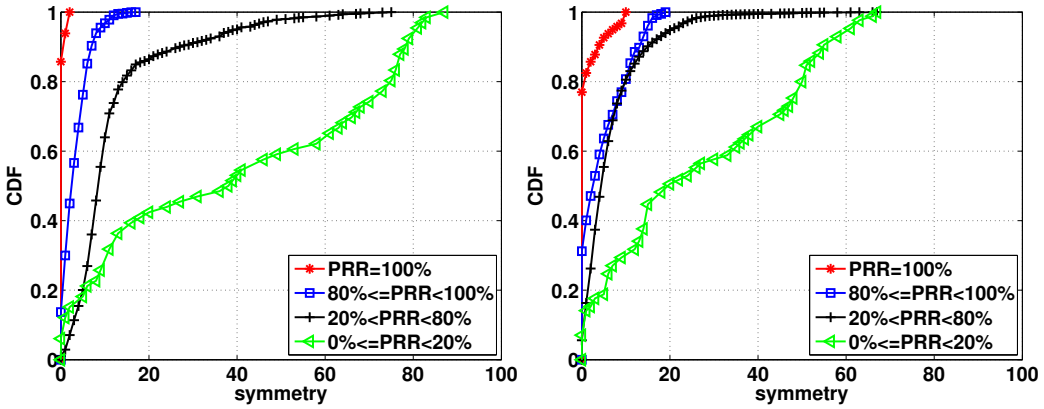

(a) 6 byte packets size at 0dBm.

(b) 110 byte packets size at 0dBm.

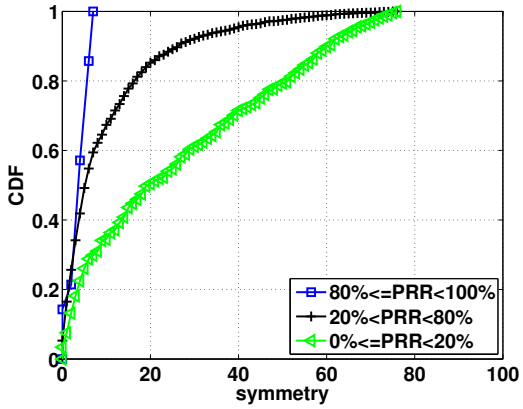

(c) 110 byte packets size at -10dBm.

Figure 3.17: The RSSI symmetry for perfect ($PRR = 100\%$), good ($80\% \leq PRR \leq 99\%$), intermediate ($20\% \leq PRR < 80\%$), bad ($0 < PRR < 20\%$) links for CC2420: a) 6 bytes, output power of 0dBm, b) 110 bytes, output power of 0dBm, c) 110 bytes, output power of 0dBm -15dBm.

strong asymmetry.

3.7 Discussion

In this chapter, we have analyzed the empirical data from indoors testbed with CC1101 and CC2420 radio chips to better understand the proprieties of links. The study focuses on the link dynamics and the link asymmetry for specific categories of links. We have considered several aspects such as the percentage of formed links, average and standard deviation of RSSI/LQI, and the asymmetry of links.

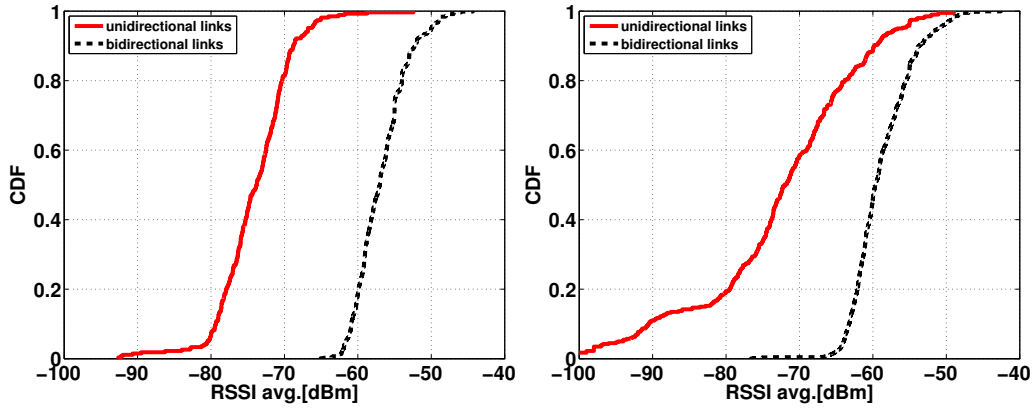

(a) 6 byte packets size at 0dBm.

(b) 110 byte packets size at 0dBm.

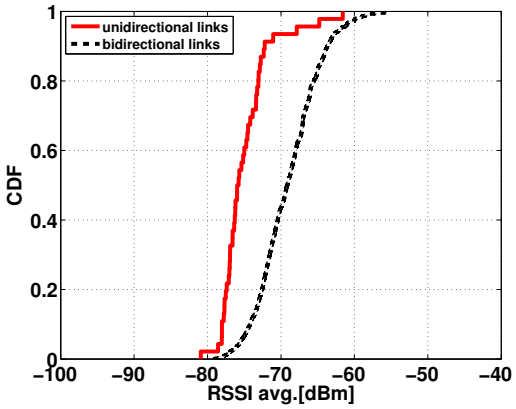

(c) 110 byte packets size at -10dBm.

Figure 3.18: The cumulative distribution function of unidirectional links (with a PRR>0% in just one direction) and the bidirectional links as a function of RSSI for CC1101 radio: a) 6 bytes, 0dBm, b) 110 bytes, 0dBm, c) 110 bytes, -10dBm.

Good Link proportion

First, we have presented a link classification as good ($PRR \geq 80\%$), intermediate ($20\% \leq PRR < 80\%$), bad ($0 < PRR < 20\%$) due to temporal fluctuation of hardware metrics. Moreover, we have observed a large proportion of good links. Also, we have noticed that third tray of Strasbourg platform reduces its RSSI of about 5dBm due to multipath presence.

Namely, we have identified on Strasbourg platform the factors affecting the link quality as multipath, shadowing, and interference. Multipath effect refers to *scattering* from wall, window, ceiling, or floor surfaces, *partial/total reflection* from glass fiber, wood poles, RJ45V cables, and *diffraction* from obstacles (poles-wood/cement, light

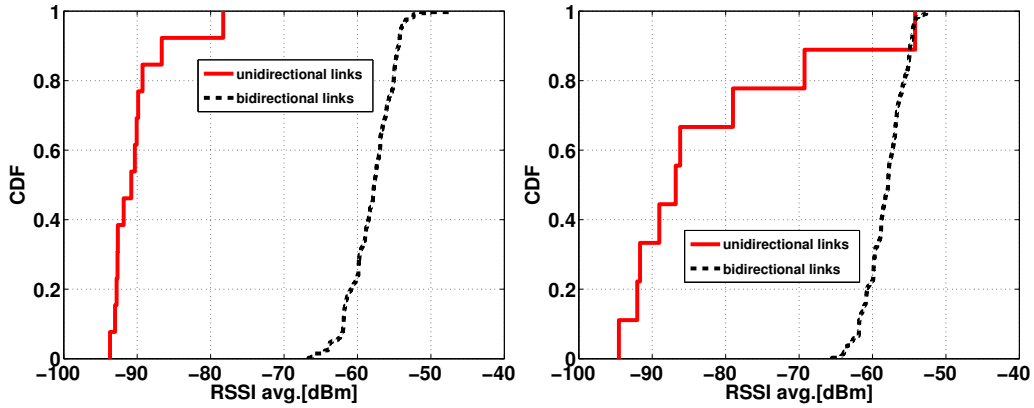

(a) 6 byte packets size at 0dBm.

(b) 110 byte packets size at 0dBm.

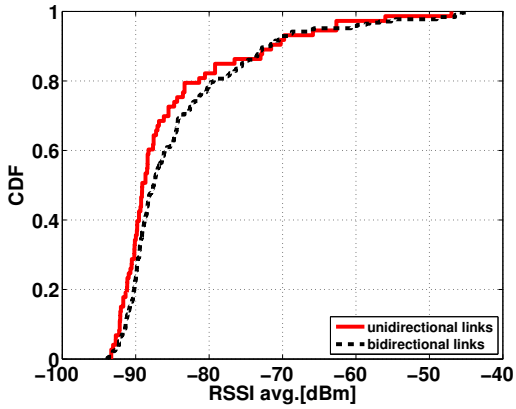

(c) 110 byte packets size at -10dBm.

Figure 3.19: The cumulative distribution function of unidirectional links (with a PRR>0% in just one direction) and the bidirectional links as a function of RSSI for CC2420 radio: a) 6 bytes, 0dBm, b) 110 bytes, 0dBm, c) 110 bytes, -10dBm.

lamps). The shadowing may occur from obstacles: poles on cement/wood. Last, the interference can occur due to the train presence that is equipped with mobile nodes.

Moreover, we have observed for CC1101 that an output power of 0dBm results in a majority of good links and a quite low proportion of intermediate links. The proportion of good links is not affected by varying the inter-packet interval (100ms, 200ms, 500ms, 1s, 30s), the packet size, also the power decrease to -10dBm slightly impacts the good links proportion.

However, in presence of the multipath effects and concurrent interference, the power decrease leads to a decay of good links of about 70%. Contrary to CC1101 where we observed a majority of good links (∼65%), CC2420 has a majority of intermediate links

(∼71%).

For CC2420, decreasing the output power to -15dBm and -25dBm leads to a link proportion decrease of good links with 80% and with 46% of intermediate. Similarly to CC1101, the inter-packet interval affects little the proportion of good links. Moreover, in terms of packet size, we observe that the proportion of good links for short packets is close to 90% and only ∼27% for long packets.

RSSI

We have noticed that the packet size and the inter-packet interval do not affect the probability density function of the averaged RSSI that concentrates around -65dBm (CC1101) and -75dBm (CC2420) at 0dBm output power. Besides, the probability density function of the standard deviation of RSSI encounters a low variation from 0.5 to 1.

We have noticed that links with a PRR above 99% are spread above -65dBm (CC1101)/-70dBm (CC2420) value that can be used as a threshold to discriminate good links, independent of the packet size. Howsoever, the threshold value does not depend on the output power neither on CC1101 nor on CC2420 radios.

Moreover, contrary to CC1101, the CDF curves of avg RSSI and std RSSI overlap less, which shows that avg RSSI and std RSSI can distinguish between good and intermediate links.

LQI

We can draw the conclusion that, for CC1101, good links show low variation of avg LQI and std LQI. On the other hand, intermediate (20%<=PRR<80%) and bad links (PRR less than 20%) have high average LQI and deviation LQI. Hence, bad links have higher average LQI and deviation LQI.

Link temporal fluctuation of link quality

The fluctuation of RSSI is about 0dBm to 4dBm for good links and increases for intermediate and bad links up to 10dBm. On the other hand, for CC2420, the RSSI variation is more important as the difference between minimum and maximum RSSI may reach 30dBm for bad links.

LQI has a minor temporal fluctuation while intermediate and bad links have a major temporal fluctuation on both radios (CC1101/CC2420).

Link asymmetry

We have observed that good links are less affected by the packet size or by output power decrease. In our study, intermediate and bad links present a high degree of asymmetry for both CC1101 and CC2420 radio chips. The asymmetry of intermediate links ($20\% \leq PRR < 80\%$) is not influenced by the packet size, whereas the decrease of the output power leads to a decay of links that present stable asymmetry. Contrastively, the packet size and the power decrease highly impact the asymmetry of bad links ($0 < PRR < 20\%$).

For instance, good links have an asymmetry below 20%, majority of intermediate links are characterized by an asymmetry between 20% and 80%. Bad links have a high asymmetry for CC1101 (a majority of strong asymmetry), and between 20% and 80% for CC2420.

3.8 Conclusions

Our analysis has shown that the network may benefit from a large proportion of good links on CC1101 and CC2420 (for 6 byte packet size).

The analysis of the CDF and PDF of RSSI (average, standard variance) and LQI (average, standard variance) enable us to observe that RSSI and LQI have distinct values—they can discriminate the quality of links.

However, on CC1101, avg RSSI may help to discriminate links with PRR=100%, since avg RSSI for links below PRR=100% overlap. Also, the deviation of RSSI (CC2420) can be an interesting measure, but not sufficient to discriminate link quality in an accurate manner.

Contrary to CC1101, the CDF curves of avg RSSI and std RSSI overlap less, which enables avg RSSI and std RSSI to distinguish better between good and intermediate links. For instance, RSSI variation is low on CC1101 (max. 10dbm), whereas for CC2420 it may reach about 30dBm.

In what it concerns asymmetry, we have observed that good links present stable asymmetry, while intermediate and bad links present intermediate and strong asymmetry for CC1101 and CC2420 radio chips. Besides, we found that the packet size and the power decrease highly impact the asymmetry of bad links ($0 < PRR < 20\%$).

We use the observations of empirical data of avg/std RSSI and avg/std LQI to find a mathematical model able to capture the link quality.

Chapter 4

Estimating Link Quality in an indoor Wireless Sensor Network

Contents

In this chapter, we analyze the link quality in a statistical way. Different empirical studies agreed on the fact that very good and very bad links can be discriminated using samples of physical metrics (RSSI, LQI). However, links with PRR<99% present significant temporal fluctuation, and large number of samples are needed to characterize the link quality.

To obtain an estimator of PRR, we have fitted a Fermi-Dirac function to the scatter diagram of the average and standard variation of LQI. The function enables us to find PRR for a given level of LQI. We evaluate the estimator by computing PRR over a varying size window of transmissions and comparing with the estimator. The aim of the estimator is to provide a better routing metric in wireless sensor networks.

4.1 Introduction

We want to design a metric that estimates PRR. Recent work on routing protocols emphasized the importance of using stable metrics of link quality .

Our observations from Chapter 3 helped to find the relationship between RSSI, LQI, and PRR. Moreover, we use RSSI as an indicator of possible anomalous behavior of sensor nodes. We characterize PRR in function of RSSI and LQI by looking for continuous distributions that fit the best the measured values of the PRR. We notify that RSSI is not a good discriminator of link categories, because the functions overlap for CC1101 and CC2420. The average LQI and the standard variation of LQI better discriminate between the categories. Our analysis confirms the main findings of the previous work and provides new insights on the link quality metrics based on LQI.

Fitting a Fermi-Dirac function to the scatter diagram of the average and standard variation of LQI, we have attained the estimation of the PRR. The found function facilitates the prediction of PRR from a given level of the average and standard deviation of LQI. To prove the functionality of the prediction, we compute PRR over variable size windows and compared the value against the estimated PRR, which we obtained from the fitting FD function.

The findings of this Chapter have been validated by the community as they have been accepted in Algotel [9] , PIMRC [10] conferences.

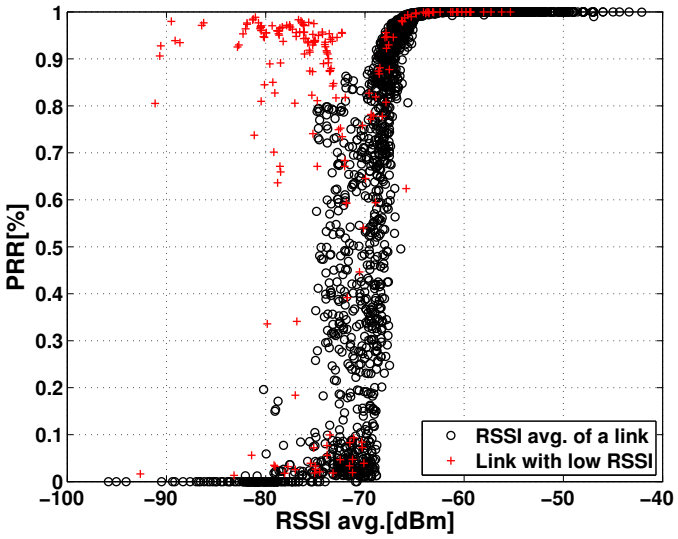

Figure 4.1: Scatter diagram of PRR in function of the average RSSI for each link.

4.2 Analysis of RSSI

We started with the analysis of RSSI and its influence on PRR for the second tray. Figure 4.1 presents the scatter diagram of PRR vs. the average RSSI for all links (each point corresponds to a link with a given average RSSI and the observed PRR). We can observe that some values (red crosses) lie in a region with high PRR and low RSSI values. The values indicate a possible anomalous behavior in the generation of RSSI values or another problem of hardware operation.

Figure 4.2 presents the distribution of the average RSSI measured by all nodes (one curve per node). A node receives packets from all other nodes placed in a regular pattern in the experiment area so that the expected range of RSSI values needs to smoothly vary from the sensitivity threshold to some large values. Cross distributions correspond to two nodes that generated the anomalous group in Figure 4.1. They are different from the distributions of other nodes.

On the contrary, on the CC2420 platform we are not aware of the existence of nodes with anomalous behavior.

Figure 4.3 shows the scatter diagram corresponding to Figure 4.1 with the two

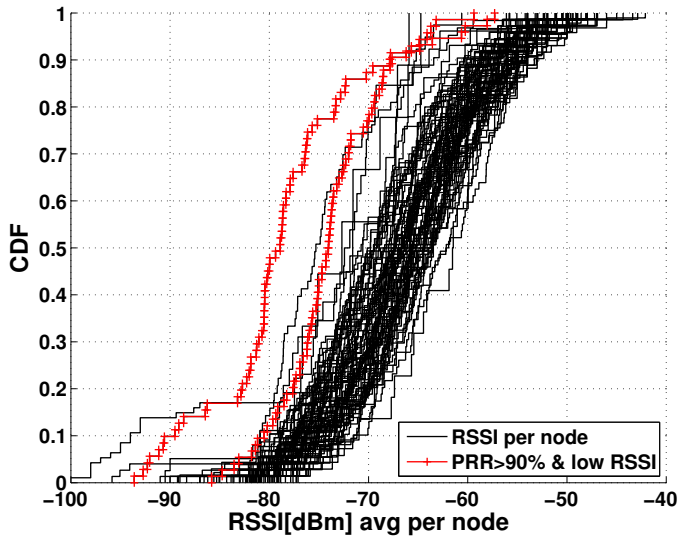

Figure 4.2: CDF of the measured average RSSI for each node (80 distributions in total). The distributions of two nodes are clearly different from other nodes.

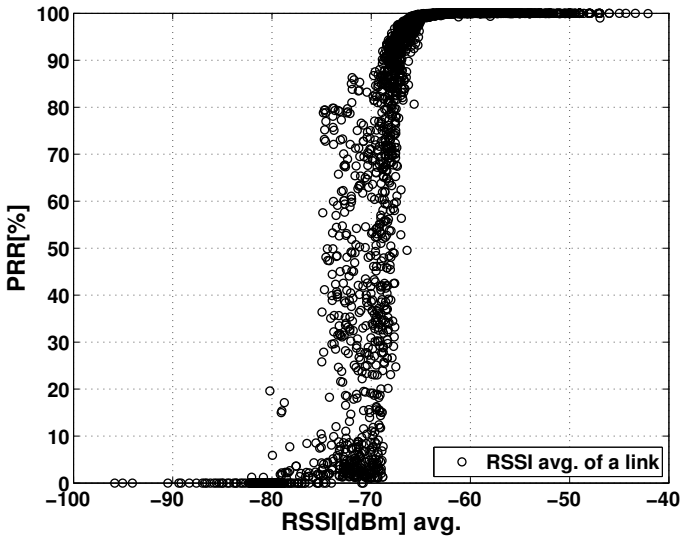

Figure 4.3: Scatter diagram of PRR in function of the average RSSI, two anomalous nodes eliminated.

anomalous nodes eliminated—crosses have disappeared. We believe that the RSSI analysis enables us to detect nodes with hardware anomalies or bad calibration that result in unlikely values of RSSI. In the case of our testbed, there are 2 anomalous nodes out of 80, a small proportion of bad nodes. We thus eliminate the results from the nodes to take away the bias of unlikely RSSI values.

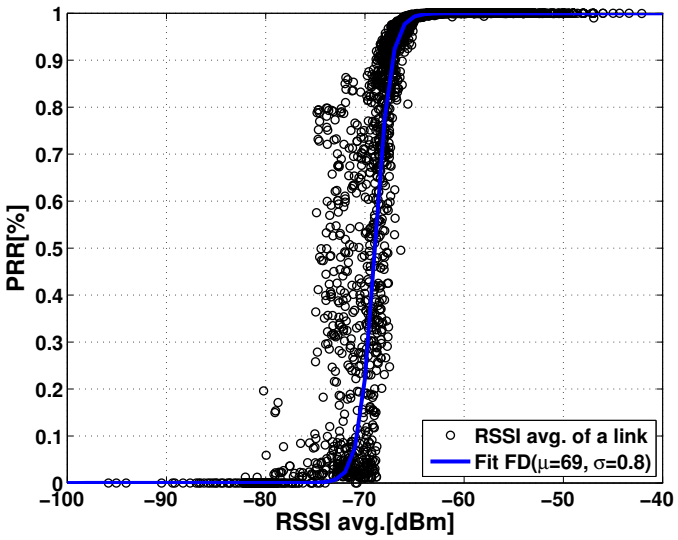

Figure 4.4: Fitting of the scatter diagram with a Fermi-Dirac function.

The next step is to explore the dependence between RSSI and PRR. Figure 4.4 presents the fitting of the scatter diagram with a Fermi-Dirac function of the form $f(x) = 1/(1 + \exp \frac{-(\mu - x)}{\sigma})$.

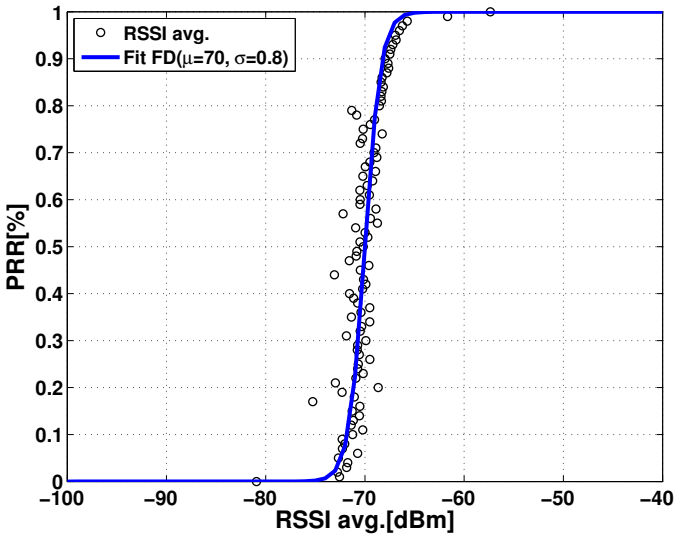

Figure 4.5: Fitting of the averaged RSSI.

We have also averaged the values of RSSI for each value of PRR (at the step of 1%)

and found the fitting function presented in Figure 4.5. We can see that the Fermi-Dirac function fits perfectly well PRR especially the values greater than 80%. We can use the function to determine a cutting threshold over which the RSSI results in a PRR of good links. The observation is valid as well for the first and third tray of Strasbourg platform.

4.3 Fitting the Distributions of RSSI and LQI

To further characterize PRR in function of RSSI and LQI, we have looked for continuous distributions that fit best the measured values of PRR. The goal is to predict PRR or at least the link category based on the observed values of RSSI and LQI. We have considered as candidate distributions the most common continuous distributions with a bounded, semi-infinite, variable support or unbounded see Table 4.1

Table 4.1: List of continuous distributions.

Bounded	**Semi-infinite**	**Variable support**	**Unbounded**
Beta	Chi-squared	Generalized Extreme Value	Cauchy
Johnson SB	Dagum	Generalized Pareto distribution	Gumbel Max
Logitnormal	Exponential	Phased Bi-Weibull	Gumbel Min
Dirac delta SB	Erlang	Wakeby	Johnson SU
Kumaraswamy	F Distribution		Logistic
Logarithmic	Fatigue Life		Normal
Pert	Frechet		Student's t
Reciprocal	Generalized Gamma		
	Log-Logistic		
	Lognormal		
	Nakagami		
	Pareto		
	Rice		
	Weibull		

We used Matlab as tool to find the best distribution fit for our data set. The distributions that fitted the best are the following:

- *Log-Logistic* distribution is defined by scale α, shape β, and location γ. Its Cumulative Distribution Function (CDF) is $F_{x;\alpha,\beta,\gamma} = (1 + (\beta/(x-\gamma)^{\alpha})^{-1}$. The Log-Logistic models the mid of the extreme values (highs and lows) of a data set of random variables.

- *Johnson SB* distribution has a bounded support that fits a bounded distribution to known moments and has CDF of $F_x = \phi(\gamma + \delta ln(z/(1-z)))$, where ϕ is the Laplace integral and z is defined as $(x-\xi)/\lambda$. It is parametrized with shape γ, two scale parameters δ and λ, and location parameter ξ.

- *Generalized Extreme Value* is a distribution that models the maxima of the extreme values of a data set. It is parametrized by shape ξ, scale σ, and location μ. Its CDF is
$F(x;\mu,\sigma,\xi) = \exp\left\{-\left[1+\xi\left(\frac{x-\mu}{\sigma}\right)\right]^{-1/\xi}\right\}$.

- *Beta* distribution is defined on the interval $[0,1]$ with two positive continuous shape parameters α and β. Its CDF is $F(x;\alpha,\beta) = B(x;\alpha,\beta)/B(\alpha,\beta) = I_x(\alpha,\beta)$, where $B(x;\alpha,\beta)$ is the incomplete beta function and $I_x(\alpha,\beta)$ is the regularized incomplete beta function. The incomplete beta function is the following: $B(x;\,a,b) = \int_0^x t^{a-1}\,(1-t)^{b-1}\,dt$.

We have used three common statistical tests: Kolmogorov-Smirnov, χ^2, and Anderson-Darling [36] to find the best distributions.

First, we account for the *Kolmogorov-Smirnov test (K-S)* [36], a nonparametric test. One-sample K–S test verifies the equality of a sample with a distribution probability reference. Especially, it estimates the vertical distance between the empirical distribution function (ECDF) of the chosen sample and cumulative distribution function (CDF) of the reference distribution, see Eq. 4.1. For two-sample K-S case, it quantifies the distance between the EDF of two data samples. The principle of the test is based on the null hypothesis that data sample is derived from the reference continuous distribution (one-sample K-S), or that both data samples follow the same distribution (two-sample K-S).

The K-S test applies only to continuous distributions, and is characterized by two hypotheses: H_0, the data follows a specific distribution, H_a the data do not follow a specific distribution, and test statistic (D), Eq. 4.1.

$$D_{K-S} = max_{1\leq i\leq N}(F(Y_i) - \frac{i-1}{n}, \frac{i}{n} - F(Y_i)), \tag{4.1}$$

where N is the number of data points, F is the theoretical cumulative distribution of the tested distribution, and $Y_1, Y_2, ..., Y_N$, are the data points.

For instance, we use the one-sample K-S where as data sample we consider averaged RSSI, averaged LQI, and standard deviation LQI. As reference continuous distributions, we use the distributions from Table 4.1.

We make use of another test, *Chi-Square test* [36]. The test compares an empirical distribution with another one. Data sample distribution approximate a chi-square distribution if the null hypothesis is true, which means that the observed distribution is close to the expected one. The test relies on Eq. 4.2.

$$\chi^2 = \sum(\frac{(O-E)^2}{E}) \tag{4.2}$$

where O is the observed distribution, E is the expected distribution.

Another test is the *Anderson-Darling test (A-D)* [36]. It evaluates if the data sample set comes from a specific distribution. For example, the test verifies if a sample set $(x_1, ..x_k)$ comes from a given distribution using the Eq. 4.3.

$$A^2 = -k - \sum_{i=1}^{n} \frac{(2i-1)}{n} [ln(F(x_i)) + ln(1 - F(x_{k+1-i}))] \tag{4.3}$$

where N is the number of data samples in the set, F is the cumulative distribution function of the chosen reference distribution.

We group into three categories (good, intermediate, and bad). Furthermore, for each link category group, we run fit tests on candidate distributions. To decrease the number of samples to handle, we average the measured values of LQI and RSSI for each link.

Figure 4.6 a)– shows that Johnson SB and Gamma density functions fit best the averaged RSSI. We can observe that average RSSI is not a good discriminator of link categories, because the functions overlap. Even the bad category overlaps the category of good links. Alike on CC1101, Figure 4.6 b) illustrates that on the CC2420 radio chip, RSSI is best fitted by Johnson SB and Gamma functions. Moreover, RSSI is not able to discriminate the quality of the links as the functions overlap.

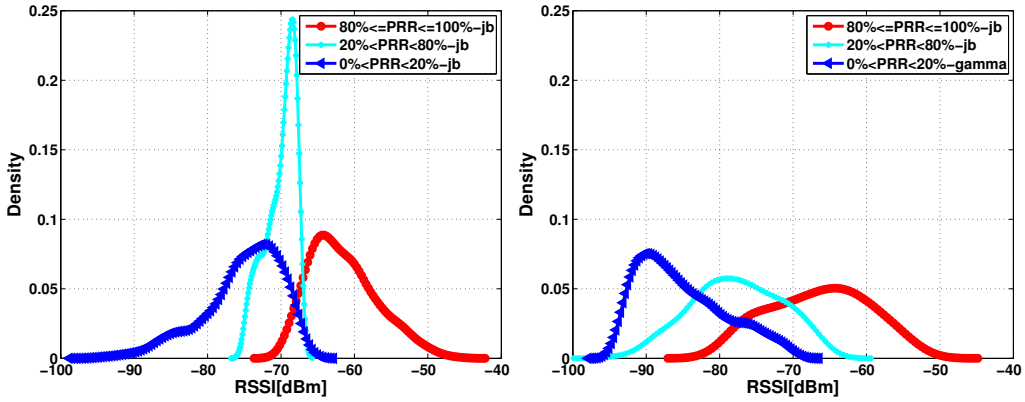

(a) Fit for CC1101.

(b) Fit for CC2420.

Figure 4.6: Density functions fitting the average RSSI: a) CC1101, b) CC2420.

The average LQI better discriminates between the categories, especially it can distinguish between good and bad links on both radios, CC1101 and CC2420. Figure 4.7 a)–depicts the best fitted functions for the averaged LQI, such as Generalized Extreme Value as well as Beta, and Johnson SB. Also, shifting to CC2420 radio, Figure 4.7 b) shows that Generalized Extreme Value and Johnson SB fit best the average LQI.

Observing the standard deviation of RSSI, we encountered a low deviation, about 1 for CC1101 that is insufficient to discriminate categories, whereas, for CC2420, the RSSI deviation is higher, about 5 for good and intermediate links, and concentrate about 20 for bad links, Figure 4.10. So, we claim that the deviation of RSSI can discriminate good from bad categories on CC2420.

Figure 4.8 a) depicts that for CC1101, the standard deviation of LQI is also a good

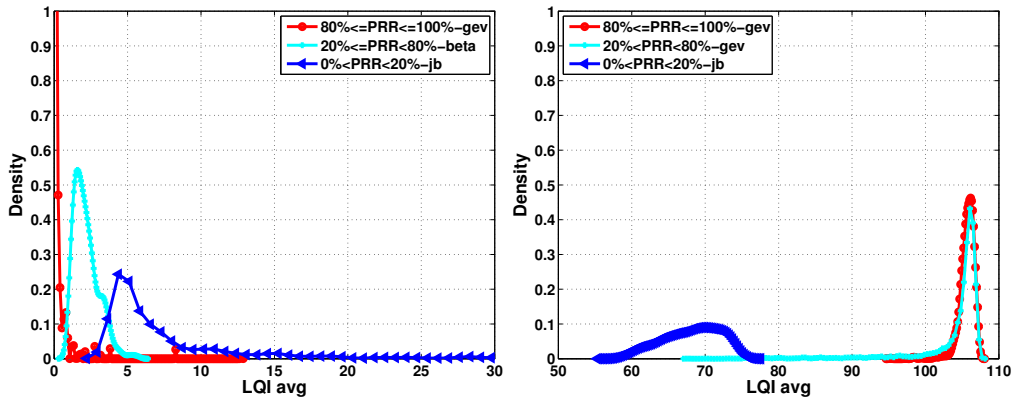

(a) Fit for CC1101. (b) Fit for CC2420.

Figure 4.7: Density functions fitting the average LQI: a) CC1101, b) CC2420.

discriminator of the link categories. Besides, for CC2420 radio, Figure 4.8 b) shows that LQI deviation can discriminate good from bad categories, same as the average LQI.

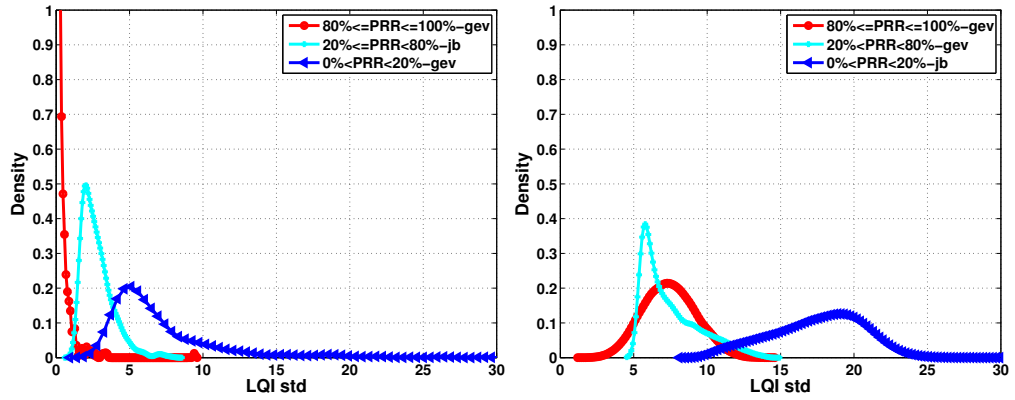

(a) Fit for CC1101. (b) Fit for CC2420.

Figure 4.8: Density functions fitting the standard deviation of LQI: a) CC1101, b) CC2420.

Figure 4.9 brings another view on the variability of LQI. It presents LQI for all packets (correctly decoded and with bad CRC) for choosing links with PRR of 100%, 80%, 20%, and 0.06%. We can observe that the average LQI and its variability increases for lower PRR.

To sum up, using average RSSI metric, bad link category overlaps the category of good links. Therefore, it cannot discriminate the link categories. Thus, the standard deviation of RSSI varies too little on CC1101, instead, on CC2420 radio, it varies more,

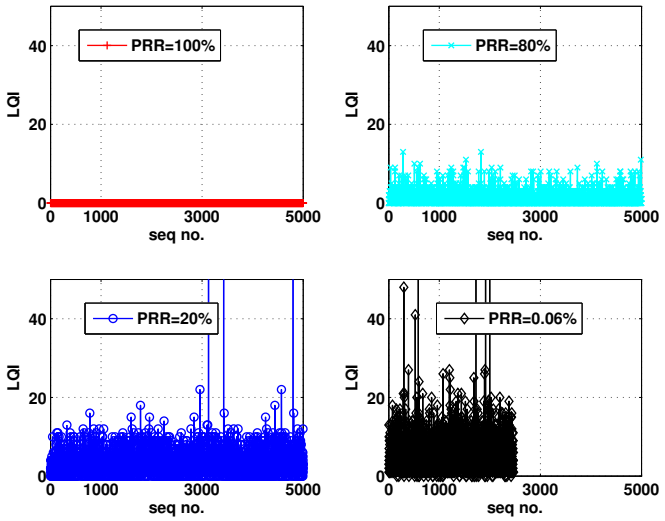

(a) CC1101 radio chip.

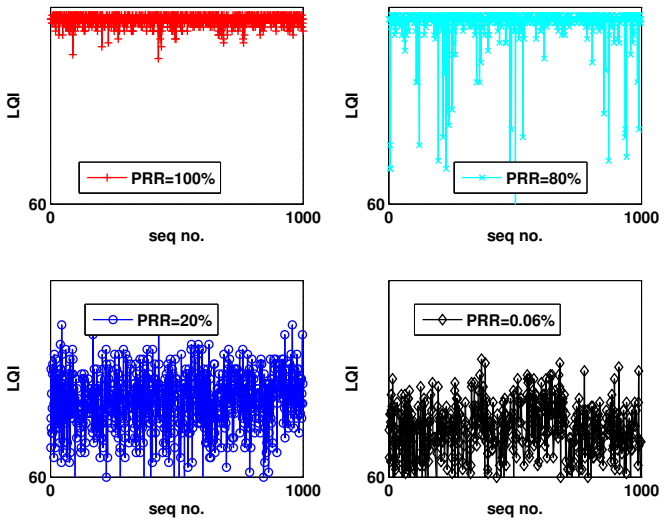

(b) CC2420 radio chip.

Figure 4.9: LQI variation of a link with PRR of 100%, 80%, 20%, and 0.06%, on CC1101 a), on CC2420 b).

so it can discriminate good from bad link categories.

On the other hand, the average LQI discriminates better between the categories, especially it can distinguish good from intermediate and bad links on CC1101 radio chip, and good and intermediate for bad links on the CC2420 radio chip. We can also observe that the standard variation of LQI is also a good discriminator of the categories for CC1101, and same as LQI average it can correctly discriminate bad from good and

intermediate links on CC2420 radio.

4.4 Fitting PRR in Function of RSSI and LQI

Figure 4.10 b) depicts the Fermi-Dirac function fit over the scatter diagram of the standard deviation of RSSI. We observe that the deviation of RSSI can easily discriminate good and intermediate from bad links, still, it overlaps for the good and intermediate links. Therefore, analyzing the average and the standard deviation for RSSI and LQI on CC2420, we found out that the ratio between RSSI std./LQI avg. fits well the F-D function, Figure 4.10 c). Hence, it discriminates best good from intermediate and bad links. In fact, we have obtained a goodness of the ratio fit characterized by: SSE: 0.2338, R-square: 0.9711, Adjusted R-square: 0.9708, and a RMSE: 0.0491.

We have applied a similar approach to LQI—fitting a Fermi-Dirac function to the scatter diagram of the average and standard variation of LQI (we use the logarithmic scale).

For CC1101, Figure . 4.11 a) displays a good fit for average LQI, accordingly LQI can discriminate the link categories. However, on CC2420, Figure . 4.11 b) presents a not so good fit of average LQI, thus, average LQI is insufficient to discriminate link categories.

On the other hand, the F-D function fits very well (with the R-value >0.98) the standard deviation of LQI, 4.12 a)–b) present the corresponding result.

4.5 Estimating PRR using F-D function

We want to find an estimator of PRR based on the measured values of RSSI and LQI. We have fitted PRR in function of RSSI, so possibly we could derive PRR from a given value of RSSI. However, using RSSI may lead to errors in the evaluation of PRR in the case of real networks—they experience contention between nodes and simultaneous transmissions. Concurrent transmissions may increase RSSI and decrease the probability of correct decoding leading to a lower PRR. In this case, the estimation based on RSSI would result in wrong values of the PRR. So, we have decided to focus on LQI and analyze estimators based on its average value and standard deviation.

First, we try to understand the impact of the window size. Figure 4.14 shows that short window of 5 presents much higher short term fluctuation which leads to link instability. Still, a good link estimator should ensure a good trade between short and long term shifts. Further we concentrate on the windows of 10 and 100 as they present less short fluctuations.

Figure 4.13 shows the temporal behavior of PRR computed over a window of 10 transmissions and its estimator derived from the average LQI. We can observe a fairly good fit between the data real PRR computed over a window of 10 and estimated PRR from the obtained Fermi-Dirac fit.

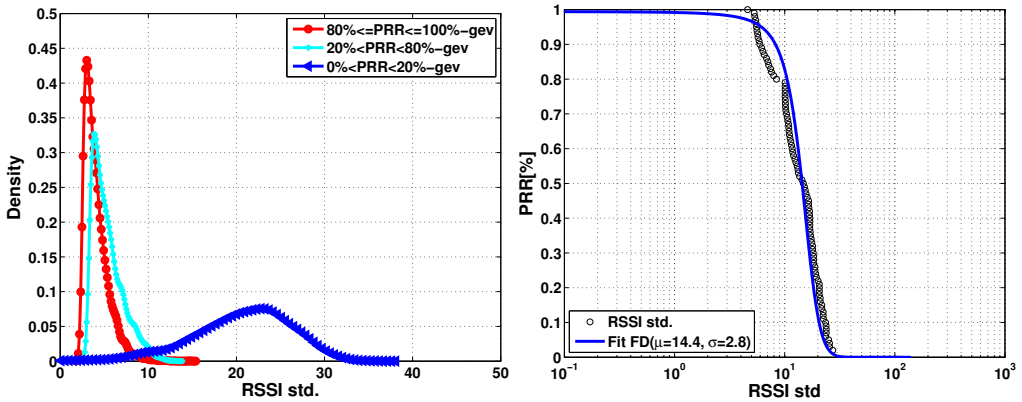

(a) Density fit of std RSSI

(b) FD fit of std RSSI

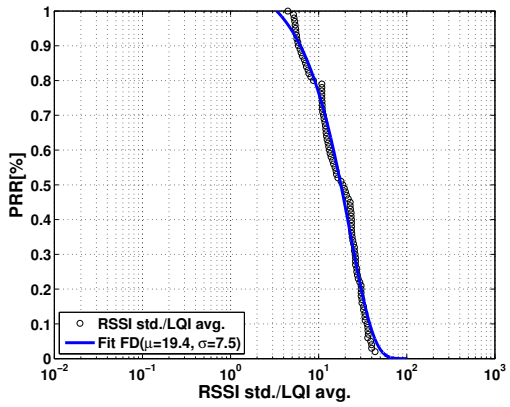

(c) FD fit of std RSSI/avg LQI.

Figure 4.10: Fitting the density and Fermi-Dirac function of the standard deviation of RSSI on CC2420: a) Fitting the density functions on standard deviation of RSSI, b) Fitting F-D on standard deviation of RSSI, c) Fitting F-D on the radio function, std RSSI/ avg LQI over links.

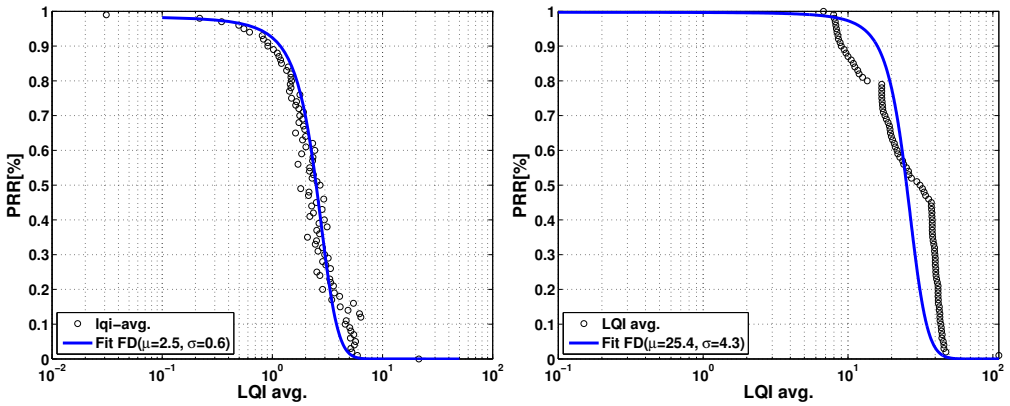

(a) CC1101 radio chip. (b) CC2420 radio chip.

Figure 4.11: Fitting averaged LQI over links.

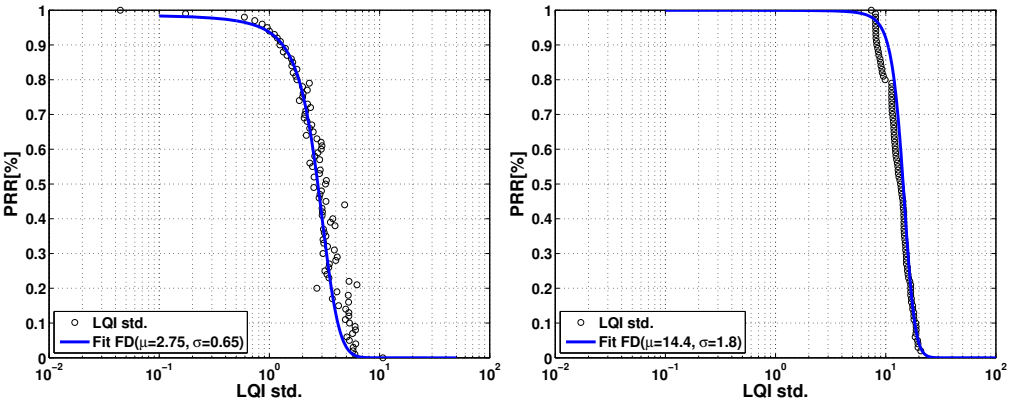

(a) CC1101 radio chip. (b) CC2420 radio chip.

Figure 4.12: Fitting the standard deviation of LQI averaged over links: a) CC1101, b) CC2420.

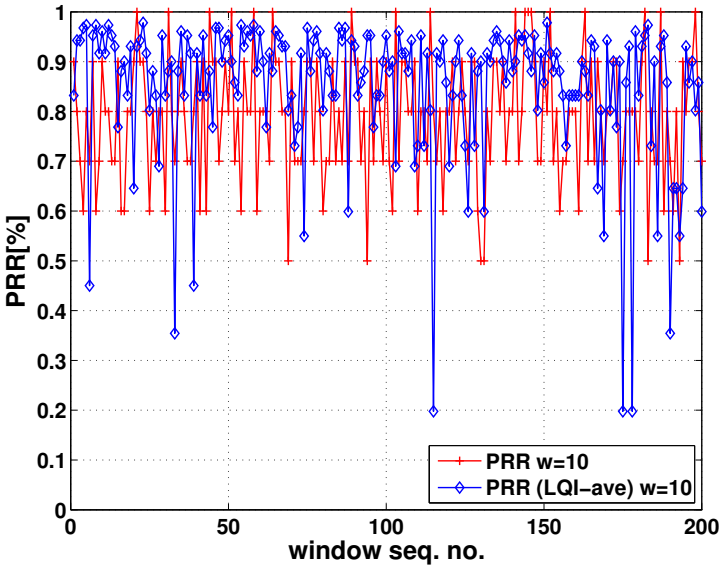

Figure 4.13: Estimation of the PRR for a link with PRR 80% with w=10. PRR vs. LQI avg.

We have tested several estimators based on the values computed on window w: $\overline{LQI}$, average LQI, $\overline{STD}$, the standard deviation of LQI, and $sqrt(\overline{LQI}^2 + \overline{STD}^2)$, the geometric mean of the previous ones. We have also derived the estimator of PRR from a moving average of LQI:

$$EWMA(\alpha, n) = EWMA(\alpha, n-1) * \alpha + (1-\alpha) * LQI \tag{4.4}$$

where $0 < \alpha < 1$.

We have considered two values of the window $w = 10, 100$.

Tables 4.2, 4.3, 4.4 present the precision of the estimators for a single link in terms of several standard error measures: AE (Absolute Error), MSE (Mean Square Error), RMSE (Root Mean Square Error).

The MSE si given by the eq. 4.5.

$$MSE(model) = \frac{1}{n} \sum_{i=1} n(prediction_i * true\_value_i) \tag{4.5}$$

We can observe that for a short window of 10 the estimation based on LQI results in an error of the order of 18% (RMSE). Considering larger windows reduces the error to 9%. EWMA with $\alpha = 0.9$ also results in a good precision for a good link.

However, tables 4.5, 4.6, 4.7 illustrate for the totality of good links the estimation triggers a precision of 93% and for a window of 10 and about 95% for a window of 100 (for EWMA with $\alpha = 0.9$, $\overline{LQI}$, and $sqrt(\overline{LQI}^2 + \overline{STD}^2)$). Oppositely, for intermediate and bad links the estimator triggers a precision of about 80%.

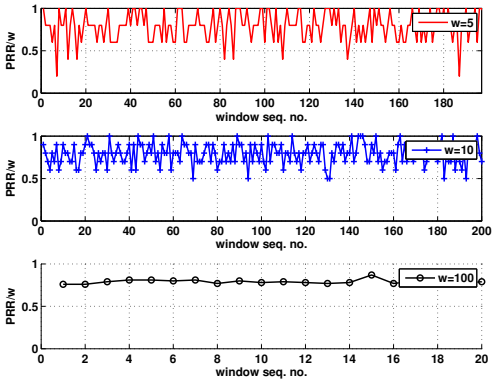

(a) PRR of link 23 → 58.

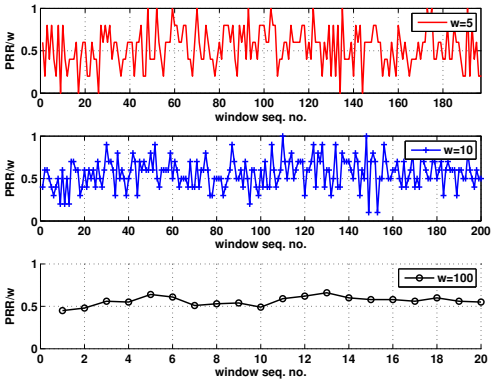

(b) PRR of link 69 → 19.

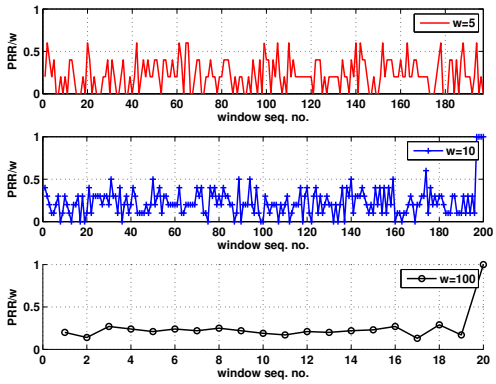

(c) PRR of link 6 → 51.

Figure 4.14: Temporal fluctuation of PRR for links: 23 → 58 with PRR 80%, 69 → 19 with PRR 50%, and 6 → 51 with PRR 20% and with a window w∈{5,10,100}.

Table 4.2: Error of estimating PRR for a link (mean PRR of 80%).

Estimator	$MSE, w = 10$	$MSE, w = 100$	$RMSE, w = 10$	$RMSE, w = 100$
$\overline{LQI}$	0.035	0.012	0.187	0.109
$\overline{STD}$	0.058	0.010	0.240	0.100
$EWMA_{LQI}(\alpha = 0.1)$	0.094	0.060	0.306	0.244
$EWMA_{LQI}(\alpha = 0.5)$	0.075	0.043	0.264	0.207

Table 4.3: Error of estimating PRR for a link (mean PRR of 50%).

Estimator	$MSE, w = 10$	$MSE, w = 100$	$RMSE, w = 10$	$RMSE, w = 100$
$\overline{LQI}$	0.081	0.039	0.284	0.197
$\overline{STD}$	0.157	0.197	0.390	0.443
$\overline{sqrt(\overline{LQI}^2 + \overline{STD}^2)}$	0.099	0.071	0.301	0.266
$EWMA_{LQI}(\alpha = 0.1)$	0.194	0.177	0.440	0.420
$EWMA_{LQI}(\alpha = 0.5)$	0.178	0.159	0.421	0.398
$EWMA_{LQI}(\alpha = 0.9)$	0.137	0.203	0.370	0.450

Table 4.4: Error of estimating PRR for a link (mean PRR of 20%).

Estimator	$MSE, w = 10$	$MSE, w = 100$	$RMSE, w = 10$	$RMSE, w = 100$
$\overline{LQI}$	0.03	0.04	0.173	0.200
$\overline{STD}$	0.076	0.040	0.275	0.200
$\overline{sqrt(\overline{LQI}^2 + \overline{STD}^2)}$	0.044	0.034	0.209	0.184
$EWMA_{LQI}(\alpha = 0.1)$	0.158	0.205	0.397	0.452
$EWMA_{LQI}(\alpha = 0.5)$	0.076	0.099	0.275	0.314
$EWMA_{LQI}(\alpha = 0.9)$	0.054	0.062	0.232	0.248

Table 4.5: Error of estimating good links (mean PRR of [80%-100%]).

Estimator	$AE, w = 10$	$AE, w = 100$	$MSE, w = 10$	$MSE, w = 100$	$RMSE, w = 10$	$RMSE, w = 100$
$\overline{LQI}$	0.063	0.032	0.010	0.002	0.100	0.044
$\overline{STD}$	0.07	0.037	0.017	0.004	0.130	0.063
$\overline{sqrt(\overline{LQI}^2 + \overline{STD}^2)}$	0.06	0.028	0.009	0.003	0.094	0.054
$EWMA_{LQI}(\alpha = 0.1)$	0.048	0.032	0.025	0.021	0.158	0.144
$EWMA_{LQI}(\alpha = 0.5)$	0.037	0.028	0.014	0.007	0.118	0.083
$EWMA_{LQI}(\alpha = 0.9)$	0.033	0.021	0.005	0.001	0.071	0.031

Table 4.6: Error of estimating intermediate links (mean PRR of [20%-80%]).

Estimator	$AE, w = 10$	$AE, w = 100$	$MSE, w = 10$	$MSE, w = 100$	$RMSE, w = 10$	$RMSE, w = 100$
$\overline{LQI}$	0.211	0.161	0.072	0.039	0.268	0.197
$\overline{STD}$	0.244	0.181	0.094	0.061	0.306	0.246
$\overline{sqrt(\overline{LQI}^2 + \overline{STD}^2)}$	0.197	0.144	0.062	0.038	0.248	0.194
$EWMA_{LQI}(\alpha = 0.1)$	0.290	0.288	0.159	0.140	0.398	0.374
$EWMA_{LQI}(\alpha = 0.5)$	0.255	0.254	0.128	0.110	0.357	0.331
$EWMA_{LQI}(\alpha = 0.9)$	0.191	0.207	0.076	0.064	0.275	0.252

Table 4.7: Error of estimating bad links (mean PRR of (0%-20%)).

Estimator	$AE, w = 10$	$AE, w = 100$	$MSE, w = 10$	$MSE, w = 100$	$RMSE, w = 10$	$RMSE, w = 100$
$\overline{LQI}$	0.160	0.158	0.047	0.216	0.034	0.464
$\overline{STD}$	0.225	0.150	0.088	0.291	0.296	0.539
$\overline{sqrt(\overline{LQI}^2 + \overline{STD}^2)}$	0.166	0.133	0.048	0.215	0.219	0.463
$EWMA_{LQI}(\alpha = 0.1)$	0.285	0.280	0.171	0.190	0.410	0.437
$EWMA_{LQI}(\alpha = 0.5)$	0.200	0.240	0.118	0.170	0.343	0.412
$EWMA_{LQI}(\alpha = 0.9)$	0.190	0.320	0.109	0.290	0.330	0.538

4.6 Conclusion

In this chapter, we have reported on the results of measurements of PRR, RSSI, and LQI on an indoor wireless sensor network testbed. First, we have analyzed RSSI and used it as an indicator of possible anomalous behavior of sensor nodes.

To further characterize PRR in function of RSSI and LQI, we have looked for continuous distributions that fit the best the measured values of the PRR. As RSSI is not a good discriminator of link categories, we have considered the average LQI and its standard variation.

We have found the density functions that fit the observed values for each link category such as Generalized Extreme Value, Johnson SB or Beta.

We have obtained an estimate of PRR by fitting the Fermi-Dirac function to the scatter diagram of the average and standard variation of LQI on both radio chip-set CC1101 and CC2420. The function decides on the level of PRR of a link from the average or standard deviation of LQI. To evaluate the estimator, we have varied the size of the observation window from 1 to 100. We have observed that at the window size of 10, we reach low MSE (0.005–0.02).

Chapter 5

Analysis of Packet Loss with 2-state Gilbert-Elliot Model

Contents

In this chapter, we aim at better understanding of channel fluctuations by investigating the number of successfully transmitted packets before a loss as well as the number of consecutive losses on 802.15.4 links.

Once we have found the PRR estimator, we want to capture the short term link dynamics. Therefore, we propose to use the Gilbert model, a 2-state Markov model, to compute the stationary probabilities to discriminate high variable link qualities. We end up the chapter by presenting our algorithm to estimate PRR across a link, derived from the obtained fitting function and the 2-state Markov model.

5.1 Introduction

In this chapter, we apply the Gilbert model, a 2-state Markov model, to packet reception sequences and the average and standard deviation values of LQI to estimate the short term PRR across high variable links. We end up by discussing the algorithm to estimate PRR employing the FD fitting function and the stationary probabilities of the 2-state Markov model.

5.2 Gilbert-Elliot (GE) Model

The GE model is widely used to represent the state of a channel (good, bad) by analyzing the errors on the channel [29] (cf. Figure 5.1). The model is memoryless as the next state depends only on the current state. The approach is simple, it has two states, a good state interprets a successful symbol arrival and a bad state denotes

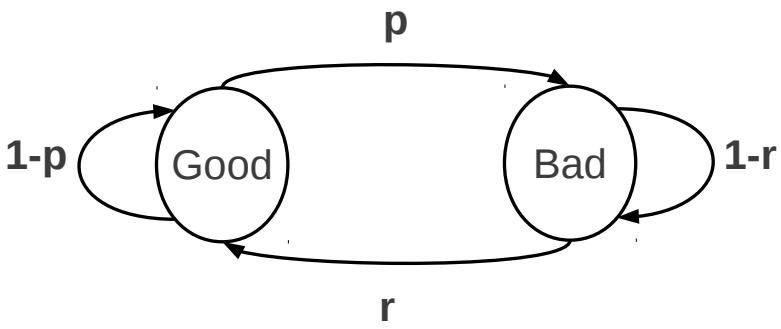

Figure 5.1: Transition probabilities of Gilbert-Elliot: 2-state Markov diagram. Good state represents a better quality channel whereas Bad state corresponds to a lower quality channel.

an erroneous symbol. In communication networks, it is used to capture the temporal correlation of packet losses [33]. To study the loss length using the two state Gilbert-Elliot model, we consider the packet reception process as a sequence of bits. Therefore, a value of 1 stands for a successful packet reception whereas a 0 value denotes a lost or corrupted packet. The GE model is shown in Figure 5.1.

It is defined by the transition matrix M between states s_t at time t:

$$M = \begin{pmatrix} 1-p & p \\ r & 1-r \end{pmatrix}$$

where $p = P(s_t = Bad|s_{t-1} = Good)$, and $r = P(s_t = Good|s_{t-1} = Bad)$, $0 < p < 1$ and $0 < r < 1$ are the transition probabilities between states, respectively.

A transition from Good (G) state to Bad (B) state takes place whenever the current packet is lost when the previous one was successful. In the opposite direction, a transition from Bad (B) to Good (G) state takes place whenever the current packet is successfully received, but the previous one was lost. The conditional loss probability of remaining in the good state (probability that a loss arises after a success) is given by $p = P(s_t = Bad|s_{t-1} = Good)$ while the conditional loss probability remaining in the bad state is denoted by $1 - r$, where $r = P(s_t = Good|s_{t-1} = Bad)$ (probability that a loss arises after a loss).

The stationary probability of the Good state π_G and the Bad state π_B are given by:

$$\pi_G = \frac{r}{p+r}, \quad \pi_B = \frac{p}{p+r}. \tag{5.1}$$

Considering the given stationary state probabilities, the loss probability is defined as:

$$\pi_{loss} = p * \pi_G + (1-r) * \pi_B = \pi_B \tag{5.2}$$

Parameter μ called *channel memory* is defined as:

$$\mu = 1 - p - r, \ -1 \leq \mu \leq 1. \tag{5.3}$$

When $\mu = 0$, the probability of getting a good or a bad symbol at any time instance is independent of the last symbol value, that is, the channel behaves as a *memory-less channel*. μ becomes negative for oscillatory links.

To show how the parameters of the GE model can be obtained from link loss observations, let us consider that the first link has $sequence_1 = [011110]$ (1 denotes a received packet, 0 denotes a lost packet). The second link is characterized by $sequence_2 = [101011]$. We see that $sequence_1$ has 4 consecutive successful packet receptions whereas $sequence_2$ records only 2.

Transition matrices $M_1(p_1, r_1)$, $M_2(p_2, r_2)$ for sequence 1 and 2 are the following:

$$M_1 = \begin{pmatrix} 0.75 & 0.25 \\ 1 & 0 \end{pmatrix}$$

$$M_2 = \begin{pmatrix} 0.33 & 0.66 \\ 1 & 0 \end{pmatrix}$$

We obtain the following transition probabilities: the first link has $p_1 = 0.25$ and $r_1 = 1$, and the second link has $p_2 = 0.66$ and $r_2 = 1$.

Table 5.1: Performance for $Link_1$ and $Link_2$.

Link	PRR	p	r	π_G	π_B	π_{loss}	μ
1	0.67	0.25	1	0.8	0.2	0.2	-0.25
2	0.67	0.66	1	0.6	0.39	0.39	-0.66

Table 5.1 summarizes the performance derived from the GE model applied to $Link_1$ and $Link_2$. Moreover, even if both links have a the same $PRR = 0.67$ (67%), $Link_1$ would be preferred over $Link_2$ as it records a higher good stationary probability (π_G of about 0.8 compared to 0.6) and a higher negative channel memory ($\mu = -0.25$ indicating that $Link_1$ is less oscillatory than $Link_2$ with $\mu = -0.66$).

The aim of the study is to use the stationary probabilities given by the GE model in link quality election and therefore, avoid links that are have faster oscillations between two states.

5.2.1 Experimental results

We call a *run length* the number of consecutive successful reception of packets and a *loss length* the number of consecutive lost packets.

Figure 5.2 a) shows that the distribution of packet losses and successful receptions depends on the link category. For instance, 98% of good links have an average 1.6 loss length, meaning that the probability of having consecutive lost packets is low. We have observed large average loss length of about 5.3 for intermediate links and about 56.8 for bad links, which shows that good links have independent losses with respect to intermediate and bad links. Yet, bad links may have bad states that last seconds.

Figure 5.2 b) illustrates that run length also varies in function of link category. Good links stick to good state for long periods, instead bad links have a quite small

run length, about 1. This means that after only one successful reception most probably bad links go to bad state.

Figure 5.2 c)–d) show that good and bad stationary probabilities can discriminate quite well link categories.

Studying the performance of μ metric, Srinivasan et al. [84] concluded that μ metrics cannot track the long term channel state. Computing the μ metric for each link, we do not obtain any interesting result as the curves overlap (cf. Figures 5.2 e) and 5.3 e)). We can conclude that μ metric is insufficient to distinguish accurately the quality of links.

Changing the radio to CC2420, we have observed that loss length is below 1.5 for good links and increases linearly with the link quality decrease (see Figure 5.3 a). Run lengths continue to be low for bad links (about 1) and high for good links (above 5), Figure 5.3 b).

Again, good stationary probability (π_G) discriminates links categories as it takes values within: 0.8-1 (good links), 0.6-0.8 (intermediate links), and 0-0.2 (bad links), Figure 5.3 c). Figure 5.3 d) depicts that bad state stationary probability (π_B) distinguishes also well link categories (0-0.2–good links, 0.2-0.4–intermediate links, 0.8-1–bad links).

Varying inter-packet interval

First, we have considered the impact of data dissemination frequency. For this reason, we vary the inter-packet interval within 100ms and 30s.

Figure 5.4 exhibits an increase with 15% of the proportion of loss lengths below 2 for IPTs above 1s. This effect is due to the expansion of the good links proportion for IPT of 1s or 30s as shown in Section 3, cf. Table 3.6.

Table 5.2 reports that run lengths are slightly affected by IPT (i.e., good links have a run length of 74 at 100ms and 88 at 500ms), still, bad links have independent successful reception, having a run length average of 2. Besides, loss lengths for good and bad links do not depend on IPT values. However, loss lengths of intermediate links may decay at larger IPTs.

For a better understanding of Table 5.2, Figure 5.5 a) illustrates that loss lengths for good links have an average less than 1 for each IPT of 100ms, 200ms, and 500ms. Observation that proves that upper layers should consider to adapt their parameters to access the channel based on the quality of the link they rely on.

Figure 5.5 b) shows that intermediate links have losses with low correlation whereas bad links have strong correlated losses (i.e., from 4s to 28s).

The table shows as well that transition probabilities $P(Good|Bad)$ and $P(Bad|Good)$ do not depend on IPT values. For instance, a low $P(Good|Bad)$ (i.e. 0.03) indicates that there are few transitions from Good to Bad state over the link. On the contrary, a low transition probability, $P(Bad|Good)$, demonstrates that links tend to preserve their bad state.

Table 5.3 presents the performance given by the 2-state Markov model in terms of stationary state probabilities π_G, π_B, loss probability π_{Loss}, and μ metric. We see that a good link has high π_G (0.96), low π_B (0.03), and low π_{Loss} ($\sim$0.03).

Packet size decrease

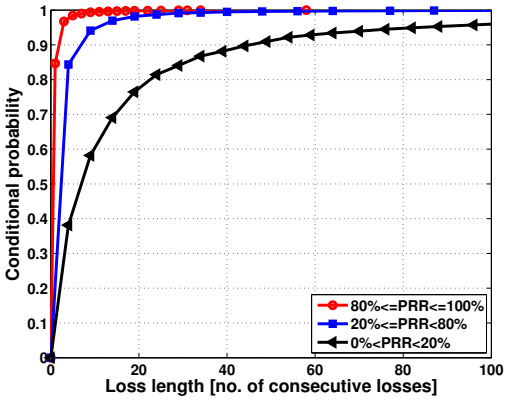

(a) Packet loss length.

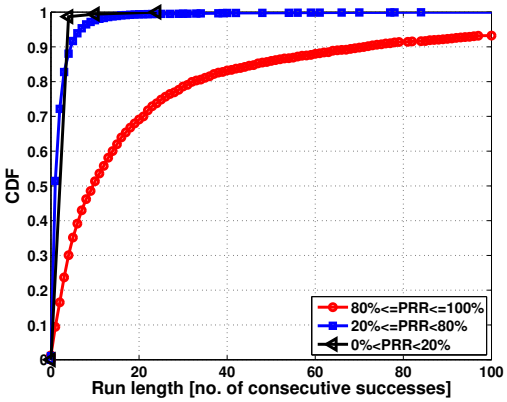

(b) Packet run length.

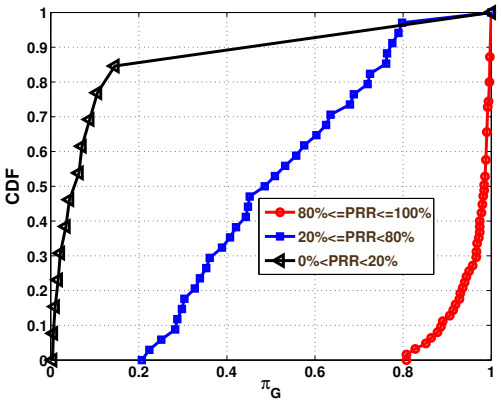

(c) Good state stationary probability π_G.

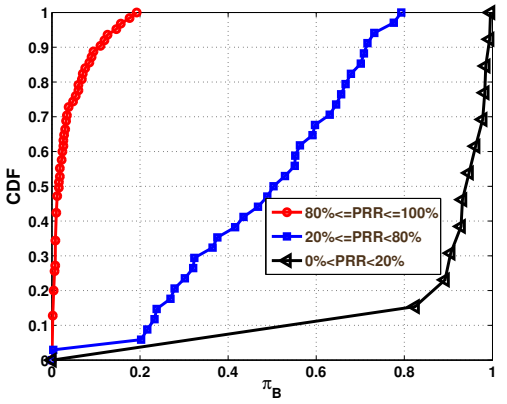

(d) Bad state stationary probability π_B.

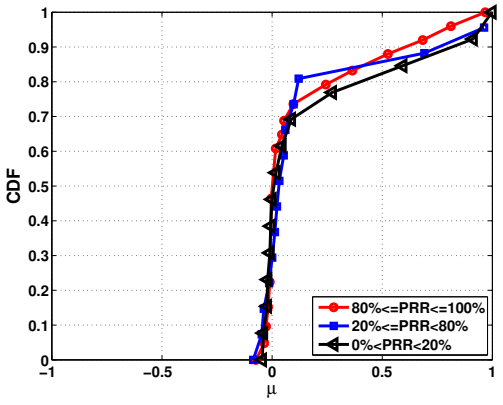

(e) Channel memory μ.

Figure 5.2: Cumulation Distribution Function for each link category: good, intermediate, bad for a) packet loss length, b) packet run length, c) stationary probability in good state π_G, d) stationary probability in bad state π_B, and e) channel memory μ on CC1101, 110B, 0dBm.

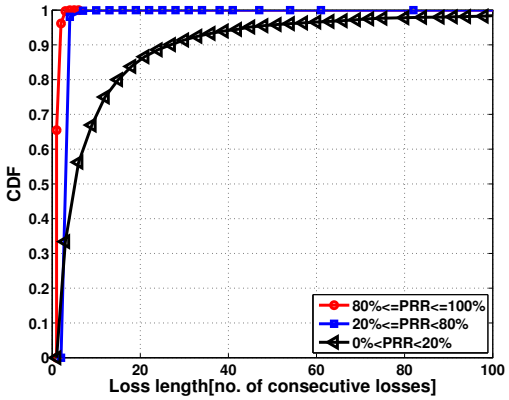

(a) Packet loss length.

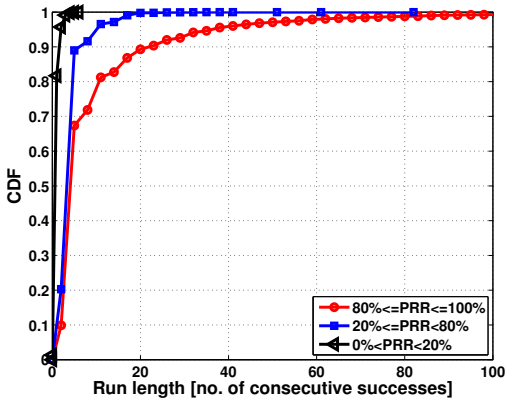

(b) Packet run length.

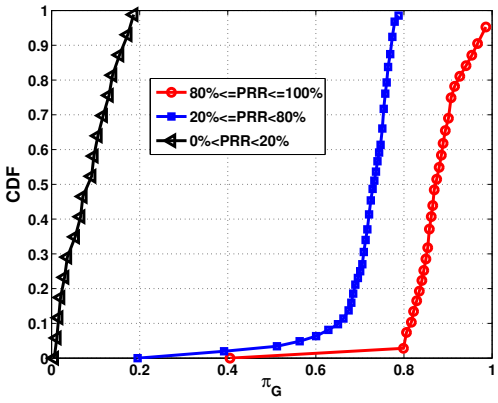

(c) Good state stationary probability π_G.

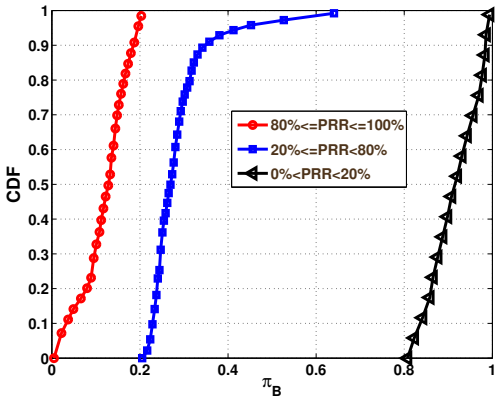

(d) Bad state stationary probability π_B.

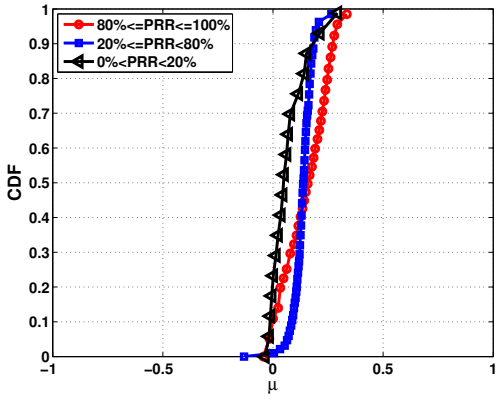

(e) Channel memory μ.

Figure 5.3: Cumulation Distribution Function for each link category: good, intermediate, bad for a) packet loss length, b) packet run length, c) stationary probability in good state π_G, d) stationary probability in bad state π_B, and e) channel memory μ on CC2420, 110B, 0dBm.

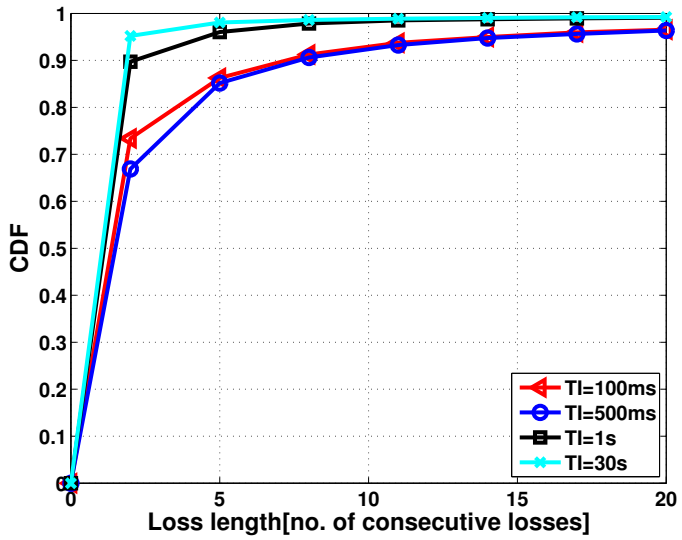

Figure 5.4: Cumulation Distribution Function of loss length at IPT of 100ms, 200ms, 500ms, 1s, 30s, CC1101, 0dBm.

Parameters		run length			loss length			GE: p			GE: r		
IPT		100ms	200ms	500ms	100ms	200ms	500ms	100ms	200ms	500ms	100ms	200ms	500ms
110B	$PRR \geq 80\%$	74.2	73.5	88.5	1.6	2	1.7	0.03	0.03	0.02	0.84	0.87	0.89
110B	$20\% \leq PRR < 80\%$	14.8	7.6	9.4	12.5	7.9	5.3	0.43	0.40	0.41	0.42	0.41	0.38
110B	$0 < PRR < 20\%$	2.2	1.4	1.5	43.4	41.1	56.8	0.81	0.82	0.82	0.07	0.08	0.05

Table 5.2: Average number of consecutive good packet receptions (run length), packet losses (loss length), the GE transition probabilities ($p = P(t_i = Bad|t_{i-1} = Good)$, $r = P(t_i = Good|t_{i-1} = Bad)$ for good ($PRR \geq 80\%$), intermediate ($20\% \leq PRR < 80\%$), bad ($0 < PRR < 20\%$) links a with 110B packet size, CC1101.

Parameters		π_G			π_B			π_{Loss}			μ		
IPT		100ms	200ms	500ms	100ms	200ms	500ms	100ms	200ms	500ms	100ms	200ms	500ms
110B	$PRR \geq 80\%$	0.96	0.96	0.97	0.03	0.03	0.02	0.03	0.03	0.02	0.13	0.1	0.09
110B	$20\% \leq PRR < 80\%$	0.49	0.50	0.48	0.50	0.49	0.51	0.50	0.49	0.51	0.15	0.19	0.21
110B	$0 < PRR < 20\%$	0.07	0.08	0.05	0.92	0.91	0.94	0.92	0.91	0.94	0.12	0.1	0.13

Table 5.3: Average stationary state probabilities π_G, π_B, loss probability π_{Loss}, and μ metric for good ($PRR \geq 80\%$), intermediate ($20\% \leq PRR < 80\%$), bad ($0 < PRR < 20\%$) links a with 110B packet size, CC1101.

To study the impact of the packet size over run and loss length, we reduce the packet size from 110B to 6B. Table 5.4 presents that good links continue to have short loss periods, about 1 to 2 for IPTs of 100ms, 200ms, 500ms, and 1s. To observe the long term distribution of packet losses, we set IPT to 30s. We can notice that loss length maintains an average of ∼1, proving that no relation exists between packet losses of good links. This is especially relevant to discriminate short term behavior of reliable

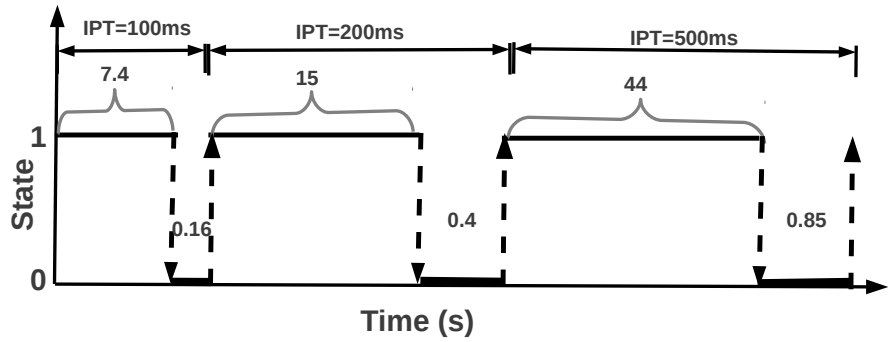

(a) Temporal behavior of good links.

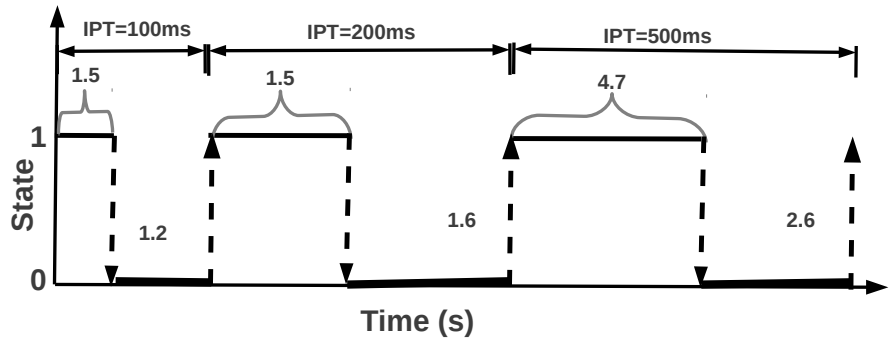

(b) Temporal behavior of intermediate links.

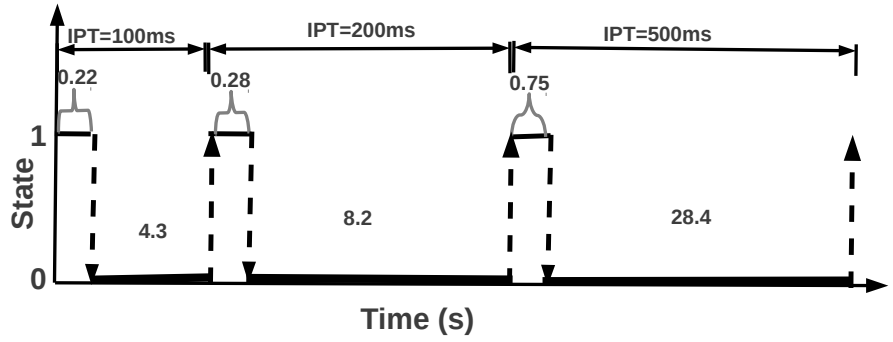

(c) Temporal behavior of bad links.

Figure 5.5: Temporal behavior between 0:Bad and 1:Good states of links belonging to categories: a) good, b) intermediate, and c) bad for long packets (110B).

links.

Additionally, $P(Good|Bad)$ is low (∼0.03) whereas $P(Bad|Good)$ is high (∼0.9) for good links; they do not depend on IPT set-up values.

Intermediate links show higher transition probability $P(Good|Bad)$ (∼0.4) and lower $P(Bad|Good)$ (max. ∼0.7). At the same time, bad links may be out of reception for long periods i.e. $P(Good|Bad)$ (∼0.8) and $P(Bad|Good)$ (max. ∼0.07). A $P(Bad|Good)$ about 0.1 means that there is only 10% chance to return from bad to a good state.

Table 5.5 shows that π_G and π_B are independent of IPT for the 6B packet size. Yet, they vary with the link category (0.03–good links, 0.52–intermediate links, 0.90–bad links).

Parameters		run length					loss length					GE: p					GE: r				
IPT		100ms	200ms	500ms	1s	30s	100ms	200ms	500ms	1s	30s	100ms	200ms	500ms	1s	30s	100ms	200ms	500ms	1s	30s
6B	$PRR \geq 80\%$	30.2	150	157	141	27	2	1.5	1.3	1	1.4	0.05	0.03	0.02	0.04	0.04	0.81	0.87	0.89	0.93	0.94
6B	$20\% \leq PRR < 80\%$	8	18.8	24.4	59.6	11.7	9	12	19	2.3	2.5	0.23	0.24	0.23	0.19	0.19	0.42	0.41	0.38	0.25	0.74
6B	$0 < PRR < 20\%$	5	2.4	3	4	1.3	52	80	107.8	16.3	19.1	0.42	0.38	0.46	0.41	0.79	0.07	0.08	0.10	0.04	0.07

Table 5.4: Average number of consecutive good packet receptions (run length), packet losses (loss length), the GE transition probabilities ($p = P(t_i = Bad|t_{i-1} = Good)$, $r = P(t_i = Good|t_{i-1} = Bad)$ for good ($PRR \geq 80\%$), intermediate ($20\% \leq PRR < 80\%$), bad ($0 < PRR < 20\%$) links with a packet size of 6B, CC1101.

Parameters		π_G					π_B					π_{Loss}					μ				
IPT		100ms	200ms	500ms	1s	30s	100ms	200ms	500ms	1s	30s	100ms	200ms	500ms	1s	30s	100ms	200ms	500ms	1s	30s
6B	$PRR \geq 80\%$	0.94	0.96	0.97	0.95	0.95	0.05	0.03	0.02	0.04	0.04	0.05	0.02	0.02	0.04	0.04	0.14	0.10	0.09	0.03	0.02
6B	$20\% \leq PRR < 80\%$	0.64	0.63	0.62	0.56	0.79	0.35	0.36	0.37	0.43	0.20	0.35	0.36	0.37	0.43	0.20	0.35	0.35	0.39	0.56	0.07
6B	$0 < PRR < 20\%$	0.14	0.17	0.17	0.08	0.08	0.85	0.82	0.82	0.91	0.91	0.85	0.82	0.82	0.91	0.91	0.51	0.54	0.44	0.55	0.14

Table 5.5: Average stationary state probabilities π_G, π_B, loss probability π_{Loss}, and μ metric for good ($PRR \geq 80\%$), intermediate ($20\% \leq PRR < 80\%$), bad ($0 < PRR < 20\%$) links with a packet size of 6B, CC1101.

Parameters		run length				loss length				GE: p				GE: r			
IPT		100ms	200ms	500ms	1s	100ms	200ms	500ms	1s	100ms	200ms	500ms	1s	100ms	200ms	500ms	1s
110B	$PRR \geq 80\%$	13.1	14.6	17.4	7.6	1.2	1.2	1.4	1.1	0.13	0.12	0.09	0.10	0.84	0.85	0.82	0.87
110B	$20\% \leq PRR < 80\%$	3.5	3.7	4.2	3.1	1.9	2.4	2.7	2.3	0.29	0.27	0.24	0.32	0.78	0.76	0.65	0.64
110B	$0 < PRR < 20\%$	1.0	1.0	1.1	1.0	28.0	35.2	26.7	22.6	0.92	0.92	0.85	0.88	0.08	0.08	0.07	0.08
6B	$PRR \geq 80\%$	12.1	9.0	10.3	9.8	1.5	1.8	1.9	1.3	0.11	0.09	0.09	0.10	0.89	0.91	0.86	0.93
6B	$20\% \leq PRR < 80\%$	2.8	3.4	3.8	3.5	2.9	2.14	3	8.3	0.32	0.31	0.24	0.32	0.79	0.63	0.61	0.75
6B	$0 < PRR < 20\%$	1.1	1.0	1.6	1.0	24.2	30.2	15.7	21.6	0.86	0.94	0.85	0.91	0.04	0.02	0.02	0.04

Table 5.6: Average number of consecutive good packet receptions (run length), packet losses (loss length), the GE transition probabilities ($p = P(t_i = Bad|t_{i-1} = Good)$, $r = P(t_i = Good|t_{i-1} = Bad)$ for good ($PRR \geq 80\%$), intermediate ($20\% \leq PRR < 80\%$), bad ($0 < PRR < 20\%$) links for short (6B) and long (110B) packets, at 0dBm output power, CC2420.

Parameters		π_G				π_B				π_{Loss}				μ			
IPT		100ms	200ms	500ms	1s	100ms	200ms	500ms	1s	100ms	200ms	500ms	1s	100ms	200ms	500ms	1s
110B	$PRR \geq 80\%$	0.86	0.87	0.90	0.89	0.13	0.12	0.09	0.10	0.13	0.12	0.09	0.10	0.03	0.03	0.09	0.03
110B	$20\% \leq PRR < 80\%$	0.72	0.73	0.73	0.66	0.27	0.26	0.26	0.33	0.27	0.26	0.26	0.33	-0.07	-0.03	0.11	0.04
110B	$0 < PRR < 20\%$	0.08	0.07	0.07	0.08	0.92	0.92	0.92	0.91	0.92	0.92	0.92	0.91	0	0	0.08	0.04
6B	$PRR \geq 80\%$	0.89	0.91	0.90	0.90	0.11	0.09	0.09	0.09	0.11	0.09	0.09	0.09	0	0	0.05	-0.03
6B	$20\% \leq PRR < 80\%$	0.71	0.67	0.71	0.70	0.28	0.32	0.28	0.29	0.28	0.32	0.28	0.29	-0.11	0.06	0.15	-0.07
6B	$0 < PRR < 20\%$	0.04	0.02	0.02	0.04	0.95	0.97	0.97	0.95	0.95	0.97	0.97	0.95	0.1	0.04	0.13	0.05

Table 5.7: Average stationary state probabilities π_G, π_B, loss probability π_{Loss}, and μ metric for good ($PRR \geq 80\%$), intermediate ($20\% \leq PRR < 80\%$), bad ($0 < PRR < 20\%$) links for short (6B) and long (110B) packet, at 0dBm output power, CC2420.

Considering the CC2420 radio, Table 5.6 highlights that like CC1101, losses are independent for good links with the maximum 1.9 average loss length per link for both 110B and 6B packet sizes. Intermediate links may encounter losses with an average length ranging from 2 to 10 for 110B and 6B packet size. Also, bad links show a loss length above 15, independent of the packet size. Again, transition probabilities are linearly dependent to the link category, exhibiting a $P(Good|Bad)$ of ∼0.10 (good links), ∼0.3 (intermediate links), and ∼0.9 (bad links). On the other hand, $P(Bad|Good)$ probability decreases from ∼0.80 for good links to ∼0.04 for bad links.

According to Table 5.7, on CC2420, good and bad stationary probabilities are independent of the packet length or the IPT. Thus, the probability loss remains a good link quality discriminator (0.13–good links, 0.27–intermediate links, 0.92–bad links).

Power decrease

We next decrease the output power to -10dBm and -30dBm on the CC1101 radio to verify the validity of our assumption. Table 5.8 presents that transition probabilities $P(Good|Bad)$, $P(Bad|Good)$ continue to be linearly dependent on the links category. Moreover, good links keep having large run lengths (may reach 120 consecutive successes) and low loss lengths (∼1.2) at -10dBm and -30dBm output power.

The output power decrease does not affect stability of good links, instead, intermediate links decay the stationary good probability from 0.66 at -10dBm to 0.57 at -30dBm (cf. Table 5.9). Additionally, bad links reduce their stationary probability from 0.14 at -10dBm to 0.05 at -30dBm.

On the CC2420 radio, to assess the effect of power decrease, we set up the output power to -15dBm and the -25dBm (lowest bound of CC2420). We observe that we may have at maximum two consecutive losses for good links and maximum 4-5 for intermediate links. Similarly to CC1101, the probability to transit from good to bad state is about 10% for good links at -15dBm and -25dBm.

The output power decrease contributes to the decrease of the intermediate and bad links good stationary probability from 0.62 at -15dBm to 0.56 at -25dBm and from 0.07 at -15dBm to 0.05 at -25dBm (cf. Table 5.11).

It is interesting to investigate how the loss length may discriminate the quality of links. To illustrate this point, we study the correlation between the probability of consecutive successes P(Good|Good) and the real PRR.

Parameters		run length	loss length	GE: p	GE: r
IPT		500ms	500m	500ms	500ms
110B, TX=-10dbm	$PRR \geq 80\%$	120	1.2	0.04	0.94
110B, TX=-10dbm	$20\% \leq PRR < 80\%$	54	3	0.3	0.59
110B, TX=-10dbm	$0 < PRR < 20\%$	1.3	24	0.7	0.12
110B, TX=-30dbm	$PRR \geq 80\%$	117	1	0.05	0.94
110B, TX=-30dbm	$20\% \leq PRR < 80\%$	34	2	0.4	0.55
110B, TX=-30dbm	$0 < PRR < 20\%$	0.9	63	0.8	0.05

Table 5.8: Average number of consecutive good packet receptions (run length), packet losses (loss length), the GE transition probabilities ($p = P(t_i = Bad|t_{i-1} = Good)$, $r = P(t_i = Good|t_{i-1} = Bad)$ for good ($PRR \geq 80\%$), intermediate ($20\% \leq PRR < 80\%$), bad ($0 < PRR < 20\%$) links at -10 dbm and -30dBm output power, CC1101.

Parameters		π_G	π_B	π_{Loss}	μ
IPT		500ms	500m	500ms	500ms
110B, TX=-10dbm	$PRR \geq 80\%$	0.95	0.04	0.04	0.02
110B, TX=-10dbm	$20\% \leq PRR < 80\%$	0.66	0.33	0.33	0.11
110B, TX=-10dbm	$0 < PRR < 20\%$	0.14	0.85	0.85	0.18
110B, TX=-30dbm	$PRR \geq 80\%$	0.94	0.05	0.05	0.01
110B, TX=-30dbm	$20\% \leq PRR < 80\%$	0.57	0.42	0.42	0.05
110B, TX=-30dbm	$0 < PRR < 20\%$	0.05	0.94	0.94	0.15

Table 5.9: Average stationary state probabilities π_G, π_B, loss probability π_{Loss}, and μ metric for good ($PRR \geq 80\%$), intermediate ($20\% \leq PRR < 80\%$), bad ($0 < PRR < 20\%$) links at -10 dbm and -30dBm output power, CC1101.

5.2.1.1 *Fitting the GE P(Good|Good) probability*

In Figure 5.6, we fit the probability of successful receptions express as $1 - p$ (probability that a success is followed by a success) with a first order polynomial function, $F(x) = p_1 * x + p_2$, where $p_1 = 0.9785$ and $p_2 = 0.01309$. The goodness of the fit is given by: a) CC1101 – R^2: 0.9818, a SSE of 5.495, and a RMSE of 0.0394, b) CC2420 – R^2: 0.977, a SSE of 2.675, and a RMSE of 0.017974.

5.2.2 Estimating PRR using stationary probabilities

Previously, we have obtained an estimation of PRR through a F-D function applied over avg and std LQI measured values; RSSI is recommended only for the detection of anomalous behavior.

Parameters		run length	loss length	GE: p	GE: r
IPT		500ms	500m	500ms	500ms
110B, TX=-15dbm	$PRR \geq 80\%$	8.5	1.1	0.09	0.90
110B, TX=-15dbm	$20\% \leq PRR < 80\%$	4.5	1.5	0.32	0.54
110B, TX=-15dbm	$0 < PRR < 20\%$	1.2	8	0.90	0.07
110B, TX=-25dbm	$PRR \geq 80\%$	8.2	1.1	0.10	0.88
110B, TX=-25dbm	$20\% \leq PRR < 80\%$	3.6	2	0.39	0.54
110B, TX=-25dbm	$0 < PRR < 20\%$	1.1	23	0.94	0.05

Table 5.10: Average number of consecutive good packet receptions (run length), packet losses (loss length), the GE transition probabilities ($p = P(t_i = Bad|t_{i-1} = Good)$, $r = P(t_i = Good|t_{i-1} = Bad)$ for good ($PRR \geq 80\%$), intermediate ($20\% \leq PRR < 80\%$), bad ($0 < PRR < 20\%$) links at -15 dbm and -25dBm output power on CC2420 radio.

Parameters		π_G	π_B	π_{Loss}	μ
IPT		500ms	500m	500ms	500ms
110B, TX=-15dbm	$PRR \geq 80\%$	0.90	0.09	0.09	0.01
110B, TX=-15dbm	$20\% \leq PRR < 80\%$	0.62	0.37	0.37	0.14
110B, TX=-15dbm	$0 < PRR < 20\%$	0.07	0.92	0.92	0.03
110B, TX=-25dbm	$PRR \geq 80\%$	0.89	0.10	0.10	0.02
110B, TX=-25dbm	$20\% \leq PRR < 80\%$	0.56	0.43	0.43	0.11
110B, TX=-25dbm	$0 < PRR < 20\%$	0.05	0.94	0.94	0.01

Table 5.11: Average stationary state probabilities π_G, π_B, loss probability π_{Loss}, and μ metric for good ($PRR \geq 80\%$), intermediate ($20\% \leq PRR < 80\%$), bad ($0 < PRR < 20\%$) links at -15 dbm and -25dBm output power on CC2420 radio.

Also, we have noticed that stationary probabilities (π_G and π_B) are good discriminators of link quality. Therefore, to refine the prediction of PRR using the obtained F-D fitting function, we apply the 2-state Markov model over avg and std LQI measured values for highly variable links.

We consider avg and std LQI values of the received packets as a sequence of bits:

$$f(\overline{lqi}) = \begin{cases} 1, & \text{if } \overline{lqi} \leq \overline{LQI_{threshold}}. \\ 0, & \text{otherwise.} \end{cases} \tag{5.4}$$

$$f(\sigma_{lqi}) = \begin{cases} 1, & \text{if } \sigma_{lqi} \leq \sigma_{LQI_{threshold}}. \\ 0, & \text{otherwise.} \end{cases} \tag{5.5}$$

where $\overline{LQI_{threshold}}$ and $\sigma_{LQI_{threshold}}$ are the threshold values of avg LQI and std LQI that may be elected with respect to the used hardware or to the environment. More

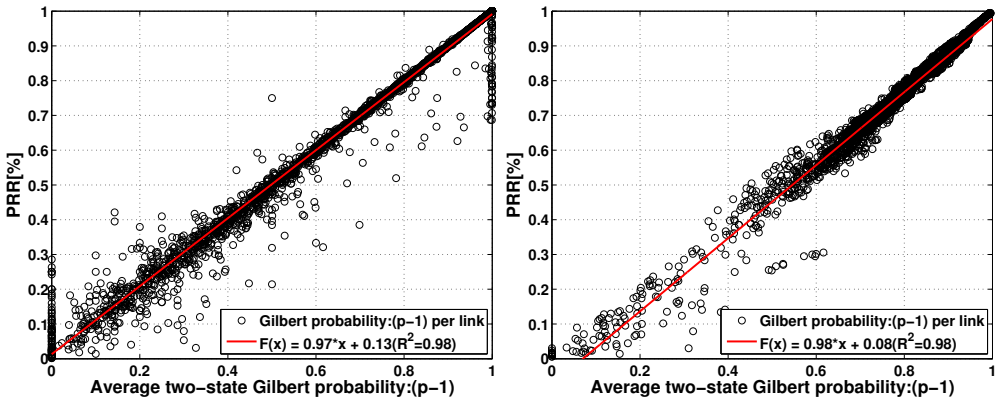

(a) CC1101 – PRR vs. GE:(1-p). (b) CC2420 – PRR vs. GE:(1-p).

Figure 5.6: Fitting of the scatter diagram of PRR in function of $P(Good|Good)$ probability $(1-p)$ with a linear function.

specifically, we chose a $\overline{LQI_{threshold}}$ of 1.7; an avg LQI value below 1.7 corresponds to 1 (good reception) whereas an avg LQI above 1.7 corresponds to a 0 (bad reception), Equation 5.4. The avg LQI value of 1.7 was decided observing the obtained F-D fit, Figure 4.7.

Similarly, for std LQI, we consider a bound ($\sigma_{LQI_{threshold}}$) of 1.5, values below are associated with 1 (good reception) while values above 1.5 are associated with 0 (bad reception) (cf. Equation 5.5).

Figure 5.8 a) depicts the temporal evolution of avg LQI computed over windows of size 2 whereas Figure 5.8 b) shows the temporal evolution of std LQI. Given the overlapping of avg LQI and std LQI for the link with PRR=50% and PRR=20%, we associate each value of avg and std LQI to a sequence of bits; then, we compute the stationary probability π_G for each sequence of five values as in Figure 5.7.

Stationary probability π_G computed over avg LQI, Figure 5.8 c), shows that the link with PRR of 80% can be easily distinguish between links with 50% or 20% of PRR. Not only π_G of avg LQI, but also π_G of std LQI helps to discriminate links with 80%, 50% or 20% of PRR (cf. Figure 5.8 d)).

Considering that a node has in its neighborhood only intermediate links, we explore the effect of estimating PRR of available intermediate links through the FD fit as well as by computing the stationary probability π_G of avg and std LQI. As intermediate links, we pick three links such as: $6 \rightarrow 20$ (PRR=64%), $6 \rightarrow 57$ (PRR=54%), $6 \rightarrow 34$ (PRR=34%).

We show the measured PRR over an observation window of 10 in Figure 5.9 a). Figure 5.9 b)–c) present the temporal evolution of avg LQI that ranges within 0.5 and ∼3 and std LQI with values concentrated within 0.5 and 5. Both avg LQI and std LQI have curves that overlaps.

To perform the PRR estimation, we fit the Fermi-Dirac function with the following

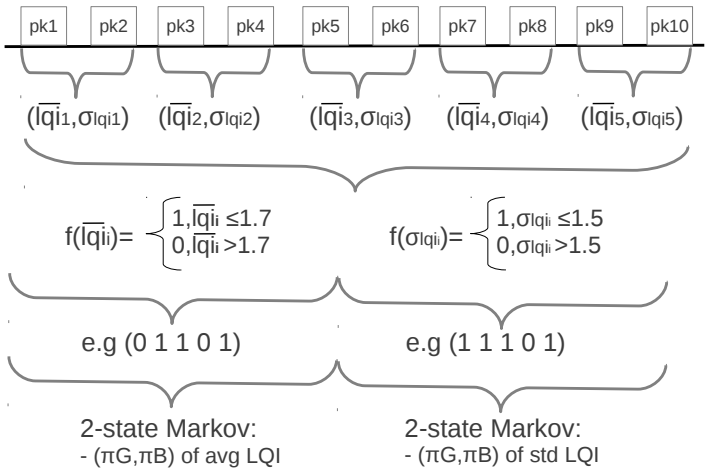

Figure 5.7: Computation process of the stationary probabilities from avg and std LQI values.

parameters: (μ = 2.5, σ = 0.6) for avg LQI and (μ = 2.75, σ = 0.65) for std LQI. Figure 5.9 d) shows that using FD for avg LQI, the link 6 → 20 (PRR=64%) overlaps the link 6 → 57 (PRR=54%). On the other hand, when we use FD for std LQI all three links overlaps, see Figure 5.9 e).

To attain a better estimation of such high variable links, we calculate the stationary probability given by 2-state Markov model.

Figure 5.10 a) points out that π_G of avg LQI gives a fairly good differentiation between the link of PRR=64%, PRR=54%, and PRR=34% π_G of std LQI is also able to determine the best link within links of PRR=64%, PRR=54%, and PRR=34%.

We have also evaluated the relevance and the efficiency of using stationary probabilities to categorize high variable CC2420 links. Like CC1101, we assess the temporal fluctuation of intermediate links with different reception ratio: 174 → 127 (PRR=60%), 99 → 179 (PRR=40%), 188 → 105 (PRR=20%).

At first, we plot the real PRR that clearly identifies the links by their reception ratio (cf. Figure 5.11 a)). Looking at Figure 5.11 b), we observe that the temporal evolution of average LQI for 174 → 127 and 99 → 179 are quite close. Therefore, average LQI is not able to decide which one is better. Additionally, each link varies sporadically in a large range from 0 to 15 deepen the complexity of selecting the most reliable link as shown in Figure 5.11 c) .

Trying to identify the best link, we apply the Fermi-Dirac function over average LQI (μ = 25.4, σ = 4.3) and std LQI (μ = 14.4, σ = 1.8). Figure 5.11 d) illustrates that link 174 → 127 and link 99 → 179 have short spans overlap that may mislead link selection when we use the FD fit of avg LQI. However, link 188 → 105 with 20% can be well identify from the avg LQI FD fit. Moreover, investigating the FD fit of std LQI it is hard to decide best link as we face high overlapping (cf. Figure 5.9 e)).

To cope with easy-going PRR prediction when intermediate links are difficult to be estimated from the FD fit, we compute the stationary probability conforming to Figure

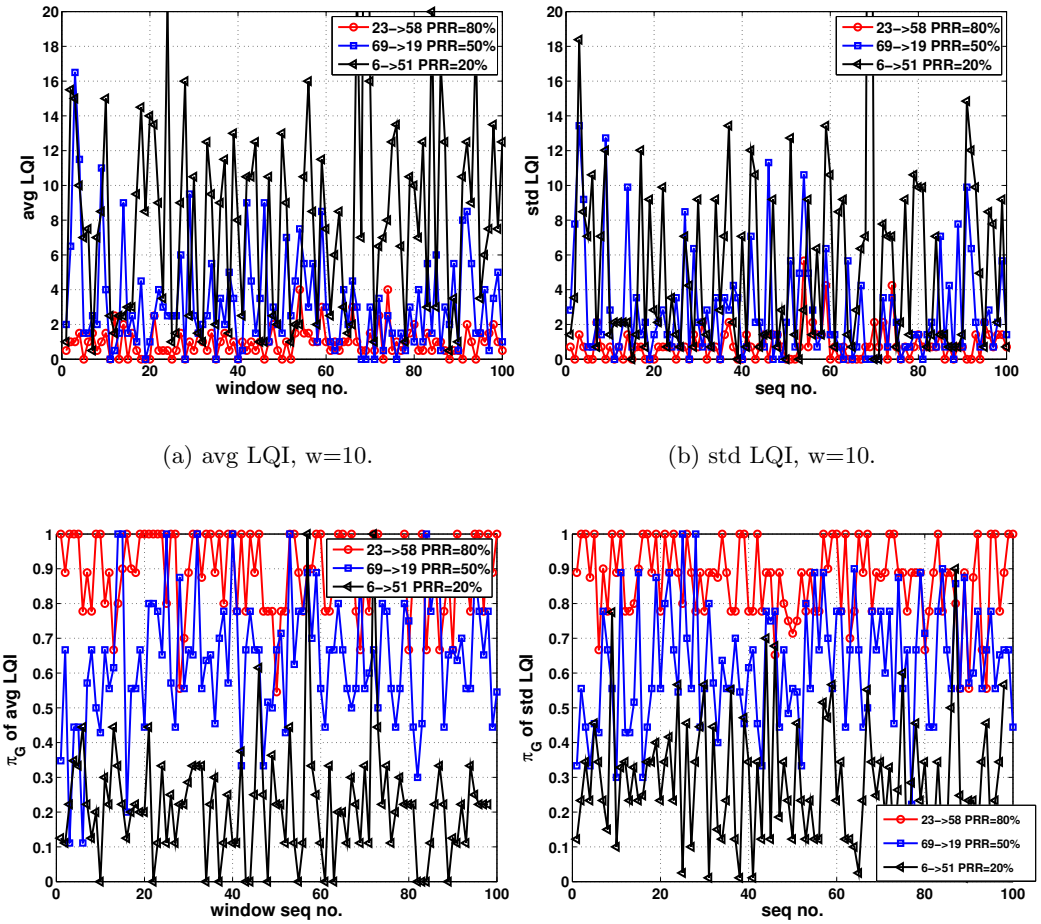

(a) avg LQI, w=10.

(b) std LQI, w=10.

(c) π_G of avg LQI.

(d) π_G of std LQI.

Figure 5.8: Stationary probability π_G of avg/std LQI derived from avg/std LQI measured values a) avg LQI, b) std LQI, c) avg LQI (threshold of 1.7), and b) std LQI (threshold of 1.5) for link 23 $\rightarrow$ 58 (PRR=80%), link 69 $\rightarrow$ 19 (PRR=50%), and link 6 $\rightarrow$ 51 (PRR=20%), w=10, CC1101, 0dBm.

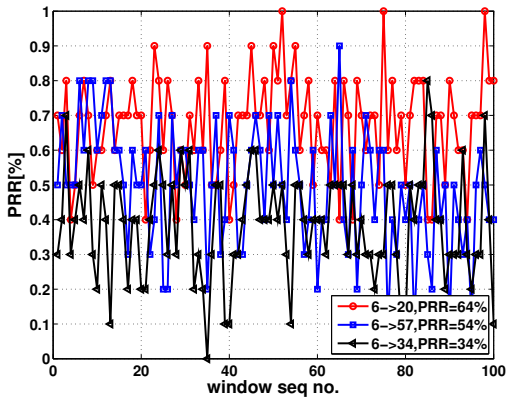

(a) Measured PRR.

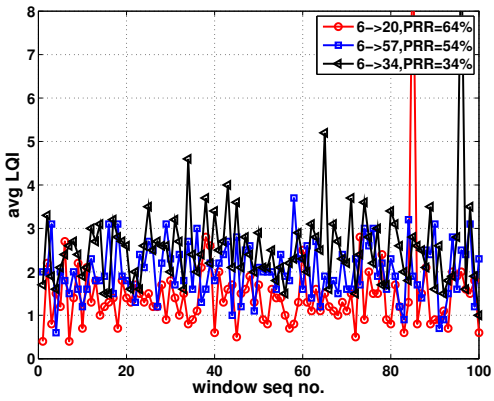

(b) avg LQI.

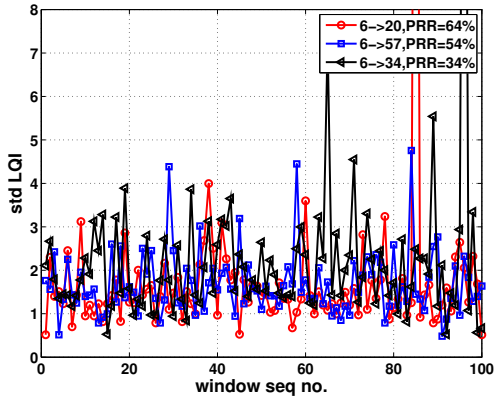

(c) std LQI.

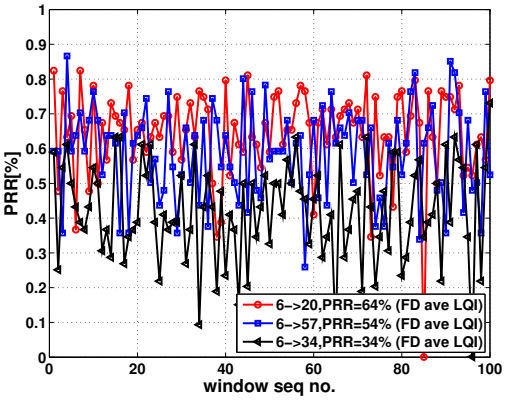

(d) Estimated PRR (FD of avg LQI).

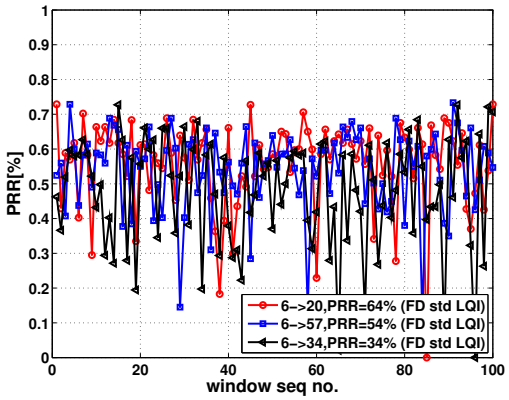

(e) Estimated PRR (FD of std LQI).

Figure 5.9: Estimating PRR using the Fermi Dirac fitting function for three intermediate links ($6 \rightarrow 20$ (PRR=64%), $6 \rightarrow 57$ (PRR=54%), $6 \rightarrow 34$ (PRR=34%)) a) measured PRR, b) avg LQI, c) std LQI, d) FD fit of avg LQI, and e) FD fit of std LQI over an observation window of 10 for CC1101, 0dBm.

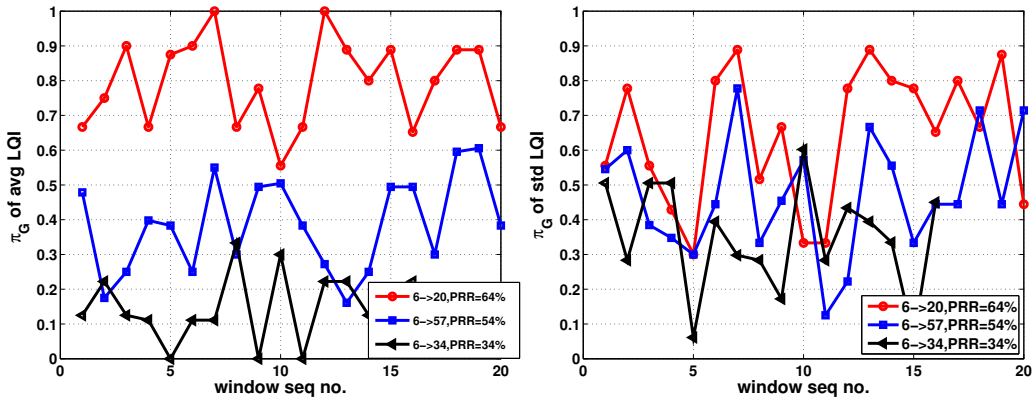

(a) π_G of avg LQI.

(b) π_G of std LQI.

Figure 5.10: Stationary probability π_G of avg/std LQI derived from avg/std LQI measured values a) avg LQI, b) std LQI, c) avg LQI (threshold of 1.7), and b) std LQI (threshold of 1.5) for link 23 → 58 (PRR=80%), link 69 → 19 (PRR=50%), and link 6 → 51 (PRR=20%), CC1101, 0dBm.

5.7 with $\overline{LQI_{threshold}} = 72$ and $\sigma_{LQI_{threshold}} = 4$.

Figure 5.12 a) shows that π_G of avg LQI can very well distinguish among CC2420 links with PRR=60%, PRR=40%, and PRR=20%. On the contrary, we cannot exploit π_G of std LQI due to the inaccurate prediction (cf. Figure 5.12 b)).

5.3 Link quality metric approach

To enable energy efficiency and reliable multi-hop communication, link quality estimators (LQE) need to be accurate independently of the network density or the noisy environments. Moreover, LQE needs to predict the quality of a link, the quality that reflects the successful data delivery across it.

To design such accurate link quality, it should be taken into consideration several requirements such as: energy efficiency, assure the stability of the route while data is transferred, avoid high rate dissemination of control packets (low overhead), or low complexity.

To meet these challenges, we propose an agile link estimator able to predict PRR on short term from existent hardware metrics (RSSI, LQI). We have concluded that RSSI manages to single out nodes with anomalous behavior (CC1101), or that low averages and standard deviations usually designate good packet receptions (CC2420). However, LQI demonstrates to characterize better link qualities via its average and standard deviation.

To assess short term link estimation, we use our statistical approach (Fermi-Dirac fitting function–coefficient of correlation up to 0.98 and the 2-state Markov model) driven from the carried out experiments on large scale indoor Senslab testbed (CC1101,

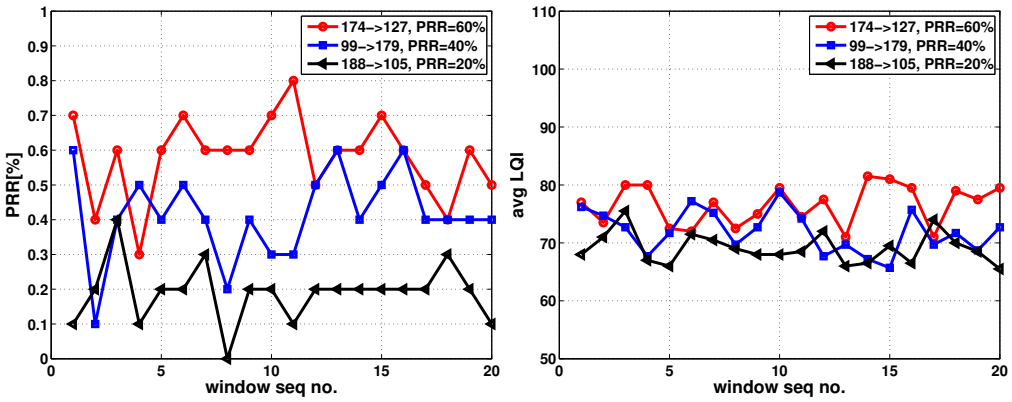

(a) Measured PRR.

(b) avg LQI.

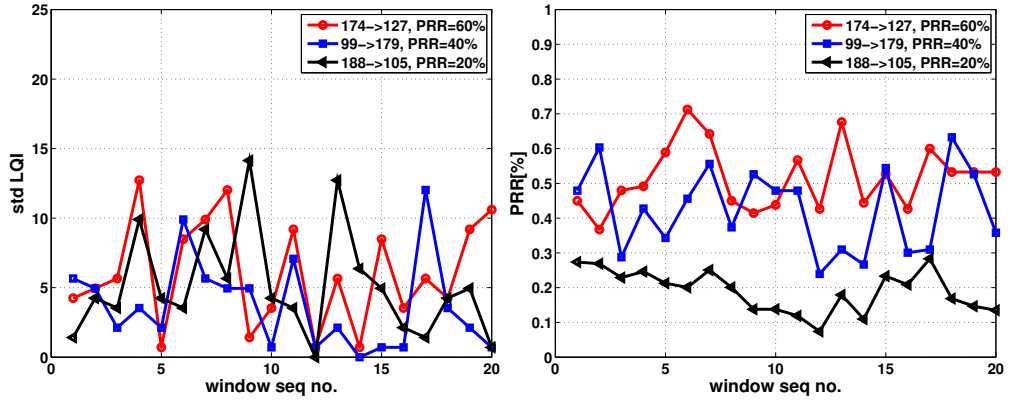

(c) std LQI.

(d) Estimated PRR (FD of avg LQI).

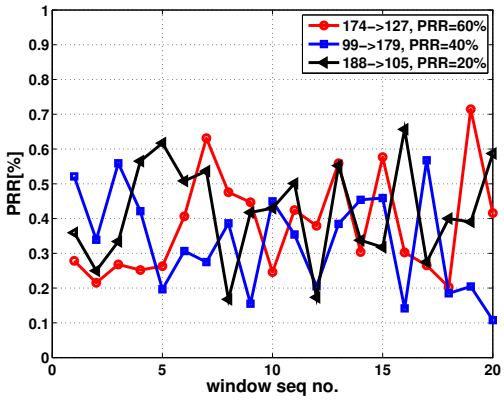

(e) Estimated PRR (FD of std LQI).

Figure 5.11: Estimating PRR using the Fermi-Dirac fitting function for three intermediate links (174 → 127 (PRR=60%), 99 → 179 (PRR=40%), 188 → 105 (PRR=20%)) a) measured PRR, b) avg LQI, c) std LQI, d) FD fit of avg LQI, and e) FD fit of std LQI over an observation window of 10 for CC2420, 0dBm.

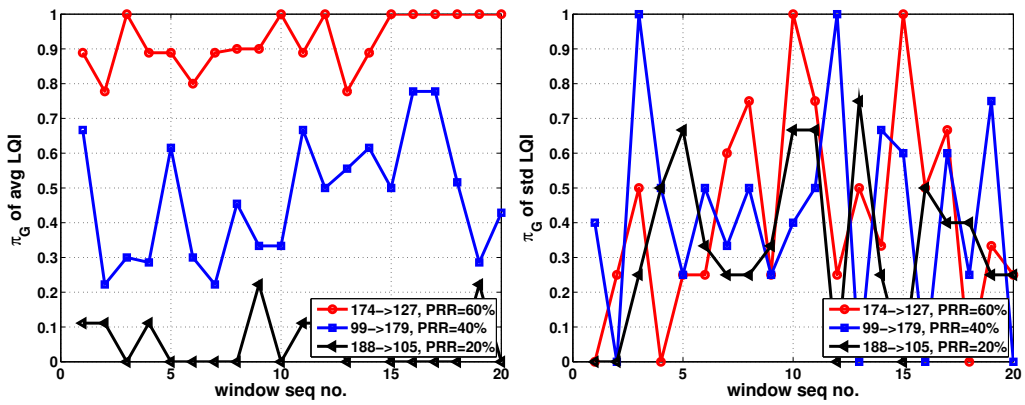

(a) π_G of avg LQI.

(b) π_G of std LQI.

Figure 5.12: Stationary probability π_G of avg/std LQI derived from avg/std LQI measured values a) avg LQI, b) std LQI, c) avg LQI (threshold of 70), and b) std LQI (threshold of 3.5) for 174 $\rightarrow$ 127 (PRR=60%), 99 $\rightarrow$ 179 (PRR=40%), 188 $\rightarrow$ 105 (PRR=20%), CC2420, 0dBm.

CC2420).

Considering the RPL routing protocol, we count for the couples (lqi_i,$rssi_i$) recorded with each reception of packets such as NS/NA, RS/RA (neighbor discovery), DIO/DIS/DAO (routing), and data.

Our approach of PRR estimation is two-folded. First, we consider the Fermi-Dirac model:

$$f(x) = 1/(1 + \exp \frac{-(\mu - x)}{\sigma}), \tag{5.6}$$

where $f(x)$ gives the PRR prediction of sample x that may denote the lqi_i, the $rssi_i$ of a single packet, or $\overline{lqi_i}$, σ_{lqi_i} computed over an observation window of size w; We obtained good performance for $w = 10$ ($\mu = 2.5$, $\sigma = 0.6$) for avg LQI and ($\mu = 2.75$, $\sigma = 0.65$) for std LQI. The Fermi-Dirac model has proven to predict PRR by achieving more than 80% accuracy. The significance of the Fermi-Dirac function is pictured by μ (cf. Equation 5.6) that gives the inflection point value and σ that indicates the slope of the curve. Both parameters are hardware reliable.

Second, to overcome spare spaces with prevalent poor links that present high variation, we compute additional to F-D, the stationary good state probability (π_G), where a high value of the link demonstrates reliable packet reception across it.

We further plan to integrate the algorithm 1 described above with RPL so that nodes may decide as preferred parent neighbors with good quality.

Algorithm 1 Estimating PRR of link (i,j): LQ_{ij}

Require: (lqi_i,$rssi_i$) for each received packet (DIO/DIS/DAO, data, NS/NA, RS/RA),$0 \geq lqi_i > 60$ for CC1101, $60 \geq lqi_i > 110$ for CC2420

1: $n \Leftarrow$ size of w (observation window)
2: **for all** $link(i,j) \in neighborhood$ **do**
3: $seq(k)_{ij} \Leftarrow \{(lqi_1,rssi_1), ..., (lqi_n,rssi_n)\}$
4: $\overline{lqi} \Leftarrow \frac{1}{n} * \sum_{l=1}^{n} lqi_l$
5: $\sigma_{lqi} \Leftarrow \sqrt{\frac{1}{n}\sum_{l=1}^{n}(lqi_l - \overline{lqi_{seq(p)}})}$
6: $PRR_{\overline{lqi}} \Leftarrow 1/(1+\exp\frac{-(\mu-\overline{lqi})}{\sigma})$
7: $PRR_{\sigma_{lqi}} \Leftarrow 1/(1+\exp\frac{-(\mu-\sigma_{lqi})}{\sigma})$
8: $PRR_{ij} \Leftarrow \frac{1}{2}(PRR_{\overline{lqi}} + PRR_{\sigma_{lqi}})$
9: **end for**
10: **if** Only intermediate links **then**
11: Compute π_G
12: Choose link with higher π_G as preferred parent.
13: **else if** Good links detected **then**
14: Choose link with higher PRR_{ij} as preferred parent.
15: **end if**

5.4 Conclusions

Investigating the correlation of losses, the first aspect to be pointed out is that losses are independent for good links, no matter the packet size. Moreover, on a short period of time, about seconds, we observed that loss length depends on the link quality. Varying the inter-packet time interval, we have noticed, that $P(Good|Bad)$ and $P(Bad|Good)$ probabilities are not impacted. We argue that upper layer may adapt their mechanism to access the channel (decaying retransmissions to 400ms for low IPT and 1s for higher IPT values), this way, they overcome extensive retransmissions due to short term loss correlation. Since the upper layer relies only on intermediate links the timing to delay further packet transmissions may be set up to 1.5s-2s.

We further analyzed the channel memory metric μ together with transitional and stationary probabilities (π_G, π_B) of the GE model. We concluded that due to curve overlapping, the channel memory it is not a good link quality predictor neither for CC1101 nor for CC2420. Good and Bad state stationary probabilities measured for packet reception sequences or over sequences derived from avg and std LQI assess good link quality estimation. For example π_G may range within 0.8-1 (good links), 0.6-0.8 (intermediate links), 0-0.2 (bad links)).

We have decreased the output power and we concluded that good links are not affected while intermediate and bad links can reduce with 10%, 50%, respectively the good stationary probability when they go from -10dBm to 0.57 -30dBm.

We have shown that estimating PRR using the F-D fitting function may have short spans overlap that may mislead link prediction when links are high variable (i.e links with PRR=64%, PRR=40%, PRR=20%). Therefore, to overcome this issue, we employ the computation of the stationary probabilities associated to the avg and std LQI.

In order to measure π_G and π_B of avg LQI, we found that filtering avg LQI with a $\overline{LQI_{threshold}}$ of 1.7 (CC1101), 72 (CC2420) leads to a fairly good estimation of link quality. However, as links vary sporadically in wide ranges, the π_G and π_B of std LQI is versatile as curves overlap.

Finally, we propose a PRR estimation algorithm based on hardware metrics by combining the obtained Fermi-Dirac fit with the stationary probability of the 2-state Markov model. The approach aims to discriminate between good, intermediate, and bad links using the F-D fit. Once we rely only on intermediate links we differentiate them by favoring links with the highest good stationary probability π_G corresponding to the avg LQI.

Chapter 6

Conclusions and Future Work

Conclusions

The main contribution of this dissertation is to investigate the link quality estimation in large scale dense Wireless Sensor Networks. We focus our attention on a large scale WSN testbed (Senslab) to identify the factors that impact the pattern deviation of the hardware metrics that result in energy waste when communication protocols are used.

In Chapter 2 we give an overview of the main factors that influence link quality whereas we focus our attention on the hardware metrics (RSSI/LQI/SNR). We provide a critical study of existing link assessment mechanisms in terms of RSSI, LQI, PRR that relies on link or a composite link and routing information. Also, we overview the main aspects of several distance-vector based routing protocols (RPL, LOAD, CTP).

We concluded the chapter by several observations:

- An ideal link estimator needs to: assure a good delivery, be accurate, be reactive (adapt to network changes), consider the link asymmetry, have low overhead, be reliable in dense and noisy networks, be stable (able to smooth small fluctuations of links).
- Hardware metrics provide good information of the link properties (delivery, stability, asymmetry, reactivity).
- Composite metrics outperformed single metrics but require further investigation in terms of the required computation time, complexity, memory footprint, and temporal behavior in noisy environments and dense networks.
- To reduce the computation complexity and the memory footprint, link estimators should integrate mathematical models able to capture the dynamics of the hardware metrics (average RSSI, std RSSI, average LQI, deviation LQI).

In Chapter 3, we report on the results of measurements on SensLAB [75] testbed equipped with CC1101/CC2420 radio chips. We recorded RSSI (Received Signal Strength Indicator) and LQI (Link Quality Indicator) hardware metrics for which we consider several aspects such as average and standard deviation of RSSI/LQI, asymmetry of links, and percentage of formed links to find the best way of detecting *good* links in comparison to *weak* ones. Besides, we investigate various scenarios by varying the output power, the inter-packet time interval, and the length of the packet. We propose a link classification function of link degree of hardware metric fluctuation (LQI, RSSI) as good ($80\% \leq PRR \leq 100\%$), intermediate ($20\% < PRR \leq 80\%$), and bad

($0\% < PRR < 20\%$). Based on the classification, we report on the proportion of link categories.

Our analysis has shown that:

- The network may benefit from a large proportion of good links on CC1101 and CC2420 (for 6 byte packets). However, for CC2420 radio, we record for 110 byte packets a majority of intermediate links.

- The CDF and PDF of RSSI (average, standard variance) and LQI (average, standard variance) can discriminate the quality of links. For example, on CC1101 the avg RSSI may help to discriminate links with PRR=100%, since avg RSSI for links below PRR=100% overlap. Also, the deviation of RSSI (CC2420) can be interesting but not sufficient to discriminate link quality. On CC2420, because CDF curves of avg RSSI and std RSSI overlap less we can use avg RSSI and std RSSI to distinguish between good and intermediate links. Furthermore, we can conclude that RSSI can fairly well differentiate good and bad links while LQI can help discriminate intermediate links.

- Good links present strong asymmetry (in Chapter 4 we called strong asymmetry a link with an asymmetry below 20) whereas intermediate and bad links present a high degree of asymmetry for CC1101 and CC2420 radio chips. Hence, the asymmetry of intermediate links ($20\% \leq PRR < 80\%$) is not influenced by the packet size, even though decreasing the output power we lose links that present strong asymmetry. Moreover, the packet size and the power decrease highly impact bad links ($0 < PRR < 20\%$).

In Chapter 4 we analyze the link quality in a statistical way. We have fitted a Fermi-Dirac function to the scatter diagram of the average and standard variation of RSSI and LQI to obtain an estimator of packet reception ratio (PRR). The function can estimate the level of PRR given the average and standard deviation of LQI and RSSI. To evaluate the estimator, we vary the observation window size over which we compare the obtained PRR to average and deviation of RSSI and LQI.

We concluded that:

- Looking for continuous distributions fitting the measured values of RSSI and LQI, we have found that Generalized Extreme Value, Johnson SB or Beta fits best.

- RSSI can be used it as an indicator of possible anomalous behavior of sensor nodes on CC1101, whereas on CC2420 its average and standard deviation can be used to discriminate link categories.

- The resulting Fermi-Dirac fitting function managed to predict accurately PRR over few samples for CC1101 and CC2420 from a given level of average and standard deviation of LQI.

- We have observed that having a window size of 10 we reach low MSE (0.005–0.02).

The work of this chapter has been published in the Algotel conference [9] and the PIMRC conference [10].

In Chapter 5, to detect the short term link dynamics, we study the loss and run length by applying the 2-state Markov model to each link. We next compute the probability of successive packet successes and losses for each link called as stationary probabilities. Probabilities that can offer fine discrimination of high variable links.

Lastly, we discuss on how we can take advantage of our Fermi-Dirac fit together with the two state Markov model metrics by integrating them within a RPL metric.

We concluded the chapter as follows:

- Investigating 2-state Markov model, we conclude that packet size and power decrease do not affect the successes and losses correlations. Moreover, packet losses and successful receptions depend on the link category. For example, a good link has no correlation of packet losses which means that losses are independent for good links. The packet loss length increases with the degradation of the quality of the link.

- We have observed that for low inter-packet interval time $\sim$ 200ms the loss correlation for good links reaches 400ms, whereas for intermediate links it may be down to 1.5s–2s.

- The channel memory is not a good link quality (μ) as is not able to estimate properly the link quality as curves overlap for each category.

- The π_G, π_B of the Markov model derived from avg and std LQI can accurately distinguish between high variable links; π_G ranges within 0.8-1 (good links), 0.6-0.8 (intermediate links), 0-0.2 (bad links)). To convert the avg and std LQI, we recommend a $\overline{LQI_{threshold}}$ of 1.7 (CC1101), 72 (CC2420), and a $\sigma_{LQI_{threshold}}$ of 1.5 (CC1101) and 4 (CC2420).

- The power decrease from -10dBm to -30dBm leads to a reduction with 10% (intermediate links) and 50% (bad links) of the good stationary probability (π_G).

- Our approach of identifying link categories from the obtained Fermi-Dirac fit offers low prediction errors for the measures obtained from Senslab testbed. Also, intermediate links with high variation are well differentiated by good stationary probability π_G corresponding to the avg LQI.

Future work

The work presented in this dissertation provides valuable insight on the link quality estimation issues on real testbeds. We highlight what appears to us the most promising research directions:

Integration and testing the approach

In Chapter 4 and Chapter 5, we have evaluated the relevance of the received signal strength indication (RSSI) and the link quality indicator (LQI) hardware metrics to

predict the PRR using distribution models (e.g Log-logistic, Johnson, Beta).), Fermi-Dirac function, and 2-state Markov model. The promising way of estimating PRR that looks for stable links of good quality and adapt to slowly changing conditions is important for nodes joining the network and to improve overall network performance.

An interesting aspect that remains to be explored is the integration of the found model with the RPL (hop count, ETX) and LOAD (weak links) metrics.

A step forward is to prove its performance against common routing metrics as ETX, LQI, MinLQI, Hops, Weak links (cf. Chapter 2) by deploying it on Contiki OS and testing it on Senslab testbed.

Channel hopping

It is claimed by the literature that the channel hopping is the best solution to avoid bad links when multipath factors or Wi-Fi interference is present. More specifically, a protocol may perform well on a chosen channel whereas on a different channel the performance may be far different. So, in order to generalize our findings, it is needed to check the applicability of our model on different channels.

Impact of the link estimation model on different hardware platforms

Considering the PRR prediction coupled together with ETX estimation, we plan to validate the above mentioned results of the link characterization on different ready-to-use large scale testbeds such as Mirage [18] (Mica2 and Mica2Dot), Kansei, TWIST testbed [32, 106] (Tmote Sky), Wisebed (Telos B, iSense) [90], Greenorbs (Greenorbs nodes) [31].

Smoothing to a single value

Another direction that remains unexplored is the need to check the inefficiency of smoothing the link estimation to a single value. We believe that tracking simultaneously different values such as the average/deviation of the hardware metrics (layer 1), the number of retransmissions (layer 2), and at the same time routing information such as density, delay will lead to more accurate link estimation.

Opportunistic routing

Another direction that requires investigation is the opportunistic routing that takes advantage from a set of links at the same time.

It would be quite interesting to be able to choose dynamically the set of links on the basis of the short term quality. The idea is to rely on the observations driven from the FD fit and the GE model to predict the PRR on short terms, and therefore, to be able to guarantee high reception independently of the fluctuation degree.

Bibliography

[1] Daniel Aguayo, John Bicket, Sanjit Biswas, Glenn Judd, and Robert Morris. Link-level Measurements from an 802.11b Mesh Network. In *Proceedings of the 2004 conference on Applications, technologies, architectures, and protocols for computer communications*, SIGCOMM '04, pages 121–132, New York, NY, USA, 2004. ACM. 32

[2] Muhammad Hamad Alizai, Olaf Landsiedel, Jo Agila Bitsch Link, Stefan Götz, and Klaus Wehrle. Bursty Traffic over Bursty Links. In *SenSys'09: Proceedings of the 7th ACM Conference on Embedded Networked Sensor Systems*, Berkeley, California, November 2009. 32

[3] Nouha Baccour, Anis Koubaa, Maissa Ben Jamâa, Habib Youssef, Marco Zuniga, and Mário Alves. A Comparative Simulation Study of Link Quality Estimators in Wireless Sensor Networks. In *MASCOTS*, pages 1–10, 2009. 38, 47

[4] Nouha Baccour, Anis Koubâa, Luca Mottola, Marco Antonio Zúñiga, Habib Youssef, Carlo Alberto Boano, and Mário Alves. Radio Link Quality Estimation in Wireless Sensor Networks: A survey. *ACM Trans. Sen. Netw.*, 8(4):34:1–34:33, September 2012. 31

[5] Nouha Baccour, Anis Koubâa, Habib Youssef, Maissa Ben Jamâa, Denis do Rosário, Mário Alves, and Leandro B. Becker. F-LQE: A Fuzzy Link Quality Estimator for Wireless Sensor Networks. In *Proceedings of the 7th European conference on Wireless Sensor Networks*, EWSN'10, pages 240–255, Berlin, Heidelberg, 2010. Springer-Verlag. 35, 36, 40, 46, 47, 55

[6] Nouha Baccour, Anis Koubía, Maissa Ben Jamía, Denis do Rosário, Habib Youssef, Mário Alves, and Leandro B. Becker. RadiaLE: A Framework for Designing and Assessing Link Quality Estimators in Wireless Sensor Networks. *Ad Hoc Netw.*, 9(7):1165–1185, September 2011. 20, 21, 29, 37, 46, 47, 58

[7] C. Umit Bas and Sinem Coleri Ergen. Spatio-temporal Characteristics of Link Quality in Wireless Sensor Networks. In *WCNC*, pages 1152–1157, 2012. 65

[8] Monique Becker, Andre-Luc Beylot, Riadh Dhaou, Ashish Gupta, Rahim Kacimi, and Michel Marot. Experimental Study: Link Quality and Deployment Issues in Wireless Sensor Networks. In *Proceedings of the 8th International IFIP-TC 6 Networking Conference*, NETWORKING '09, pages 14–25, Berlin, Heidelberg, 2009. Springer-Verlag. 46

[9] Ana Bildea, Olivier Alphand, and Andrzej Duda. Métriques de Qualité de Lien pour Réseaux de Capteur sans Fil en Intérieur et à Large Échelle. In *AlgoTel*, Pornic, France, May 2013. 88, 127

[10] Ana Bildea, Olivier Alphand, Franck Rousseau, and Andrzej Duda. Link Quality Metrics in Large Scale Indoor Wireless Sensor Networks. In *Proceedings of the 24th IEEE International Symposium on Personal, Indoor and Mobile Radio Communication (PIMRC'13)*, London, England, Sep 2013. 88, 127

[11] Carlo Alberto Boano, James Brown, Nicolas Tsiftes, Utz Roedig, and Thiemo Voigt. The Impact of Temperature on Outdoor Industrial WSN Applications. *IEEE Trans. on Industrial Informatics*, 6(3):451–459, 2010. 30

[12] Carlo Alberto Boano, Thiemo Voigt, Adam Dunkels, Fredrik Osterlind, Nicolas Tsiftes, Luca Mottola, and Pablo Suarez. Poster Abstract: Exploiting the LQI Variance for Rapid Channel Quality Assessment. In *Proceedings of the 2009 International Conference on Information Processing in Sensor Networks*, IPSN '09, pages 369–370, Washington, DC, USA, 2009. IEEE Computer Society. 30, 66, 70

[13] Carlo Alberto Boano, Marco Antonio Zúñiga Zamalloa, Thiemo Voigt, Andreas Willig, and Kay Römer. The Triangle Metric: Fast Link Quality Estimation for Mobile Wireless Sensor Networks. In *ICCCN*, pages 1–7, 2010. 23, 29, 40, 55

[14] A. Brandt, J. Buron, and G. Porcu. Home Automation Routing Requirements in Low-Power and Lossy Networks. RFC 5826, IETF, Apr. 2010. 54

[15] Alberto Cerpa Naim Busek and Deborah Estrin. SCALE: A tool for Simple Connectivity Assessment in Lossy Environments. In *Tech. Rep. CENS-21*, 2003. 21, 23, 29, 31, 45, 58

[16] Alberto Cerpa, Jennifer L. Wong, Miodrag Potkonjak, and Deborah Estrin. Temporal Properties of Low Power Wireless Links: Modeling and Implications on Multi-hop Routing. In *Proceedings of the 6th ACM International Symposium on Mobile Ad Hoc Networking and Computing*, MobiHoc '05, pages 414–425, New York, NY, USA, 2005. ACM. 20, 21, 23, 34, 35, 37, 38

[17] Octav Chipara, Chenyang Lu, Thomas C. Bailey, and Gruia-Catalin Roman. Reliable Clinical Monitoring using Wireless Sensor Networks: Experiences in a Step-down Hospital Unit. In *Proceedings of the 8th ACM Conference on Embedded Networked Sensor Systems*, SenSys '10, pages 155–168, New York, NY, USA, 2010. ACM. 49

[18] B. N. Chun, P. Buonadonna, A. AuYoung, Chaki Ng, D. C. Parkes, J. Shneidman, A. C. Snoeren, and A. Vahdat. Mirage: a Microeconomic Resource Allocation System for Sensornet Testbeds. In *Proceedings of the 2nd IEEE Workshop on Embedded Networked Sensors*, EmNets, pages 19–28, Washington, DC, USA, 2005. IEEE Computer Society. 45, 128

[19] T. Clausen, A. Colin de Verdiere, J. Yi, A. Niktash, Y. Igarashi, H. Satoh, U. Herberg, C. Lavenu, T. Lys, C. Perkins, and J. Dean. The Lightweight On-demand

Ad hoc Distance-vector Routing Protocol - Next Generation (LOADng). Work in Progress draft-clausen-lln-loadng-08, IETF, January 2013. 37, 48, 50

[20] Thomas Clausen and Ulrich Herberg. Some Considerations on Routing in Particular and Lossy Environments. *IETF Workshop on Interconnecting Smart Objects with the Internet*, 2011. 54

[21] Thomas Heide Clausen and Ulrich Herberg. Some Considerations on Routing In Particular and Lossy Environments. Research Report RR-7540, INRIA, February 2011. 54

[22] 2.4 GHz IEEE 802.15.4 compliant RF transceiver. Chipcon Product Data Sheet. `http://www.ti.com/product/cc2420`. 5, 21, 24, 27, 28

[23] Crossbow. MICA, Wireless measurement system. `http://www.xbow.com`. 21

[24] Douglas S. J. De Couto, Daniel Aguayo, John Bicket, and Robert Morris. A High-throughput Path Metric for Multi-hop Wireless Routing. In *Proceedings of the 9th annual international conference on Mobile computing and networking*, MobiCom '03, pages 134–146, New York, NY, USA, 2003. ACM. 34, 42, 46, 53

[25] M. Dohler, T. Watteyne, T. Winter, and D. Barthel. Routing Requirements for Urban Low-Power and Lossy Networks. RFC 5548, IETF, May 2009. 54

[26] A. Dunkels. The Contiki Operating System. `http://www.sics.se/contiki/`. 50

[27] Rodrigo Fonseca, Omprakash Gnawali, Kyle Jamieson, and Philip Levis. Four Bit Wireless Link Estimation . In *Proceedings of the Sixth Workshop on Hot Topics in Networks (HotNets VI)*, 2007. 34, 35, 44, 46, 49, 55

[28] D. Ganesan, B. Krishnamachari, A. Woo, D. Culler, D. Estrin, and S. Wicker. Complex Behavior at Scale: An Experimental Study of Low-Power Wireless Sensor Networks. In *Technical Report UCLA/CSD-TR 02-0013*, 2002. 21, 25, 29

[29] E. N. Gilbert. Capacity of a Burst-noise Channel. volume 39, pages 1253–1265, September 1960. 103

[30] O. Gnawali and P. Levis. The ETX Objective Function for RPL. Internet Draft 1, IETF, November 2010. 52

[31] GreenOrbs. GreenOrbs: A Long-Term Kilo-Scale Wireless Sensor Network. `http://www.greenorbs.org/`. 49, 128

[32] Vlado Handziski, Andreas Köpke, Andreas Willig, and Adam Wolisz. TWIST: a Scalable and Reconfigurable Testbed for Wireless Indoor Experiments with Sensor Networks. In *Proceedings of the 2nd International Workshop on Multi-hop Ad Hoc Networks: from Theory to Reality*, REALMAN '06, pages 63–70, New York, NY, USA, 2006. ACM. 45, 128

[33] Gerhard Hasslinger and Oliver Hohlfeld. The Gilbert-Elliott Model for Packet Loss in Real Time Services on the Internet. In *Measuring, Modelling and Evaluation of Computer and Communication Systems (MMB), 2008 14th GI/ITG Conference*, pages 1–15, 2008. 104

[34] Pirmin Heinzer, Pirmin Heinzer, Vincent Lenders, Vincent Lenders, Franck Legendre, and Franck Legendre. Fast and Accurate Packet Delivery Estimation based on DSSS Chip Errors. In *INFOCOM 2012. Proceedings*, pages 2916–2920, Orlando, Florida, USA, March 2012. IEEE. 32

[35] Derek Ho and Shahriar Mirabbasi. Low-Voltage Low-Power Low-Noise Amplifier for Wireless Sensor Networks. In *CCECE*, pages 1494–1497. IEEE, 2006. 74

[36] Peter. J. Huber. *Robust Statistics*. Wiley, 2004. 92

[37] IETF. The Internet Engineering Task Force (IETF). `http://www.ietf.org/`. 17

[38] IFTF. Constrained RESTful Environments (Active WG). `http://tools.ietf.org/wg/core/`. 17

[39] IFTF. Routing Over Low power and Lossy networks. `http://tools.ietf.org/wg/roll/`. 17

[40] Raj Jain and Shawn A. Routhier. Packet Trains: Measurements and a New Model for Computer Network Traffic. *IEEE Journal on Selected Areas In Communications*, 4:986–995, 1986. 32

[41] Wenyu Jiang and Henning Schulzrinne. Modeling of Packet Loss and Delay and their Effect on Real-Time Multimedia Service Quality. In *Proceedings of NOSSDAV*. ACM, 2000. 32

[42] Ankur Kamthe, Miguel Á. Carreira-Perpiñán, and Alberto E. Cerpa. Multilevel markov model for wireless link simulations. In *Proceedings of the 7th ACM Conference on Embedded Networked Sensor Systems*, SenSys '09, pages 57–70, New York, NY, USA, 2009. ACM. 32

[43] Syed A. Khayam and Hayder Radha. Markov-based Modeling of Wireless Local Area Networks. In *ACM Mobicom Workshop on Modeling, Analysis and Simulation of Wireless and Mobile Systems (MSWiM)*, pages 100–107, 2003. 32

[44] JeongGil Ko, Tia Gao, and Andreas Terzis. Empirical Study of a Medical Sensor Application in an Urban Emergency Department. In *Proceedings of the Fourth International Conference on Body Area Networks*, BodyNets '09, pages 10:1–10:8, ICST, Brussels,Belgium, 2009. 49

[45] Dhananjay Lal, Arati Manjeshwar, Falk Herrmann, Elif Uysal-Biyikoglu, and Abtin Keshavarzian. Measurement and Characterization of Link Quality Metrics

in Energy Constrained Wireless Sensor Networks. In *GLOBECOM*, pages 446–452, San Francisco, 2003. 46

[46] Jungwook Lee and Kwangsue Chung. An Efficient Transmission Power Control Scheme for Temperature Variation in Wireless Sensor Networks. *Sensors*, 11(3):3078–93, January 2011. 30

[47] P. Levis, T. Clausen, J. Hui, O. Gnawali, and J. Ko. The Trickle Algorithm. RFC 6206 (Proposed Standard), March 2011. 49, 51, 53

[48] P. Levis, A. Tavakolli, and S. Dawson-Haggerty. Overview of Existing Routing Protocols for Low Power and Lossy Networks. Internet draft, IETF, 2009. 54

[49] Philip Levis, Sam Madden, Joseph Polastre, Robert Szewczyk, Alec Woo, David Gay, Jason Hill, Matt Welsh, Eric Brewer, and David Culler. TinyOS: An Operating System for Sensor Networks. In *Ambient Intelligence*. Springer Verlag, 2004. 50

[50] Shan Lin, Gang Zhou, Kamin Whitehouse, Yafeng Wu, John A. Stankovic, and Tian He. Towards Stable Network Performance in Wireless Sensor Networks. In *RTSS*, pages 227–237, 2009. 30, 70

[51] Tao Liu, Ankur Kamthe, Lun Jiang, and Alberto Cerpa. Performance Evaluation of Link Quality Estimation Metrics for Static Multihop Wireless Sensor Networks. In *Proceedings of the 6th Annual IEEE communications society conference on Sensor, Mesh and Ad Hoc Communications and Networks*, SECON'09, pages 583–591, Piscataway, NJ, USA, 2009. IEEE Press. 47

[52] RFM-TR1000 low power radio system. `www.rfm.com/products/data/tr1000.pdf`. 21

[53] Andreas F. Meier, Tobias Rein, Jan Beutel, and Lothar Thiele. Coping with Unreliable Channels: Efficient Link Estimation for Low-Power Wireless Sensor Networks. In *Proc. 5th Intl. Conf. Networked Sensing Systems (INSS 2008)*, pages 19–26, Kanazawa, Japan, Jun 2008. 34, 35, 37, 39

[54] Moteiv. *Tmote Sky Datasheet http://www.sentilla.com/pdf/eol/tmote-sky-datasheet.pdf*, 2006. 21

[55] Luca Mottola, Gian Pietro Picco, Matteo Ceriotti, Ştefan Gună, and Amy L. Murphy. Not all Wireless Sensor Networks are created Equal: A Comparative Study on Tunnels. *ACM Trans. Sen. Netw.*, 7(2):15:1–15:33, September 2010. 20, 26, 30, 31, 63

[56] Dimosthenis Pediaditakis, Yuri Tselishchev, and Athanassios Boulis. Performance and Scalability Evaluation of the Castalia Wireless Sensor Network Simulator. In *Proceedings of the 3rd International ICST Conference on Simulation Tools and Techniques*, SIMUTools '10, pages 53:1–53:6, ICST, Brussels, Belgium, 2010. 50

[57] C. Perkins, E. Belding-Royer, and S. Das. Ad hoc On-Demand Distance Vector (AODV) Routing. RFC 3561, IETF, 2003. 50

[58] K. Pister and P. Thubert. Industrial Routing Requirements in Low-Power and Lossy Networks. RFC 5673, IETF, Oct. 2009. 54

[59] Joseph Polastre, Jason Hill, and David Culler. Versatile Low Power Media Access for Wireless Sensor Networks. In *Proceedings of the 2nd International Conference on Embedded Networked Sensor Systems*, SenSys '04, pages 95–107, New York, NY, USA, 2004. ACM. 26

[60] Joseph Polastre, Robert Szewczyk, and David Culler. Telos: Enabling Ultra-low Power Wireless Research. In *Proceedings of the 4th International Symposium on Information Processing in Sensor Networks*, IPSN '05, Piscataway, NJ, USA, 2005. IEEE Press. 21

[61] Joseph Polastre, Robert Szewczyk, Alan Mainwaring, David Culler, and John Anderson. Analysis of Wireless Sensor Networks for Habitat Monitoring. *Kluwer Academic Publishers*, pages 399–423, 2004. 16

[62] D. Puccinelli and M. Haenggi. Arbutus: Network-Layer Load Balancing for Wireless Sensor Networks. In *Wireless Communications and Networking Conference*, pages 2063–2068. IEEE Computer Society, 31 2008-April 3. 46

[63] Daniele Puccinelli and Martin Haenggi. Multipath Fading in Wireless Sensor Networks: Measurements and Interpretation. In *Proceedings of the International Conference on Wireless Communications and Mobile Computing*, IWCMC, pages 1039–1044, New York, NY, USA, 2006. ACM. 23, 24, 25, 26, 30, 58

[64] Daniele Puccinelli and Martin Haenggi. DUCHY: Double Cost Field Hybrid Link Estimation for Low-Power Wireless Sensor Networks. In *Proceedings of Fifth Workshop on Embedded Networked Sensors*, HotEmNets, 2008. 35, 44, 46

[65] Bhaskaran Raman and Kameswari Chebrolu. Censor Networks: A Critique of Sensor Networks from a Systems Perspective. *SIGCOMM*, 2008. 16

[66] Bhaskaran Raman, Kameswari Chebrolu, Naveen Madabhushi, Dattatraya Y. Gokhale, Phani K. Valiveti, and Dheeraj Jain. Implications of Link Range and (In)stability on Sensor Network Architecture. In *Proceedings of the 1st international workshop on Wireless network testbeds, experimental evaluation and characterization*, WiNTECH, pages 65–72. ACM Press, 2006. 30, 35, 65

[67] Niels Reijers, Gertjan Halkes, and Koen Langendoen. Link Layer Measurements in Sensor Networks. In *Proccidings of the First IEEE International Conference on Mobile Ad-hoc and Sensor Systems, Fort Lauderdale (FL)*, MASS, pages 24–27. Society Press, 2004. 23, 29, 46

[68] Christian Renner, Sebastian Ernst, Christoph Weyer, and Volker Turau. Prediction Accuracy of Link-quality Estimators. In *Proceedings of the 8th European conference on Wireless sensor networks*, EWSN'11, pages 1–16. Springer-Verlag, 2011. 35, 41, 46, 55

[69] Rodrigo Fonseca, Omprakash Gnawali, Kyle Jamieson, Sukun Kim, Philip Levis, and Alec Woo. The Collection Tree Protocol (CTP), `http://www.tinyos.net/tinyos-2.x/doc/html/tep123.html`. Internet Draft 1.8, Network Working Group, August 2006. 49

[70] Michele Rondinone, Junaid Ansari, Janne Riihijärvi, and Petri Mähönen. Designing a Reliable and Stable Link Quality Metric for Wireless Sensor Networks. In *Proceedings of the workshop on Real-world wireless sensor networks*, REALWSN '08, pages 6–10, New York, NY, USA, 2008. ACM. 31

[71] Michele Rondinone, Junaid Ansari, Janne Riihijärvi, and Petri Mähönen. Designing a Reliable and Stable Link Quality Metric for Wireless Sensor Networks. In *Proceedings of the Workshop on Real-World Wireless Sensor Networks*, REALWSN '08, pages 6–10, 2008. 37, 38

[72] Bor rong Chen, Kiran kumar Muniswamy-reddy, and Matt Welsh. Ad-hoc Multicast Routing on Resource-limited Sensor Nodes. In *Proceedings of the 2nd International Workshop on Multi-hop Ad*, pages 87–94. ACM Press, 2006. 34, 35, 43, 44, 46

[73] H. Sanneck and G. Carle. A Framework Model for Packet Loss Metrics Based on Loss Runlengths. In *Proceedings of Multimedia Computing and Networking Conference*, SPIE/ACM SIGMM, pages 177–187. ACM, 2000. 32

[74] Murat Senel, Krishna Chintalapudi, Dhananjay Lal, Abtin Keshavarzian, and Edward J. Coyle. A Kalman Filter Based Link Quality Estimation Scheme for Wireless Sensor Networks. In *GLOBECOM*, 2007. 34, 38

[75] Senslab. Very large scale open wireless sensor network testbed. `http://www.senslab.info/`. 11, 57, 59, 61, 125

[76] Low-Power Sub-1GHz RF Transceiver. Chipcon Product Data Sheet. . `www.ti.com/lit/ds/symlink/cc1101.pdf`. 5, 21, 24, 27

[77] Z. Shelby and S. Chakrabarti. E. Nordmark," Neighbor Discovery Optimization for Low Power and Lossy Networks (6LoWPAN)", draft-ietf-6lowpan-nd-18 (work in progress), 2011. 17

[78] S. V. Srikanth, Pramod P.J., Dileep K.P., Tapas S., Mahesh U. Patil, and Sarat Chandra Babu N. Design and Implementation of a Prototype Smart PARKing (SPARK) System Using Wireless Sensor Networks. In *Proceedings of the 2009 International Conference on Advanced Information Networking and Applications Workshops*, WAINA '09, pages 401–406, Washington, DC, USA, 2009. 16

[79] Kannan Srinivasan, Prabal Dutta, Arsalan Tavakoli, and Philip Levis. Understanding the Causes of Packet Delivery Success and Failure in Dense Wireless Sensor Networks. In *Proceedings of the 4th International Conference on Embedded Networked Sensor Systems*, SenSys '06, pages 419–420, New York, NY, USA, 2006. ACM. 26, 29, 30, 31, 46, 66

[80] Kannan Srinivasan, Prabal Dutta, Arsalan Tavakoli, and Philip Levis. An Empirical Study of Low-power Wireless. *ACM Trans. Sen. Netw.*, 6(2):16:1–16:49, March 2010. 20, 21, 26, 29, 31, 64, 66

[81] Kannan Srinivasan, Maria A. Kazandjieva, Saatvik Agarwal, and Philip Levis. The beta-factor: Measuring Wireless Link Burstiness. In *Proceedings of the 6th ACM conference on Embedded network sensor systems*, SenSys, pages 29–42, New York, NY, USA, 2008. ACM. 30, 32, 35, 36, 39, 46, 50, 65

[82] Kannan Srinivasan, Maria A. Kazandjieva, Mayank Jain, Edward S. Kim, and Philip Levis. Demo Abstract: SWAT: Know your Network. In *IPSN*, pages 431–432, 2009. 46

[83] Kannan Srinivasan and Philip Levis. RSSI is Under Appreciated. In *Proceedings of the Third Workshop on Embedded Networked Sensors*, EmNets, 2006. 21, 23, 30, 35, 37, 70

[84] Kannan Srinivasan, Philip Levis, Fouad A Tobagi, and Sachin Katti. Towards a Wireless Lexicon. In *Thesis-PhD*, pages 1–165. Stanford University Dept. of Electrical Engineering., 2010. 106

[85] IEEE 802.15.4 MAC standard. Available at. `http://www.ieee802.org/15/pub/TG4.html`. 22

[86] Zhi Sun, Pu Wang, Mehmet C. Vuran, Mznah Al-Rodhaan, Abdullah Al-Dhelaan, and Ian F. Akyildiz. BorderSense: Border Patrol Through Advanced Aireless Aensor Networks. *Ad Hoc Networks*, 9(3):468–477, 2011. 16

[87] Lei Tang, Kuang-Ching Wang, Yong Huang, and Fangming Gu. Channel Characterization and Link Quality Assessment of IEEE 802.15.4-Compliant Radio for Factory Environments. In *Industrial Informatics, IEEE Transactions*, volume 3, pages 99–110, 2007. 30

[88] P. Thubert and et al. RPL: IPv6 Routing Protocol for Low power and Lossy Networks. RFC 6553, IETF, March 2012. 37, 48, 50, 52

[89] TI. Calculation and Usage of LQI and RSSI. `http://e2e.ti.com/support/low_power_rf/w/design_notes/calculation-and-usage-of-lqi-and-rssi.aspx`. 57

[90] Torsten Braun and Philipp Hurni and Markus Anwander and Gerald Wagenknecht. Wireless Sensor Network Testbeds (Wisebed). ERCIM Workshop

on E-Mobility, in conjunction with WWIC 2010, June 1-5, Lulea, Sweden, 2010. 128

[91] JP. Vasseur, M. Kim, K. Pister, N. Dejean, and D. Barthel. Routing Metrics Used for Path Calculation in Low-Power and Lossy Networks. RFC 6551 (Proposed Standard), March 2012. 52

[92] T. Watteyne, S. Lanzisera, A. Mehta, and K. S. J. Pister. Mitigating Multipath Fading through Channel Hopping in Wireless Sensor Networks. In *Proc. of IEEE International Conference on Communications*, pages 1–5. Ieee, May 2010. 23, 24, 26, 29, 30, 58

[93] Geoffrey Werner-Allen, Patrick Swieskowski, and Matt Welsh. MoteLab: a Wireless Sensor Network Testbed. In *Proceedings of the 4th international symposium on Information processing in sensor networks*, IPSN '05, Piscataway, NJ, USA, 2005. IEEE Press. 45

[94] Andreas Willig and Robert Mitschke. Results of Bit Error Measurements with Sensor Nodes and Casuistic Consequences for Design of Energy-efficient Error Control Schemes. In *Proceedings of the Third European conference on Wireless Sensor Networks*, EWSN'06, pages 310–325, Berlin, Heidelberg, 2006. Springer-Verlag. 46

[95] M. Woehrle, M. Bor, and K. Langendoen. 868 MHz: A Noiseless Environment, but no Free Lunch for Protocol Design. In *Networked Sensing Systems (INSS), 2012 Ninth International Conference on*, pages 1 –8, june 2012. 20, 29, 31

[96] Alec Woo and David Culler. Evaluation of Efficient Link Reliability Estimators for Low-Power Wireless Networks. Technical Report UCB/CSD-03-1270, EECS Department, University of California, Berkeley, 2003. 20, 38, 46, 47

[97] Alec Woo, Terence Tong, and David Culler. Taming the Underlying Challenges of Reliable Multihop Routing in Sensor Networks. In *Proceedings of the 1st international conference on Embedded networked sensor systems*, SenSys '03, pages 14–27, New York, NY, USA, 2003. ACM. 21, 29, 31, 34, 35, 37, 46, 58

[98] Yingqi Xu and Wang chien Lee. Exploring Spatial Correlation for Link Quality Estimation in Wireless Sensor Networks. In *Proc. IEEE PerCom*, pages 200–211, 2006. 35

[99] M I Xue, Zhao Hai, and Z H U Jian. A Novel EWMA based Link Quality Evaluation Algorithm for WSN. *International Journal of Engineering and Technology*, 11(Issue 3, p19), June 2011. 31, 66

[100] Sven Z., Thomas N., Sinead O'K., and Elfed L. Identifying Sources of Interference in RSSI Traces of a Single IEEE 802.15.4 Channel. In *ICWMC*, 2012. 30

[101] Marco Zennaro, Hervé Ntareme, and Antoine Bagula. Experimental Evaluation of Temporal and Energy Characteristics of an Outdoor Sensor Network. In *Proceedings of the International Conference on Mobile Technology, Applications, and Systems*, Mobility '08, pages 99:1–99:5, New York, NY, USA, 2008. ACM. 20, 21, 29, 30, 31, 58, 65

[102] Rongbiao Zhang, Yongxian Song, Fuhuan Chu, and Biqi Sheng. Study of Wireless Sensor Networks Routing Metric for High Reliable Transmission. *Journal of Networks*, 7(12):2044–2050, 2012. 34, 45, 46, 55

[103] Jerry Zhao and Ramesh Govindan. Understanding Packet Delivery Performance in Dense Wireless Sensor Networks. In *SenSys*, pages 1–13, 2003. 21, 23, 29, 31, 46, 58, 64

[104] Gang Zhou, Tian He, Sudha Krishnamurthy, and John A. Stankovic. Impact of Radio Irregularity on Wireless Sensor Networks. In *Proceedings of the 2nd international conference on Mobile systems, applications, and services*, MobiSys '04, pages 125–138, New York, NY, USA, 2004. ACM. 24, 30

[105] Gang Zhou, Tian He, Sudha Krishnamurthy, and John A. Stankovic. Models and Solutions for Radio Irregularity in Wireless Sensor Networks. *ACM Transactions on Sensor Networks*, 2:221–262, 2006. 21

[106] Marco Zuniga, Izabela Irzynska, Jan-Hinrich Hauer, Thiemo Voigt, Carlo Alberto Boano, and Kay Römer. Link Quality Ranking: Getting the Best out of Unreliable Links. In *DCOSS*, pages 1–8, 2011. 20, 35, 36, 42, 45, 55, 128

[107] Marco Zuniga and Bhaskar Krishnamachari. Analyzing the Transitional Region in Low Power Wireless Links. In *SECON*, pages 517–526, 2004. 64